

A STUDY OF ELECTRON-ION DISSOCIATIVE RECOMBINATION OF
SUBSTITUTED BENZENE ANALOGS RELEVANT TO THE TITAN
ATMOSPHERE

by

DAVID SAM OSBORNE, JR.

(Under the Direction of NIGEL G. ADAMS)

ABSTRACT

Because of the continuing success of the Cassini Mission to study the Titan atmosphere, a great deal of kinetic data is required. One of the types of kinetic data which is needed is for electron-Ion Dissociative Recombination (e-IDR) rate constants. This is used by Titan atmospheric modelers to explain, in part, the process by which simple compounds, such as nitrogen and methane, are transformed into larger compounds. The larger compounds, possibly poly-cyclic aromatic hydrocarbons (PAH's), are responsible for the characteristic orange haze present within the Titan atmosphere. With the confirmed presence of benzene, both in the Titan atmosphere by Cassini and on the Titan surface by the Huygens probe, the e-IDR rate constant data for benzene and various benzene analogs are needed by Titan atmospheric modelers. To satisfy this need, a study of the e-IDR rate constants for benzene substituted with varying functional groups has been completed. Another study of the e-IDR rate constants for benzene with hetero-atom substitutions has also been undertaken to address the possible presence of PAH's. When possible, the temperature dependence data have been collected

for the benzene analog under study. Trends between e-IDR rate constants and the number of hetero-atom additions and between e-IDR rate constants and the Hammett σ_{para} value are some of the observed trends in the various studies. These revealed trends in e-IDR rate constants will greatly reduced the number of e-IDR rate constants needed by Titan atmospheric modelers. The effects of isomeric form on e-IDR rate constants have also been investigated in these studies. The data on each study and its effect on Titan atmospheric modeling are discussed.

INDEX WORDS: electron-Ion Dissociative Recombination, VT-FALP, Flowing Afterglow, Interstellar Medium, Titan, Ionosphere, planetary atmospheres, PAH, Benzene Analogs, Hammett Constant

A STUDY OF ELECTRON-ION DISSOCIATIVE RECOMBINATION OF
SUBSTITUTED BENZENE ANALOGS RELEVANT TO THE TITAN
ATMOSPHERE

by

DAVID SAM OSBORNE, JR.

Bachelors of Science, Alice Lloyd College, 2007

Bachelors of Arts, Alice Lloyd College, 2007

A Dissertation Submitted to the Graduate Faculty of the University of Georgia in Partial
Fulfillment of the Requirements for the Degree

DOCTORATE OF CHEMISTRY

ATHENS, GEORGIA

2013

© 2013

David Sam Osborne, Jr.

All Rights Reserved

A STUDY OF ELECTRON-ION DISSOCIATIVE RECOMBINATION OF
SUBSTITUTED BENZENE ANALOGS RELEVANT TO THE TITAN
ATMOSPHERE

by

DAVID SAM OSBORNE, JR.

Major Professor: Nigel G. Adams

Committee: Geoffrey D. Smith
Gary E. Douberly

Electronic Version Approved:

Maureen Grasso
Dean of the Graduate School
The University of Georgia
December 2013

DEDICATION

To my son, Dirk X. Osborne, who asked many times when I would be done with school?

ACKNOWLEDGEMENTS

In the pursuit of this degree, I have obtained help from a number of amazing people, both at the University of Georgia and elsewhere. I would like to thank Nigel Adams, Patrick Lawson, Lillian Dalila Mathews, Chris Molek, Jason McLain, Geoffrey Smith, Gary Douberly, and Martha Osborne for their support and help. I would also like to thank the secretaries that helped me find materials and the engineers who built the machines I use to conduct research. To everyone who helped me, being too numerous to name, I would like to say thank you. Without the support of each and everyone one of you this endeavor would not have been possible.

TABLE OF CONTENTS

	Page
ACKNOWLEDGEMENTS	v
LIST OF TABLES	x
LIST OF FIGURES	xii
CHAPTER	
1 INTRODUCTION AND LITERATURE REVIEW	1
1-1 REFERENCES	8
2 EXPERIMENTAL ARRANGEMENT OF THE FLOWING AFTERGLOW	11
2-1 BASIC INFORMATION	11
2-2 REACTANT GAS SYSTEMS AND THE BUBBLER	
APPARATUS	14
2-3 LANGMUIR PROBE OPERATION AND DETERMINATION OF	
ELECTRON-ION DISSOCIATIVE RECOMBINATION RATE	
CONSTANTS	18
2-4 TEMPERATURE CONTROL	23
2-5 TEMPERATURE DEPENDENT PATHWAYS	24
2-6 REFERENCES	26
3 FLOWING AFTERGLOW STUDIES OF DISSOCIATIVE ELECTRON-ION	
RECOMBINATION FOR A SERIES OF SINGLE RING COMPOUNDS AT	
ROOM TEMPERATURE	28

3-1 ABSTRACT	29
3-2 INTRODUCTION	29
3-3 EXPERIMENTAL.....	32
3-4 RESULTS AND DISCUSSION	39
3-5 CONCLUSIONS	42
3-6 ACKNOWLEDGEMENTS	43
3-7 REFERENCES	43
4 THE EFFECT OF N-HETEROATOMS AND CH ₃ SUBSTITUENTS ON	
DISSOCIATIVE ELECTRON-ION RECOMBINATION OF PROTONATED	
SINGLE SIX MEMBERED RING COMPOUNDS AT ROOM	
TEMPERATURE	46
4-1 ABSTRACT	47
4-2 INTRODUCTION	47
4-3 EXPERIMENTAL.....	49
4-4 RESULTS AND DISCUSSION.....	52
4-5 CONCLUSIONS	54
4-6 ACKNOWLEDGEMENTS	58
4-7 REFERENCES	58
5 TRENDS IN ELECTRON-ION DISSOCIATIVE RECOMBINATION OF BENZENE	
ANALOGS WITH FUNCTIONAL GROUP SUBSTITUTIONS: NEGATIVE	
HAMMETT σ_{PARA} CONSTANTS	60
5-1 ABSTRACT	61
5-2 INTRODUCTION	61

5-3 EXPERIMENTAL.....	63
5-4 RESULTS AND DISCUSSION	65
5-5 CONCLUSION	68
5-6 ACKNOWLEDGEMENTS	68
5-7 REFERENCES	69
6 TRENDS IN ELECTRON-ION DISSOCIATIVE RECOMBINATION OF BENZENE ANALOGS WITH FUNCTIONAL GROUP SUBSTITUTIONS: POSITIVE HAMMETT σ_{para} CONSTANTS	
6-1 ABSTRACT	74
6-2 INTRODUCTION	74
6-3 EXPERIMENTAL.....	77
6-4 RESULTS AND DISCUSSION	78
6-5 CONCLUSION	82
6-6 ACKNOWLEDGEMENTS	83
6-7 REFERENCES	83
7 ELECTRON-ION DISSOCIATIVE RECOMBINATION RATE CONSTANTS: EFFECTS FOR BENZENE ANALOGS WITH VARYING DEGREES OF METHYLATION	
7-1 ABSTRACT	89
7-2 INTRODUCTION	89
7-3 EXPERIMENTAL	90
7-4 RESULTS AND DISCUSSION	92
7-5 CONCLUSION	96

7-6 REFERENCES	96
8 ELECTRON-ION DISSOCIATIVE RECOMBINATION RATE CONSTANTS	
RELEVANT TO THE TITAN ATMOSPHERE AND THE INTERSTELLAR	
MEDIUM	101
8-1 ABSTRACT	102
8-2 INTRODUCTION	102
8-3 EXPERIMENTAL	104
8-4 RESULTS AND DISCUSSION	106
8-5 FUTURE WORK	112
8-6 ACKNOWLEDGEMENTS	112
8-7 REFERENCES	112
9 CONCLUSION AND FUTURE WORK	116
9-1 REFERENCES	119

LIST OF TABLES

	Page
Table 3-1. Room temperature (300K) recombination rate constants, α_e , ($\text{cm}^3 \text{s}^{-1}$) for the protonated monomer (RVH^+) and proton bound dimer ($(\text{RV})_2\text{H}^+$) for the compounds indicated	40
Table 4-1. Recombination rate constants, α_e , indicated for the protonated species (RVH^+) and their proton bound dimers ($(\text{RV})_2\text{H}^+$) together with relevant data from previous studies reported in the literature. These species contain various combinations of CH_3 substituents attached to the rings and N-atoms substituted into the rings.	52
Table 5-1: 300K rate constants and electron temperature dependencies (300-550K) for the electron-ion dissociative recombination (e-IDR) of the protonated species indicated. These are all mono substituted with the functional groups indicated and have the negative Hammett (σ_{para}) values shown. The data are plotted graphically in Figs. 1 and 2. a) Data previously published.....	66
Table 6-1: 300K rate constants and temperature dependencies (300-550K) for the electron-ion dissociative recombination (e-IDR) of the protonated species indicated. These are all mono substituted with the functional groups indicated and have the positive Hammett (σ_{para}) values shown. Note that the measured e-IDR rate constants have an associated $\pm 15\%$ error.....	79
Table 6-2: List of substituted benzene compounds which fragment on proton transfer (see	

reaction (3)). The associated Hammett σ_{para} value and the functional group are included in the table. Note that all these species have positive Hammett values and are less stable.....	81
Table 7-1: 300K electron-Ion Dissociative Recombination (e-IDR) rate constants for various methyl substituted benzenes.....	93
Table 7-2: 300K electron-Ion Dissociative Recombination (e-IDR) rate constants for various methyl substituted benzene isomers.....	94
Table 8-1: Values for the room temperature electron-ion dissociative recombination rate constants and associated temperature dependencies for benzene, furan, and 1,4 dioxane. Note that the benzene data has been published previously. The 300K data for the protonated monomer and proton bound dimer of both Furan and 1,4 dioxane has been published previously.....	110
Table 8-2: Values for the room temperature electron-ion dissociative recombination rate constants of benzene and naphthalene. Note the 300K data for benzene have been published previously	111

LIST OF FIGURES

	Page
Figure 1-1: A spectrum of the positive ions taken by the Cassini CAPS instrument on the T40 flyby, at ~1000km. The black dots represent the Cassini measured data. The dotted line represents the predicted spectra according to the Vuitton model. The black line has been included to connect the dots. Ion identification of the peaks and error bars have been included to aid the viewer.....	6
Fig. 2-1: A schematic diagram of the Flowing Afterglow apparatus (FALP) located at the University of Georgia. Temperature variable facility has been omitted for clarity. Parts are labeled	12
Fig 2-2: A schematic of the flow control systems for the Reactant Gas Systems 1-4. This schematic illustrates how a reactant gas is distributed to a reactant port. The capillary tube, which is used to calculate the density of the reactant gas flowing into the system, is labeled with the pre and post stages of pressure measurement also labeled. The closer values in the system are labeled as the black boxes with “CV” inside them.....	15
Fig. 2-3: The empty bubbler apparatus prior to connection to the system. The Helium inlet, sample reservoir, ground glass joint and flow outlet have been labeled	17
Fig. 2-4: The downstream half of the glass probe assembly which holds the tungsten probe. The area of the probe exposed to the FALP plasma labeled and the location of the glass bead, which holds the probe in place, is also labeled. Note that due to	

the small diameter of the tungsten wire, it does not show up in the picture, also due to the length of the probe assembly (~58 inc.) two pictures were needed to show detail 19

Fig. 2-5: The upstream end of the probe assembly. The small diameter glass tube and the steel slug are labeled. The slug serves as the upstream connection to the computer via a metal track, not pictured. A thin nickel (0.05mm diameter) wire is insulated from the plasma by the thin glass tubing of the probe assembly and serves as the connection between the metal slug and the tungsten probe..... 20

Fig. 2-6: A schematic of the Langmuir probe circuit for the University of Georgia Flowing Afterglow (FALP). The schematic shows connections to the probe, computer input bias voltage (voltage applied to the probe to attract electrons), and the output voltage to the computer. The resistor selector switch indicated in the schematic allows the user to select the correct resistor for plasma conditions. Pin connection numbers and labels have been attached to the appropriate locations for both the LF411 and AD 210 chips..... 21

Fig. 2-7: Plot of reciprocal electron density, $1/[e^-]$, and function of flow tube distance, z . The various regions of the plasma along the length of the flow tube are labeled. The plasma region of H_3^+ , is labeled in red. The black arrow represents the introduction point of benzene vapor into the plasma. This region is followed by a region of proton transfer (the unlabeled two blue dots represent measurements of electron density during this period) before the green labeled region of protonated benzene ($C_6H_7^+$) recombination. The slope of the green line yields the e-IDR rate constant for protonated benzene. Following the recombination of protonated

benzene, we see electron loss due to ambipolar diffusion to the walls, which occurs at about 65cm down the flow tube. 23

Fig. 2-8: A plot of the e-IDR rate constants, α_e , versus temperature for protonated benzene ($C_6H_7^+$) and pyridine ($C_5H_5NH^+$) from 300K to ~550K.....26

Fig. 3-1. Variation of $1/[e]$ versus distance, z , along the flow for the electron ion recombination of protonated furan at 300K..... 33

Fig. 3-2. Schematic of the variation of α_e with reactant vapor concentration, $[RV]$, showing the regions where H_3^+ , RVH^+ or $(RV)_2H^+$ dominate the recombination. (a) Plateaus in recombination for RVH^+ and $(RV)_2H^+$ with $\alpha_e(RVH^+) < \alpha_e((RV)_2H^+)$ and asymptotic approach to H_3^+ recombination at low reactant vapor concentrations34

Fig. 3-3. Schematic of the variation of α_e with reactant vapor concentration, $[RV]$, showing the regions where H_3^+ , RVH^+ or $(RV)_2H^+$ dominate the recombination. (b) Plateau in recombination for RVH^+ with no production of $(RV)_2H^+$ and an asymptotic approach to H_3^+ recombination at low reactant vapor concentrations35

Fig. 3-4. Schematic of the variation of α_e with reactant vapor concentration, $[RV]$, showing the regions where H_3^+ , RVH^+ or $(RV)_2H^+$ dominate the recombination. (c) Plateaus in recombination for RVH^+ and $(RV)_2H^+$ with $\alpha_e(RVH^+) > \alpha_e((RV)_2H^+)$ and asymptotic approach to H_3^+ recombination at low reactant vapor concentrations35

- Fig. 3-5. Experimental data for the recombination rate constant, α_e , of protonated 4-picoline as a function of 4-picoline reactant vapor concentration showing both the monomer and the dimer plateaus. 38
- Fig. 3-6. Experimental data for the recombination rate constant, α_e , of protonated pyrrole as a function of pyrrole reactant vapor concentration. This shows that the plateaus for the dimer cannot be seen in all cases.....38
- Fig. 4-1. Plot of 2, 3, and 4 picoline rate constant (α_e) versus reactant vapor concentration. The plateaus are well defined for 4-picoline but less so for 2 and 3 picoline. Note: The three plots are vertically offset for viewing ease, and the rate constants of the protonated form and the proton bound dimer are labeled on each curve..... 50
- Fig. 4-2. A plot of the rate coefficients, α_e , ($\text{cm}^3 \text{s}^{-1}$) for a series of recombining protonated single six membered ring compounds as a function of the number of CH_3 substituents and N-atoms in the rings. 2,5 lutidine and mesitylene were also studied and show increasing values, which are included in Table 1. However, are omitted for clarity in this figure. 53
- Fig. 4-3. A plot of the recombining proton bound dimer rate constants, α_e , ($\text{cm}^3 \text{s}^{-1}$) for a series of proton bound dimers of single six membered ring compounds as a function of the number of CH_3 substituents and N-atoms in the rings. Mesitylene shows an increasing value and is included in Table 1. However it is omitted here for clarity..... 54
- Fig. 4-4. Possible parallel routes to the production of naphthalene through interactions of benzene with ions present within the Titan atmosphere. 56

Fig. 5-1: Measured 300K electron-Ion dissociative recombination (e-IDR) rate constants versus their associated negative Hammett σ_{para} values. The red square represents the previously measured e-IDR rate constant for protonated toluene. A trend line, excluding the red square, has been added to show the linearity of the measured data. The toluene data are inconsistent with the trend line for which we have no explanation. 67

Fig. 5-2: Graph of the power law temperature dependencies for the species in Table 5-1 versus their negative Hammett σ_{para} values.....68

Fig. 6-1: Measured electron-Ion dissociative recombination (e-IDR) rate constants versus their associated Hammett σ_{para} constant values. The red square represents the measured upper limit e-IDR rate constant for protonated phenyl isothiocyanate. The green square represents the e-IDR rate constant for protonated toluene. A purple line, excluding the red square and green square, has been added to show the linearity of the measured data and show the constant value for e-IDR rate constant for benzene analogs whose functional groups have a positive Hammett σ_{para} constant value. The $\pm 15\%$ error associated with each measurement is represented by the error bars attached to each point.....80

Fig. 7-1: Measured 300K electron-Ion dissociative recombination (e-IDR) rate constants versus the number of benzene methyl additions. The error bar associated with each measurement has been included in the graph, and the benzene value labeled. The red line represents the central value around which all methylated benzene analogs fluctuate. 93

Fig. 7-2: Electron-Ion Dissociative Recombination (e-IDR) rate constants between 300K and 550K for protonated benzene and toluene. The benzene data have been published previously95

Figure 8-1: A plot of the temperature dependencies of the protonated monomers for 1,4 dioxane (the red squares) and benzene (the blue diamonds). Note that benzene has been published previously108

Figure 8-2: A plot of the temperature dependencies of the proton bound dimers for 1,4 dioxane (red squares) and benzene (the blue diamonds). Note that benzene has been published previously.....108

CHAPTER 1

INTRODUCTION AND LITERATURE REVIEW

Saturn's largest moon, Titan, was discovered in 1655 by Christian Huygens[1], and has a dense silicate core surrounded by a layer of high pressure water ice[2]. Covering the high pressure ice is a layer of liquid water/liquid ammonia that in turn are enclosed by an layer of water ice and less than 5 meters thickness of organic particles[2]. These organic particles cover the surface of Titan[2, 3].

Surrounding the surface there is a dense atmosphere composed of ~98% nitrogen and ~2% methane and other compounds in trace amounts[4]. Due to a hydrolytic cycle, similar to the one found on Earth, methane can also be found in pools or lakes on the polar regions of the Titan surface[5]. This methane evaporates from the surface and condenses in the atmosphere around organic nano-particles facilitating their transfer to the surface[6]. This cycle deposits the vast array of organic compounds produced in the Titan atmosphere upon the satellites surface [6]. High winds, created by the combination of the dense atmosphere and the low gravity of Titan, create massive storms in the equatorial regions which cause the constant shifting of dunes composed of organic nano-particles and water ice crystals[7]. While a fascinating extra-terrestrial landscape, the production of organic compounds within the Titan atmosphere is of great interest due to the possible similarities between Titan and the early Earth[8].

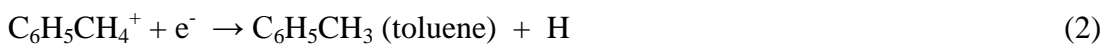
It is predicted that the complex organic compounds necessary for the formation of life on Earth may have been produced through atmospheric reactions similar to those on Titan[8]. For over half a century, there has existed a problem with modeling the appearance of life on Earth[9]. It has been estimated that the sun emitted 30-45% less luminance at the time when life arose on Earth[9, 10]. With this decrease in luminance, the surface of the Earth would have been much colder than present day. These colder temperatures would have caused any water upon the surface of the planet to be frozen[9]. While it is possible for life to arise under such harsh conditions, geological evidence indicates that life arose during a period where temperatures were at least 40°C warmer than present day[11]. This has led to the prediction that the early Earth had an organic haze present in the atmosphere[10]. The atmosphere of the early Earth is thus thought to be similar to Titan in composition; with nitrogen as the dominate species followed by lesser concentrations of methane, carbon dioxide, and water[10]. Through a process similar to that which occurs on Titan, large organic species may have been produced in the atmosphere of the early Earth [8, 10]. This protective organic haze allowed species such as methane, carbon dioxide, and ammonia to survive destruction by ultra-violet (UV) solar radiation [8, 10, 11]. These species may have provided a “greenhouse effect” which helped to raise the temperature on the surface of the planet[8]. It is even possible that due to the composition of the early Earth’s atmosphere, the building blocks of life (amino acids) could have been produced via secondary reactions in the atmosphere and then deposited upon the planet surface.

In 2004, a spacecraft arrived at Titan to conduct a definitive study of the makeup of the atmosphere of this Saturn moon [12-14]. Before this expedition there had been

three other investigations into the atmosphere of Titan with spacecraft's Pioneer 11, Voyager 1, and Voyager 2[1]. With the data sent back during these missions, a crude preliminary model of the atmosphere was created which predicted that ionization of methane was occurring and that large compounds, such as benzene, were being produced. However with the commencement of the Cassini mission in 2004, the situation changed and it was shown that the complexity of the predicted chemistry had been greatly underestimated[6]. Cassini showed that in the upper atmosphere, >900km above the satellite's surface, nitrogen and methane are ionized by solar x-ray and ultra-violet solar radiation [15-17]. Ionization also occurs by high energy electrons and oxygen anions (O^+) from Saturn's magnetosphere impacting with the Titan atmosphere [7, 12, 15]. This ionization creates charged species (such as CH_3^+ , N^+ , N_2^+ , CH_4^+) which can undergo a series of reactions (Ion-Neutral reactions, Association reactions, Proton transfer reactions, Ion-Ion Neutralization reactions and electron-Ion Dissociative Recombination) which generate larger compounds[3, 12]. However, the production of larger compounds was observed by the Cassini spacecraft following its arrival at Titan in 2004[12-14]. Small compounds, such as $HCNH^+$ and $C_3H_3^+$, were discovered in Titan's upper atmosphere by the Ion Neutral Mass Spectrometer (INMS) on Cassini, which measured positive ions having masses from 1 to 99 amu with a better than one amu resolution[14]. Larger hydrocarbon ions such as those of benzene (C_6H_6) and toluene ($C_6H_5CH_3$) have been identified with Cassini Plasma Spectrometer (CAPS) which measured positive ions with masses from 1 to 350 amu[13]. While these discoveries have helped to refine the models of Titan atmosphere, equally important was the discovery of negative ions between 50 to

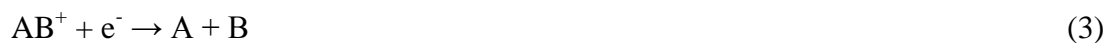
14,000 amu by the CAPS electron spectrometer which has introduced a new complication in the atmospheric models[13].

Cassini data indicates that benzene may account for ~4% of the observable hydrocarbon deposits on the surface of Titan[6]. With the efficient production of benzene through chemical reactions within the atmosphere, it is probable that large polycyclic aromatic hydrocarbons (PAH's) and Polyphenyls are produced at lower altitudes through reactions between benzene and benzene analogs[3, 6, 18]. This theory is supported by the discovery that the benzene concentrations decreases as a function of altitude, while the abundances of larger mass ions increases[18]. Current models have indicated the presence of a great number of benzene analogs within the atmosphere [3, 12]. Methyl substituted benzenes such as toluene ($C_6H_5CH_3$) and xylene ($C_6H_4(CH_3)_2$) have been observed by Cassini [6, 19] and are possibly formed through reactions such as between benzene and CH_3^+ , equations 1 and 2 [20].



Protonated toluene is produced by the association of benzene with CH_3^+ . Upon neutralization by electron-Ion Dissociative Recombination (e-IDR), neutral toluene and hydrogen are produced[20]. Similar processes could lead to the buildup of larger compounds within the Titan atmosphere[21], such as naphthalene ($C_{10}H_8$).

Atmospheric models predict that there is a buildup of larger hydrocarbons between 1000-400km which could be produced through two processes; association followed by electron-ion dissociative recombination (e-IDR), equation 3, and ion-ion neutralization reactions[3], equation 4.



In this atmospheric region the larger compounds are produced which give the Titan atmosphere its characteristic orange color. This color is produced by large nano-particles, composed of PAH's or polyphenyl compounds suspended in the atmosphere creating a haze [3, 18, 22]. The sizes increase as the particles diffuse lower in the atmosphere due to the possible condensation of benzene upon the surface of the particles and through association between particles[3, 22].

From 200km down to the surface, the atmosphere is free from particles. This is because methane then condenses on the particles facilitating the formation of methane droplets[15] [6, 23]. Methane droplets then serve as a carrier to deposit the particles upon the Titan surface [6]. Following the methane droplets arrival at the Titan surface, the droplet will evaporate and repeat the cycle [7]. The Huygens probe (a detachable part of the Cassini probe designed to land on the Titan surface) confirmed this through the monitoring of the atmosphere during its descent to the Titan surface[7]. The concentration of methane was found to increase as the probe neared the surface, indicating that liquid methane is located on the surface[6]. The probe was also able to verify the existence of benzene in the organic layer on the surface[18].

With the data sent back by Cassini, new models had to be created which incorporate large molecular ions into the reaction sequences, see Figure 1-1[12]. Of great interest, is the haze particle formation in the Titan atmosphere. With only two proposed pathways for the production of such particles, e-IDR and ion-ion recombination, Titan atmospheric models are rudimentary in nature. Their complexity arises from the large

number of kinetic rate constants of benzene analogs that must be included within the model. The need for a great deal of benzene analog data creates a problem.

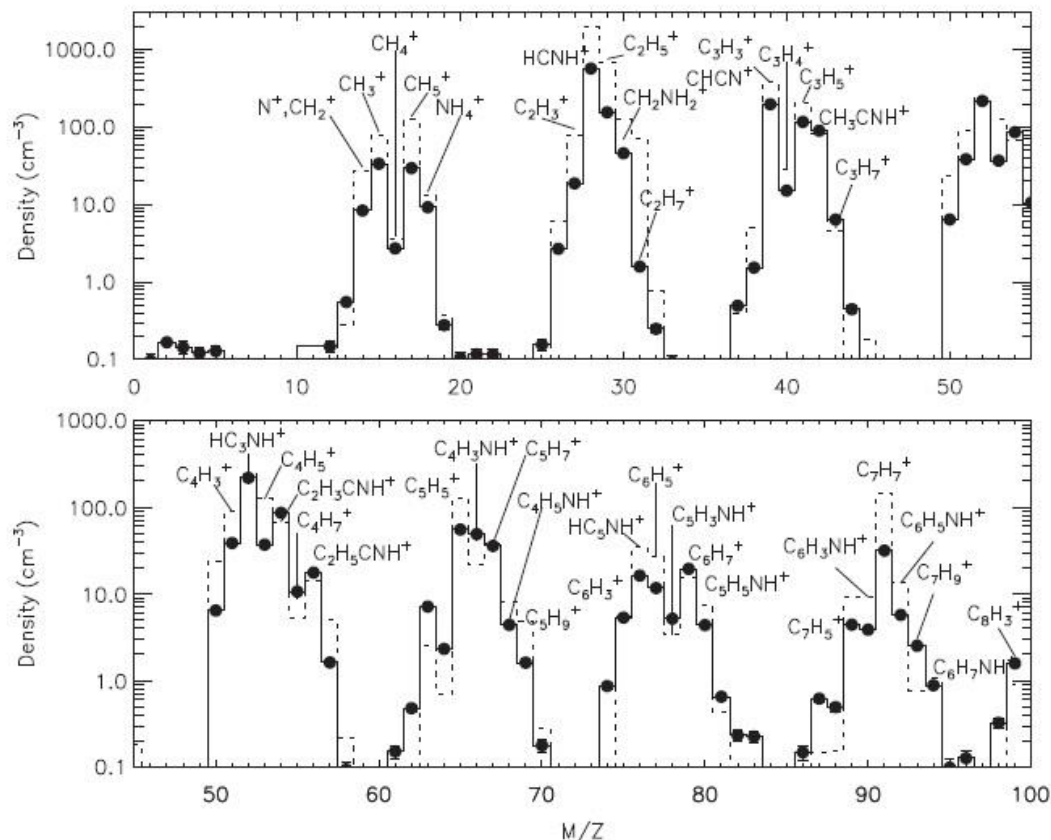


Figure 1-1: A spectrum of the positive ions taken by the Cassini CAPS instrument on the T40 flyby, at ~1000km. The black dots represent the Cassini measured data. The dotted line represents the predicted spectra according to the Vuitton model. The black line has been included to connect the dots. Ion identification of the peaks and error bars have been included to aid the viewer^[12].¹

There exists a shortage in the kinetic data available to Titan modelers, especially e-IDR kinetic data. With the need for e-IDR kinetic data, a study has been undertaken on the e-IDR rate constants for protonated benzene and its substituted analogs. The goal of the new study would not be to measure all possible e-IDR rate constants, rather to identify

¹ Reprinted from [12] with permission. Copyright 2009 by Elsevier. Full text article can be found at <http://www.sciencedirect.com/science/article/pii/S0032063309001068>.

trends which would allow the prediction of e-IDR rate constants. By determining trends, the number of rate constants that must be measured would be greatly reduced. For compounds for which it is not possible to get into the gas phase, observed trends would allow the prediction of their e-IDR rate constants. With the presence of so much benzene within the Titan atmosphere, the study should start with this compound and its most common analogs which are likely to exist on Titan. The study should look at how the e-IDR rate constants are affected by the substitution of nitrogen in place of a carbon within the benzene ring. One such compound (charged pyrimidine($C_5N_2H_4^+$)) has already been identified by the CAPS on Cassini as present within the Titan atmosphere[12]. It is likely, given the abundance of nitrogen within the Titan atmosphere, that other nitrogen substituted benzene like compounds could exist and undergo similar reactions to benzene[12]. With the abundance of CH_4^+ and CH_3^+ within the upper atmosphere, a study to see the effects of methyl substitution to benzene also needs to be carried out. Some methylated benzene species have been identified as present at ~1000km[6, 17, 19]. Toluene ($C_6H_5CH_3$) and xylene ($C_6H_4(CH_3)_2$) were identified and other methylated benzenes could be present at lower altitudes[3, 6]. These compounds could be a base for the formation of haze particles. A study of functional group substitutions to benzene should therefore be undertaken, as current experiments simulating the formation of Titan haze particles have predicted that not just benzene is formed but that various functional groups occur at the same time[18, 22, 23]. The last study that needs to be undertaken is to determine the effects of multi-rings and polyphenyls on e-IDR rate constants. This will be of great interest since it is predicted that benzene combines to form these multi-ring and polyphenyl compounds. These compounds then produce the haze particles

which give Titan its characteristic color. The proposed study will also need to determine any effect that the isomeric form has on e-IDR rate constants, since most of the benzene analogs proposed can have multiple isomeric forms. Such studies would identify trends which would help to supply the great amount of data needed to model the formation of haze particles within the Titan atmosphere.

1-1 REFERENCES

1. Raulin, F., et al., *Prebiotic-like chemistry on Titan*. Chemical Society Reviews, 2012. **41**(16): p. 5380-5393.
2. Tobie, G., et al., *Titan's internal structure inferred from a coupled thermal-orbital model*. Icarus, 2005. **175**(2): p. 496-502.
3. Waite, J.H., Jr., et al., *The Process of Tholin Formation in Titan's Upper Atmosphere*. Science, 2007. **316**(5826): p. 870-875.
4. Coustenis, A., *Formation and Evolution of Titan's Atmosphere*, in *The Outer Planets and their Moons*, T. Encrenaz, et al., Editors. 2005, Springer Netherlands. p. 171-184.
5. Sotin, C., et al., *Observations of Titan's Northern lakes at 5 μ m: Implications for the organic cycle and geology*. Icarus, 2012. **221**(2): p. 768-786.
6. Clark, R.N., et al., *Detection and mapping of hydrocarbon deposits on Titan*. Journal of Geophysical Research: Planets, 2010. **115**(E10): p. E10005.
7. Coustenis, A., *What Cassini-Huygens has revealed about Titan*. Astronomy & Geophysics, 2007. **48**(2): p. 2.14-2.20.
8. Trainer, M.G., et al., *Organic haze on Titan and the early Earth*. Proceedings of the National Academy of Sciences, 2006. **103**(48): p. 18035-18042.

9. Feulner, G., *The faint young Sun problem*. Reviews of Geophysics, 2012. **50**(2): p. RG2006.
10. Wolf, E.T. and O.B. Toon, *Fractal Organic Hazes Provided an Ultraviolet Shield for Early Earth*. Science, 2010. **328**(5983): p. 1266-1268.
11. Kasting, J.F. and M.T. Howard, *Atmospheric composition and climate on the early Earth*. Philosophical Transactions of the Royal Society B: Biological Sciences, 2006. **361**(1474): p. 1733-1742.
12. Vuitton, V., et al., *Negative ion chemistry in Titan's upper atmosphere*. Planetary and Space Science, 2009. **57**(13): p. 1558-1572.
13. Cravens, T.E., et al., *Composition and Structure of the Ionosphere and Thermosphere*, in *Titan from Cassini-Huygens*, R. Brown, J.-P. Lebreton, and J.H. Waite, Editors. 2009, Springer Netherlands. p. 259-295.
14. Cravens, T.E., et al., *Composition of Titan's Ionosphere*. Geophys. Res. Lett., 2006. **33**: p. L07105.
15. Ferris, J., et al., *The role of photochemistry in Titan's atmospheric chemistry*. Advances in Space Research, 2005. **36**(2): p. 251-257.
16. Lunine, J. and S. Hörst, *Organic chemistry on the surface of Titan*. Rendiconti Lincei, 2011. **22**(3): p. 183-189.
17. Sittler Jr, E.C., et al., *Heavy ion formation in Titan's ionosphere: Magnetospheric introduction of free oxygen and a source of Titan's aerosols?* Planetary and Space Science, 2009. **57**(13): p. 1547-1557.
18. Delitsky, M.L. and C.P. McKay, *The photochemical products of benzene in Titan's upper atmosphere*. Icarus, 2010. **207**(1): p. 477-484.

19. Jacovi, R., et al., *Chemical composition of simulated Titan's midatmospheric aerosols*. Journal of Geophysical Research: Planets, 2010. **115**(E7): p. E07006.
20. Osborne Jr, D., P.A. Lawson, and N.G. Adams, *Flowing afterglow studies of dissociative electron-ion recombination for a series of single ring compounds at room temperature*. International Journal of Mass Spectrometry, 2011. **305**(1): p. 35-39.
21. Osborne Jr, D.S., P.A. Lawson, and N.G. Adams, *The effect of N-heteroatoms and CH₃ substituents on dissociative electron-ion recombination of protonated single six membered ring compounds at room temperature*. International Journal of Mass Spectrometry, 2011. **308**(1): p. 114-117.
22. Derenne, S., et al., *New insights into the structure and chemistry of Titan's tholins via ¹³C and ¹⁵N solid state nuclear magnetic resonance spectroscopy*. Icarus, 2012. **221**(2): p. 844-853.
23. Bernard, J.M., et al., *Reflectance spectra and chemical structure of Titan's tholins: Application to the analysis of Cassini-Huygens observations*. Icarus, 2006. **185**(1): p. 301-307.

CHAPTER 2

EXPERIMENTAL ARRANGEMENT OF THE FLOWING AFTERGLOW

2-1 BASIC INFORMATION

Experiments were carried out using the University of Georgia's Variable Temperature Flowing Afterglow equipped with an electrostatic Langmuir probe (VT-FALP). This chapter will include; (i) an overview of the Flowing Afterglow, (ii) a detailed description of the bubbler apparatus, (iii) a detailed description of the Langmuir probe's construction and operation, and (iv) an overview of how the reaction temperature is controlled and its importance in the experiments.

The Flowing Afterglow at the University of Georgia, see figure 2-1[1], is composed of a upstream ion source, a stainless steel flow tube, and a downstream detection system. The flow tube is constructed of two materials, glass and stainless steel (stainless steel alloy 316L). The upstream portion of the flow tube is constructed out of a borosilicate glass custom made in the UGA glass shop. This glass portion of the flow tube is connected to a stainless steel bellows which allows the flow tube to expand and contract with changes in temperature. The remaining portion of the flow tube is a stainless steel pipe. This flow tube is ~1 meter in length overall, with a diameter of 7.3 cm. Along the length of the flow tube there are eight reaction ports (RP) which allow the introduction of gases into the system. At the end of the flow tube is an Extrel quadrupole mass filter with a discrete dynode electron multiplier (ETP type AF566).

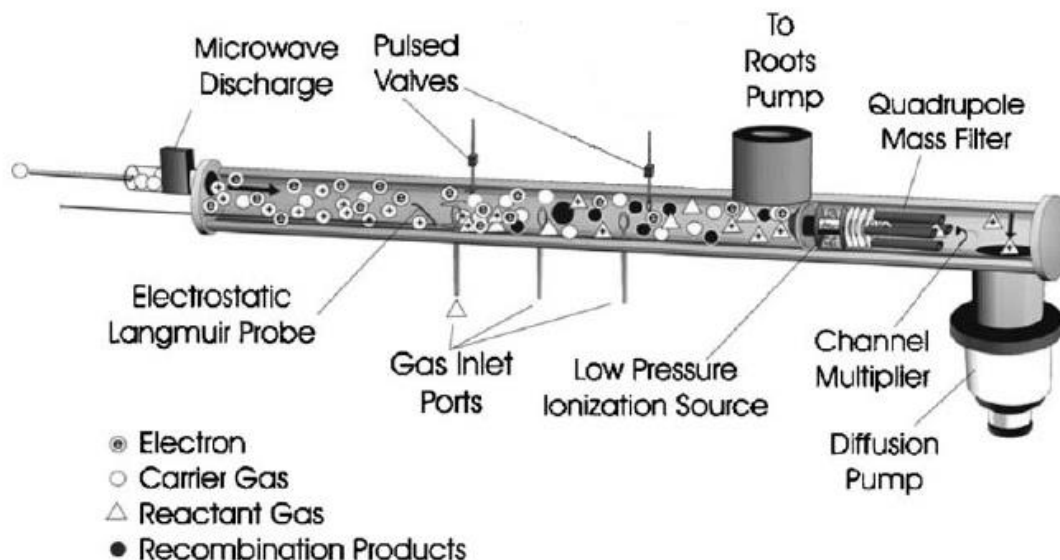


Fig. 2-1: A schematic diagram of the Flowing Afterglow apparatus (FALP) located at the University of Georgia. The temperature variable facility has been omitted for clarity. Parts are labeled.²

In this part of the experiment, plasma is created upstream, in the glass portion of the flow tube, by the ionization of the helium carrier gas in a microwave discharge source (Ophos MPG-4M 393). The helium gas (Airgas grade UHP helium) is purified before ionization by passage through two traps filled with a 30%/70% mixture of the molecular sieves 13X and 5A respectively. To further remove contaminants from the helium, the two traps are cooled to 77K by liquid nitrogen. Two ports are allocated for the introduction of the helium carrier gas into the flow tube, RP 1 and RP 2A. RP 1 is rarely used, while RP 2A was used in all experiments conducted in this study. RP 2A allows the helium, following purification by liquid nitrogen, to flow through a stainless steel 1/4" diameter tubing along the length of the flow tube to equilibrate the temperature to that of the flow tube. This port is also equipped with a specialized glass tube which is

² Reprinted from [1] with permission. Copyright 2006 by Elsevier. Full text article can be found at <http://www.sciencedirect.com/science/article/pii/S0370157306001463>.

positioned inside of the main glass flow tube. This tube transports the helium upstream and then undergoes a 180° bend downstream. Following this bend, the helium is injected into the flow tube. At the point of helium injection, a plasma is produced by microwave ionization. By adjusting the position of the microwave cavity upstream or downstream of RP 2A, it is possible to vary the upstream plasma density between 10^8 and 10^{11} cm^{-3} . In most experiments, a maximum plasma density was desired and the microwave cavity was positioned to create a plasma density of 10^{11} cm^{-3} .

Following creation of a helium plasma (He^+ , $\text{He}_{\text{metastables}}$, and He_2^+ with electrons, see equation (1)), argon (National Welders grade UHP) is introduced through RP 2B. RP 2B is located ~22cm downstream from the point of ionization. Similar to RP 2A, RP 2B is constructed of stainless steel tubing which runs the length of the flow tube allowing the temperature of the argon to become equilibrated before its introduction into the flow tube. Following the introduction of argon, the helium ions and helium metastables react with the argon creating an Ar^+/e^- plasma, see reaction (2 and 3). The complete ionization scheme for a standard hydrocarbon ion study is given in reactions 1 to 7.



The reaction of helium metastables with argon creates not only Ar^+ , but more electrons further increasing the electron density within the plasma by reaction (3). Hydrogen is then introduced through RP 4, so that the Hydrogen reacts with the Ar^+ to form an H_3^+/e^- plasma, reactions (4) and (5). Following the creation of a H_3^+/e^- plasma either a secondary gas is added to make another type of plasma or the reactant gas is added. In the cases where the desired ion cannot be produced, in reaction (6), due to fragmentation upon proton transfer from H_3^+ , another protonated species must be used to create a (softer) less exothermic proton transfer. In these cases, a secondary gas such as N_2 , CO, or benzene vapor (C_6H_6) is introduced into the system via RP 5 upstream of the reactant gas to create N_2H^+ , HCO^+ , or C_6H_7^+ respectively. Once the “softer” plasma is created, the reactant gas (RV) is introduced via RP 6, and created by the reaction sequence in equations 8 and 9. Note nitrogen used in equations 8 creates a less energetic proton transfer.



Following reaction (9), RVH^+ undergoes recombination as shown in reaction (7).

2-2 REACTANT GAS SYSTEMS AND BUBBLER APPARATUS

2-2a OVERVIEW

Reactant gases, (RV), are introduced into the Flowing Afterglow with a measured flow through one of four reactant gas systems. These systems are composed of stainless steel tubing (stainless alloy 316, of two sizes used 1/16” OD and 1/4” OD) which connect to the various reactant ports along the flow tube, see Fig. 2-2. These systems allow the user to input a reactant gas (RV) through one of the four ports along the flow tube and at

a controlled and measured flow. The flow is controlled by a Granville-Phillips 216 Pressure and Flow Controller which regulates the flow by opening and closing a valve driven by a servo motor. One reactant gas system is used solely for the introduction of hydrogen (Airgas grade UHP hydrogen). The remaining three systems are available for introduction of reactant gases. When a “softer” proton transfer is needed, system 1 is used to introduce the secondary gas into the system. The remaining two systems, systems 3 and 4, are used for the introduction of various molecules into the flow tube (these are the hydrocarbons included in this study). System 3 was used primarily for the introduction of gaseous mixtures of hydrocarbons with helium, where system 4 was used in combination with the bubbler apparatus to introduce hydrocarbons into the flow tube.

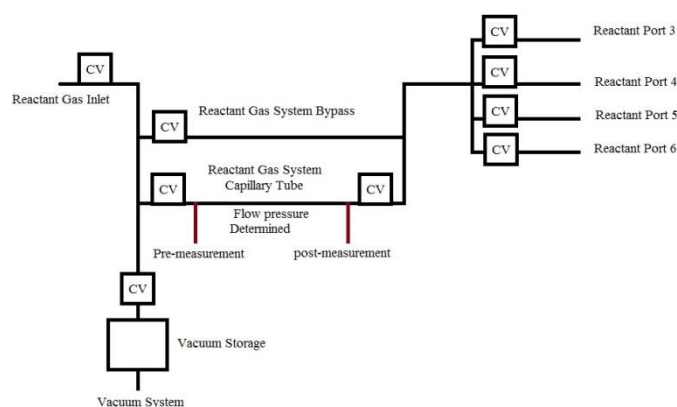


Fig 2-2: A schematic of the flow control systems for the Reactant Gas Systems 1-4. This schematic illustrates how a reactant gas is distributed to a reactant ports. The capillary tube, which is used to calculate the density of the reactant gas flowing into the system, is labeled with the pre and post stages of pressure measurement also labeled. The closer values in the system are labeled as the black boxes with “CV” inside them.

2-2b INTRODUCTION OF HYDROCARBONS WITH HIGH VAPOR

PRESSURE

The hydrocarbon species studied in this dissertation were introduced into the system either as a gaseous mixture with helium or through the action of the bubbler

apparatus. For hydrocarbon species, where mixtures were used, these mixtures were made by using the neat vapor from a pure sample of the hydrocarbon which had been purified by the pump/freezing method. This method of pumping on the sample and then freezing it with liquid nitrogen; drives off any dissolved gases that may contaminate the sample. This process is usually repeated a few times to ensure that all the dissolved gases are removed. Once the dissolved gases are removed, the neat vapor is taken off the sample to create a mix of ~1% of the hydrocarbon in helium (Airgas grade UPC helium). The creation of a mixture with the neat vapor of hydrocarbons in this way requires the hydrocarbon to have a significant vapor pressure at room temperature (usually the vapor pressure must be above 5 mmHg (torr) at room temperature). Following the production of the hydrocarbon/helium mixture, the mixture is allowed to sit for ~24 hours to ensure complete diffusive mixing. Then, the mixture is introduced into the flow tube through system 3. System 3 allows the user to maintain a constant flow of the mixture into the flow tube. In cases where the hydrocarbons species did not have significant vapor pressure to make a mixture, a bubbler apparatus was used to introduce the hydrocarbon into the flow tube.

2-2c LIQUID HYDROCARBON SAMPLES AND THE BUBBLER

APPARATUS

This apparatus consists of a sample reservoir into which a glass tube allows helium to bubble through a liquid hydrocarbon sample, see Fig 2-3. Before helium was passed through the liquid, a vacuum was applied to the hydrocarbon sample and the sample was frozen with liquid nitrogen (the pump/freeze method). Following freezing, the sample was allowed to melt under vacuum.

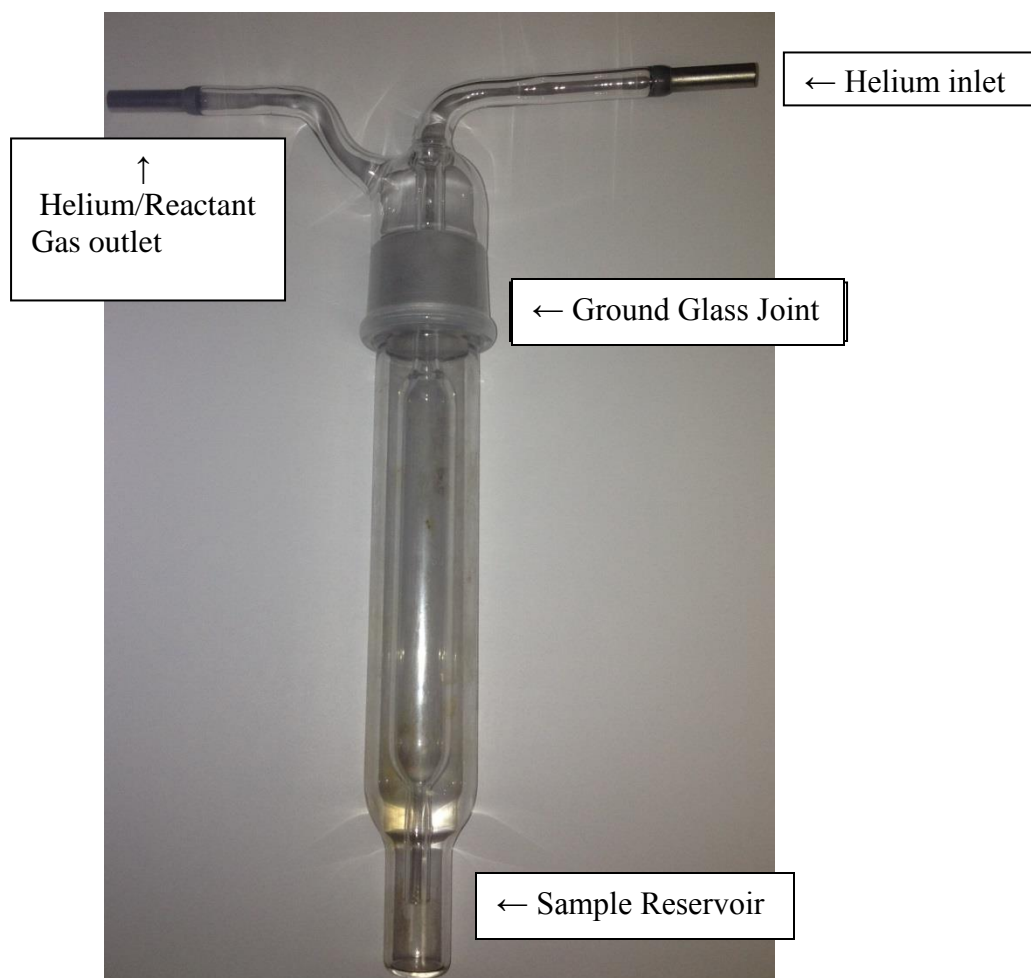


Fig. 2-3: The empty bubbler apparatus prior to connection to the system. The Helium inlet, sample reservoir, ground glass joint and flow outlet have been labeled.

Once the sample reached room temperature, a flow of helium is bubbled through the hydrocarbon sample carrying it into the flow tube. In experiments where the hydrocarbon to be studied was a liquid with a smaller vapor pressure (less than 5 torr at 300K), the exit tubing connecting the output flow of the bubbler to the system was slightly heated. This heating was needed to insure that the sample vapor did not condense on the walls of the tubing.

2-2d SOLID HYDROCARBON SAMPLES AND THE BUBBLER

APPARATUS

In cases where the hydrocarbon was solid at room temperature, a finely ground sample was placed in the bubbler sample reservoir. A vacuum was then applied to the reservoir to remove any contaminants and any atmospheric gases that may be in the sample reservoir. Following this, helium was passed through the solid sample carrying hydrocarbon vapor into the flow tube. A piece of Pyrex glass wool was put into the top of the sample reservoir to keep any small grains of the hydrocarbon “dust” from being blown into the tubing by the helium gas. As before, the stainless steel exit tubing of the bubbler was heated slightly to reduce condensation.

The sample reservoir is connected to the bubbler apparatus by a ground glass joint. This glass joint also acts as a safety valve. In cases where the helium pressure within the bubbler increases due to clogged lines, the joint can separate, venting the excess helium. This venting of excess helium pressure keeps the apparatus from being destroyed. The bubbler apparatus was successful in getting many compounds into the flow tube which it was not previously possible to study. Success was possible for almost all hydrocarbon compounds, which had a vapor pressure greater than 0.1 torr at room temperature.

2-3 LANGMUIR PROBE OPERATION AND DETERMINATION OF E-IDR RATE CONSTANTS

Once the hydrocarbon reactant gas had been introduced into the flow tube and the protonated form produced, the species can then undergo recombination with free electrons in the plasma, as in reactions 7 or 9. The axial Langmuir probe allows the

measurement of the rate of electron depletion within the plasma. The Langmuir probe is a thin piece of tungsten wire, 50 microns in diameter and is between 5 and 8 mm long; this configuration of probe length and plasma ion density is called the electron orbital limited region determining electron density, $[e]$ [2]. In this configuration a positive potential on the probe draws in the surrounding electrons and the plot of I^2 vs. Applied voltage, V_p , is linear[2]. The tungsten wire is held in the center of a piece of small diameter glass tubing (known as the probe assembly) which holds the tungsten wire in the center of the flow tube, see Fig. 2-4.

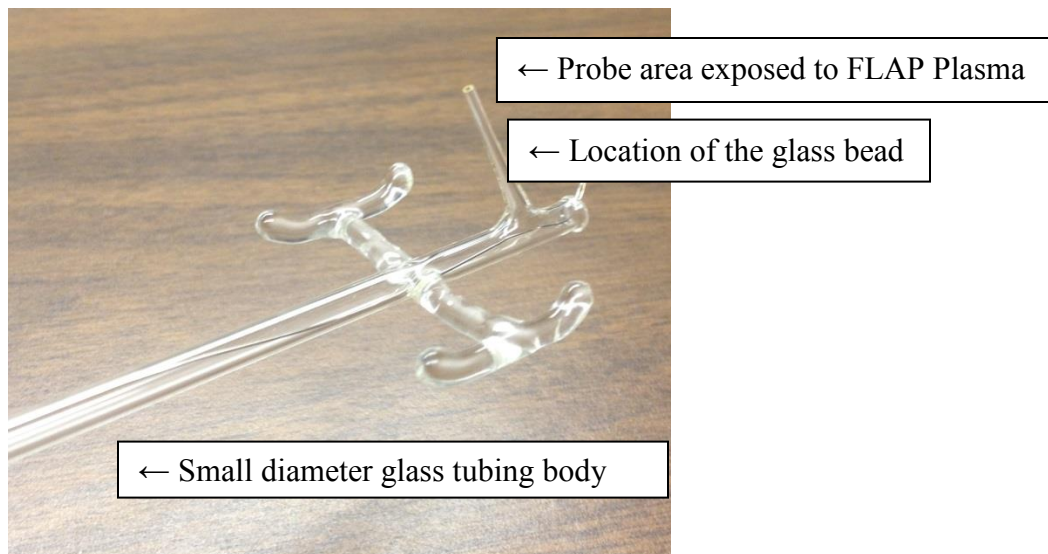


Fig. 2-4: The downstream half of the glass probe assembly which holds the tungsten probe. The area of the probe exposed to the FALP plasma is labeled and the location of the glass bead, which holds the probe in place, is also labeled. Note that due to the small diameter of the tungsten wire, it does not show up in the picture, also due to the length of the probe assembly (~58 inc.) two pictures were needed to show detail.

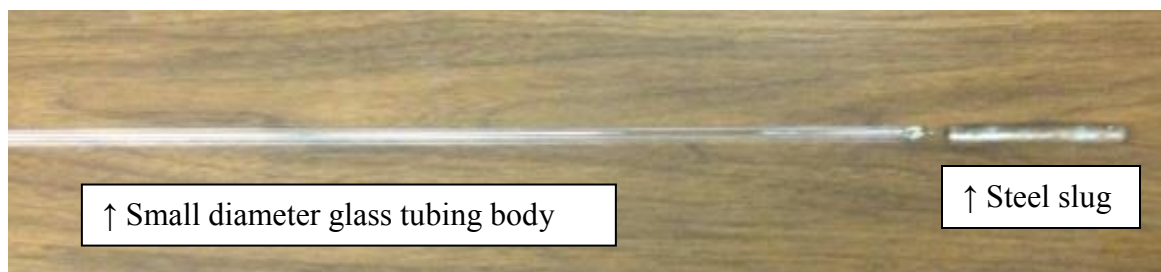


Fig. 2-5: The upstream end of the probe assembly. The small diameter glass tube and the steel slug are labeled. The slug serves as the upstream connection to the computer via a metal track, not pictured. A thin nickel (0.05mm diameter) wire is insulated from the plasma by the thin glass tubing of the probe assembly and serves as the connection between the metal slug and the tungsten probe.

The tungsten wire has a small glass bead attached to it which serves to hold the probe in the center of the flow tube. The probe assembly is composed of a long glass tube which has an iron slug attached, Fig. 2-5. The probe assembly insulates the probe from the plasma and keeps it located in the center of the plasma. The iron slug allows the user to adjust the position of the probe location along the length of the flow tube with the use of a magnet. The iron slug also acts as a point of contact for voltage application and current measurement to the probe. A voltage, between 0.5-1.5 volts DC, is applied to the probe and is also applied by a computer. The current of electrons to the probe (which has a positive voltage applied to it for attracting electrons) is converted into a voltage with a resistor. This voltage is then amplified by an isolation amplifier and transferred to the computer, see schematic of probe circuit in Fig. 2-6. Using the equation below, the electron flux can be determined by the computer^[2],

$$[e^-] = \sqrt{\frac{m \cdot \pi^2 \cdot M_e}{2 \cdot a^2 \cdot e^3}} \quad (11)$$

In this expression the measured slope, m , is obtained from the plot of I^2 (current squared) vs V_p (applied voltage). The term a , represents the area of the cylindrical tungsten probe (this cylindrical area is determined by $2\pi rh$, where r is the radius of the tungsten probe sheath and h is the length.). M_e and e are the mass of an electron and the charge of an electron respectively. From the measurement of the electron density, the computer program can determine the slope from a plot of I^2 vs V_p . Using the electron-Ion

Dissociative Recombination (e-IDR) expression, reaction 12, it is possible to write an equation in which the electron density is expressed, see equation 13.



$$\frac{d[s^-]}{dt} = -\alpha_s [X^+][e^-] \quad (13)$$

$$\frac{d[s^-]}{dt} = -\alpha_s [e^-]^2 \quad (14)$$

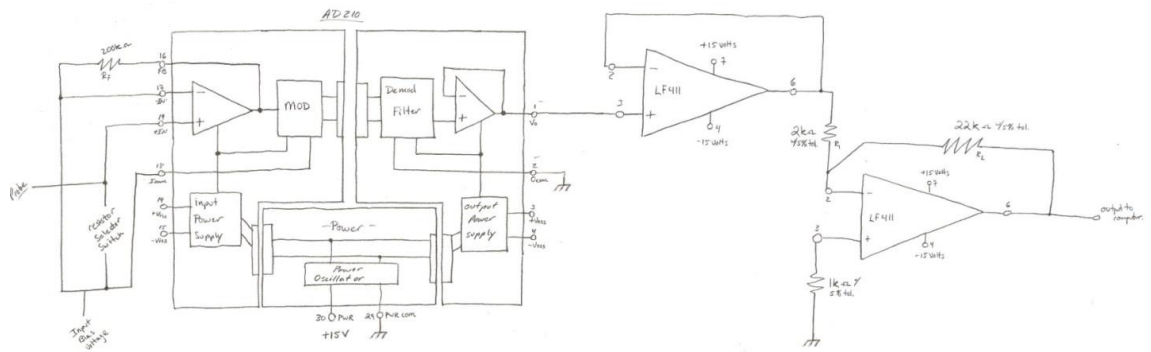


Fig. 2-6: A schematic of the Langmuir probe circuit diagram for the University of Georgia Flowing Afterglow (FALP). The schematic shows connections to the probe, computer input bias voltage (voltage applied to the probe to attract electrons), and the output voltage to the computer. The resistor selector switch in the schematic allows the user to select the correct resistor for plasma conditions. Pin connection numbers and labels have been attached to the appropriate locations for both the LF411 and AD 210 chips.

Since the Flowing Afterglow creates a quasi-neutral plasma, the electron density is equal to the ion density. This leads to the formation of equation 14. Integration then yields the following.

$$-\frac{1}{[s^-]} = -\alpha_s t + C \quad (15)$$

Where C, is the constant of integration. For time zero, $t=0$, where $[e^-]=[e^-]_0$, equation 16 is the value for the constant of integration.

$$-\frac{1}{[s^-]_0} = C \quad (16)$$

By substituting equation 16 into equation 15 and rearranging terms, it is possible to create equation 17.

$$-\frac{1}{[e^-]} + \frac{1}{[e^-]_0} = -\alpha_e t \quad (17)$$

Dividing both sides of equation 17 by -1 creates equation 18.

$$\frac{1}{[e^-]} - \frac{1}{[e^-]_0} = \alpha_e t \quad (18)$$

With replacement of time by terms for the velocity of the plasma, V_{plasma} , and the probe's position along the flow tube, z , it is possible to create equation 19, the e-IDR expression.

$$\frac{1}{[e^-]} - \frac{1}{[e^-]_0} = \frac{\alpha_e z}{V_{\text{plasma}}} \quad (19)$$

With the determination of electron densities from plots of I^2 vs V_p , the e-IDR rate constant, α_e , can be determined from a plot of $1/[e^-]$ vs z . An example of this plot is seen in Fig. 2-7[3].

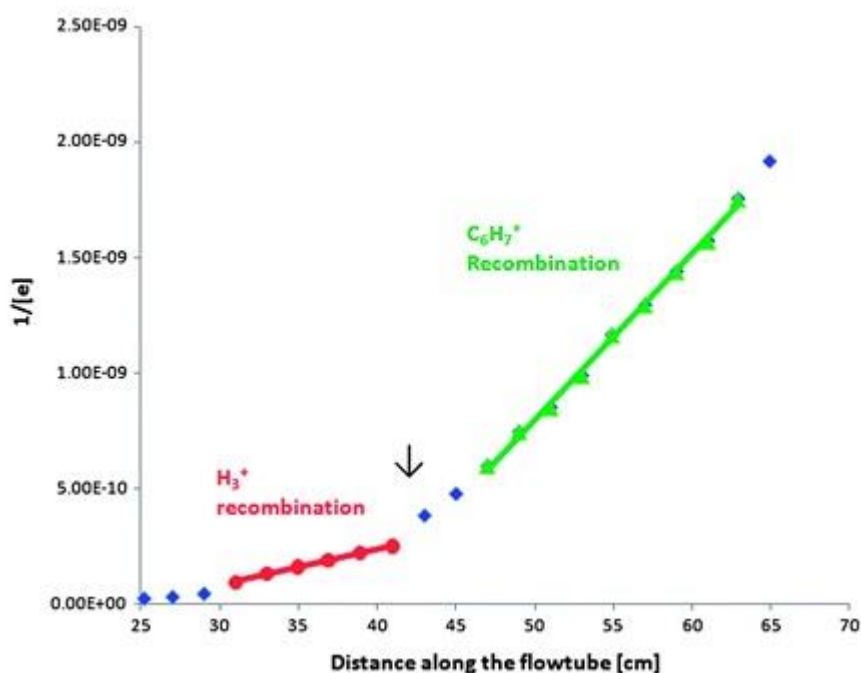


Fig. 2-7: Plot of reciprocal electron density, $1/[e^-]$, and function of flow tube distance, z . The various regions of the plasma along the length of the flow tube are labeled. The plasma region of H_3^+ , is labeled in red. The black arrow represents the introduction of benzene vapor into the plasma. This introduction is followed by a region of proton transfer (the unlabeled two blue dots represent measurements of electron density during this period) before the green labeled region of protonated benzene ($C_6H_7^+$) recombination. The slope of the green line yields the e-IDR rate constant for protonated benzene. Following the recombination of protonated benzene, we see electron loss due to ambipolar diffusion to the walls, which occurs at about 65cm down the flow tube.³

2-4 TEMPERATURE CONTROL

Temperature dependence data are obtained by measuring the e-IDR rate constants at a series of different temperatures. The flow tube can be cooled by the passage of liquid nitrogen through a series of 3/8 copper tubes attached to the outside of the flow tube (known as the copper jacket). The use of liquid nitrogen allows the system to be cooled down to a 77K. Temperatures between 77K and 300K can be obtained and maintained through the pulsed pumping of liquid nitrogen through the copper tubing. The flow tube

³ Reproduced from [3] with permission from The Royal Society of Chemistry.

can be heated resistively through 10 Watlow firesticks. Six 300 watt and four 200 watt firesticks are attached to the flow tube's copper jacket. These heaters have a maximum temperature of 700K, and are controlled by use of Variac power supplies. While it is possible to obtain a flow tube temperature of 700K, at such a high temperature the O-rings sealing the detection system would fail. The O-rings on the flowing afterglow are only able to withstand temperatures of 600K; for this reason the maximum temperature which reactions are studied is 550K. The flow tube temperature is monitored through the use of six type K thermocouples. These thermocouples are evenly spaced along the flow tube. To determine the flow tube temperature an average of these measured temperatures is used. With the use of firestick heaters or liquid nitrogen cooling it is possible to maintain the flow tube temperature to within $\pm 5\text{K}$ during the course of a 30 minute measurement at any temperature between 77K and 550K. To further isolate the flow tube, there is a vacuum vessel around it. This vessel permits the creation of a vacuum (a vacuum of 10^{-6} torr is held inside the vacuum vessel) between the flow tube and the outside atmosphere. This vacuum layer greatly reduces the convective heat transfer to and from the flow tube. A layer of aluminum shielding covers the flow tube, further reducing the amount of radiative heat transfer between the flow tube and the surroundings.

2-5 TEMPERATURE DEPENDENT PATHWAYS

When electrons collide with the protonated hydrocarbon molecules, two mechanisms are possible for recombination; the direct mechanism and the indirect mechanism[[1](#), [4](#)]. In the direct mechanism, the neutralized ion undergoes a direct transition to a repulsive potential curve, as illustrated by equation 20[[1](#)].



This has been investigated by Bates[5] and shows a $T_e^{-0.5}$ dependence on electron temperature. In the indirect mechanism, the neutralized ion undergoes a radiationless transition to high lying Rydberg state and then to a repulsive potential curve available only in the Rydberg state, illustrated by equation 21[1]. Here, Bardsley showed that the electron temperature dependence was $T_e^{-1.5}$ [1]. For large molecules, such as hydrocarbons, there are many curve crossings available allowing the direct and indirect mechanisms to both occur simultaneously and interfere with each other. This interference causes the measured electron temperature dependence to be between $T_e^{-0.5}$ and $T_e^{-1.5}$, showing that both pathways are accessed[6]. It should be noted that, in a flowing afterglow, the temperatures of the ions and electrons are equal due to thermalization in collisions with the helium buffer gas. The helium buffer gas is thermalized through collisions with the flow tube walls. The temperature dependence of the hydrocarbon ion can be determined by plotting the measured e-IDR rate constant vs. measurement temperature, illustrated in Fig. 2-8. By determining the e-IDR rate constant over a series of temperatures it is possible to determine the mechanism by which dissociative recombination is occurring. These data will help in the understanding of trends between hydrocarbon species.

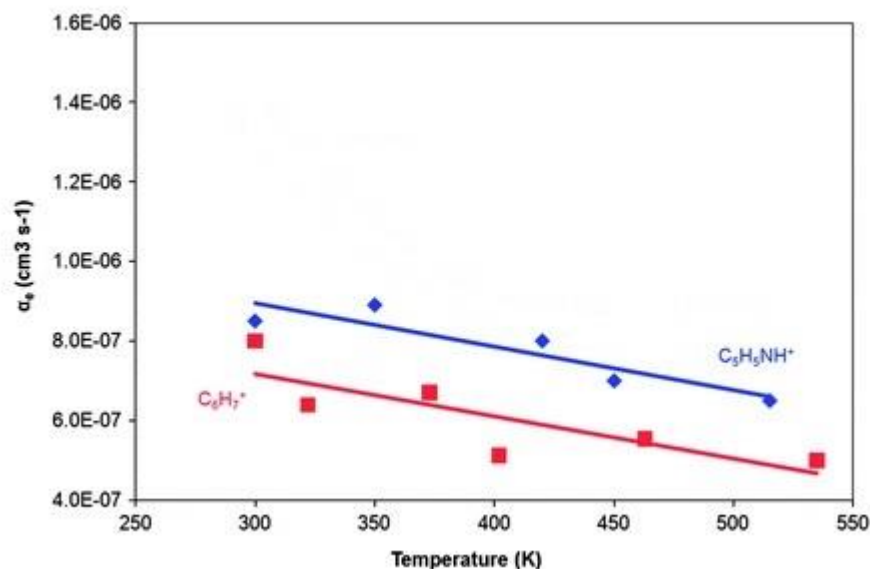


Fig. 2-8: A plot of the e-IDR rate constants, α_e , verse temperature for protonated benzene ($C_6H_7^+$) and pyridine ($C_5H_5NH^+$) from 300K to ~550K.⁴

2-6 REFERENCES

1. Florescu-Mitchell, A.I. and J.B.A. Mitchell, *Dissociative recombination*. Physics Reports, 2006. **430**(5–6): p. 277-374.
2. Goodall, C.V. and D. Smith, *A comparison of the methods of determining electron densities in afterglow plasmas from langmuir probe characteristics*. Plasma Physics, 1968. **10**(3): p. 249.
3. Adams, N.G., L.D. Mathews, and D.S. Osborne, *Laboratory Chemistry Relevant to Understanding and Modeling the Ionosphere of Titan*. Farad. Disc., 2010. **147**: p. 1-323-335.
4. Mitchell, J.B.A. and C. Rebrion-Rowe, *The recombination of electrons with complex molecular ions*. International Reviews in Physical Chemistry, 1997. **16**(2): p. 201-213.

⁴ Reproduced from [3] with permission from The Royal Society of Chemistry.

5. Bates, D.R., *Dissociative Recombination*. Phys. Rev., 1950. **78**: p. 492-493.
6. Larsson, M., *Dissociative recombination of molecular ions*. 2008: Cambridge University Press.

CHAPTER 3

FLOWING AFTERGLOW STUDIES OF DISSOCIATIVE ELECTRON-ION
RECOMBINATION FOR A SERIES OF SINGLE RING COMPOUNDS AT ROOM
TEMPERATURE⁵

⁵ D.S. Osborne Jr., P. A. Lawson, and N.G. Adams. 2011. International Journal of Mass Spectrometry. 305:35-39. Reprinted here with permission of the publisher.

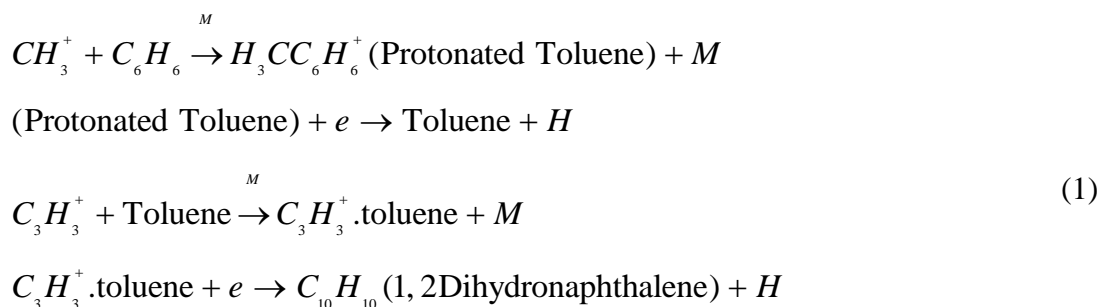
3-1 ABSTRACT

A series of dissociative electron-ion recombination reactions has been studied at room temperature using a Flowing Afterglow with Langmuir Probe (FALP) to determine the rate constants. Studied species include protonated five and six membered single rings with the heteroatoms, N, O and S and with or without CH_3 substituent groups attached to the rings. The compounds studied are protonated benzene, C_6H_7^+ ; toluene, $\text{C}_6\text{H}_5\text{CH}_4^+$; pyridine, $\text{C}_5\text{H}_5\text{NH}^+$; pyrimidine, $\text{C}_4\text{H}_4\text{N}_2\text{H}^+$; 4-picoline, $\text{C}_6\text{H}_7\text{NH}^+$; cyclohexane, $\text{C}_6\text{H}_{13}^+$; 1,4 dioxane, $\text{C}_4\text{H}_8\text{O}_2\text{H}^+$ all six membered rings (all but the last two have π electrons in the ring) with furan, $\text{C}_4\text{H}_4\text{OH}^+$; pyrrole, $\text{C}_4\text{H}_5\text{NH}^+$; 1-methylpyrrole, $\text{C}_5\text{H}_7\text{NH}^+$; thiophene, $\text{C}_4\text{H}_4\text{SH}^+$ and pyrrolidine, $\text{C}_4\text{H}_9\text{NH}^+$ all five membered rings (with only the last mentioned having no π electrons in the ring). Comparison is made with literature data on some of the multi-ring systems (PAH's and PANH's). The involvement of π electrons in the rings is discussed. Protonated six membered rings have been shown to recombine ~2 times faster than five membered rings with the exception of 1, 4, dioxane which has no π electrons. The situation is very different for the proton bound dimers, where five membered rings recombine somewhat more rapidly than six membered rings, again with 1, 4, dioxane behaving very differently. These data are critically important in chemically modeling the Titan ionosphere which is presently being probed by apparatus onboard the Cassini spacecraft.

3-2 INTRODUCTION

Interest has increased in the electron-ion dissociative recombination (DR) of protonated single ring compounds since their discovery in the interstellar medium, ISM, (C_6H_6 , benzene)[[1](#)] and the atmosphere of Titan (C_6H_6 , benzene; $\text{C}_5\text{H}_5\text{N}$, pyridine; C_7H_8 ,

toluene).[2-4] In particular, an enormous amount of detail on the atmosphere of Titan has been obtained by the highly successful Cassini space probe using the on board positive ion-neutral mass spectrometer (INMS) with a mass range from 1 to 99 amu and better than 1 amu mass resolution. The Cassini plasma spectrometer (CAPS) has detected positive ions up to 350 amu and negative ions from 20 to 8,000 amu.[5] Some of these positive ions have been tentatively identified as naphthalene, anthracene derivatives and an anthracene dimer.[2] In these regions, polycyclic aromatic hydrocarbons (PAH's) and polycyclic aromatic nitrogen heterocycles (PANH's) have also been detected as the unidentified infrared bands and diffuse interstellar bands in the ism,[6, 7] and surprisingly as negative ions in the Titan atmosphere.[2] In the latter atmosphere, they are believed to be precursors for aerosol and tholin formation. For Titan, it has recently been suggested that sequential ion-molecule associations of ring compounds with the dominant ions (CH_3^+ , C_3H_3^+ , etc.) followed by dissociative electron-ion recombination would provide a route to building of multi-ring compounds from the observed, and likely, single rings.[8] For example, $\text{CH}_3^+ + \text{C}_6\text{H}_6$ (benzene) leads to an association compound with the composition of protonated toluene ($\text{C}_6\text{H}_5\text{CH}_4^+$). After recombination, the $\text{C}_3\text{H}_3^+ + \text{C}_6\text{H}_5\text{CH}_3$ (toluene) reaction could lead to the protonated 1, 2 dihydronaphthalene ($\text{C}_{10}\text{H}_{11}^+$)(double ring). See equation (1).



Note that associations with CH_3^+ followed by recombinations may also lead eventually to 1, 2 dihydronaphthalene.[8] The recombination of these compounds also helps to maintain the ionization balance in the ISM and the Titan atmosphere. In addition, in the association of these species with CH_3^+ , it has been shown that the association component of the reaction mechanism is dependent on the presence or absence of π electrons in the rings[8]. It is of interest to pursue the recombination studies to determine whether recombination also exhibits a dependence on the presence of π electrons. Note that since the Titan atmosphere is mostly N_2 (98%), heterocyclic rings incorporating N-atoms are likely to be an important component of the atmosphere. Few oxygen containing compounds have been observed in the Titan atmosphere (CO , CO_2 , O)[9] so oxygen atoms in the ring are unlikely to be important there although they may be important in the ISM where more oxygen containing species exist. As a contribution to an understanding of the chemistry of these regions, we have studied the dissociative electron-ion recombinations of the protonated six membered rings benzene, C_6H_7^+ ; toluene, $\text{C}_6\text{H}_5\text{CH}_4^+$; pyridine, $\text{C}_5\text{H}_5\text{NH}^+$; pyrimidine, $\text{C}_4\text{H}_4\text{N}_2\text{H}^+$; 4-picoline, $\text{C}_6\text{H}_7\text{NH}^+$; 1,4 dioxane, $\text{C}_4\text{H}_8\text{O}_2\text{H}^+$; cyclohexane, $\text{C}_6\text{H}_{13}^+$ and the five membered rings, furan, $\text{C}_4\text{H}_4\text{OH}^+$; pyrrole, $\text{C}_4\text{H}_5\text{NH}^+$, n-methylpyrrole, $\text{C}_5\text{H}_7\text{NH}^+$; pyrrolidine, $\text{C}_4\text{H}_9\text{NH}^+$ and thiophene, $\text{C}_4\text{H}_4\text{SH}^+$. Note that 1, 4 dioxane, cyclohexane and pyrrolidine have no π electrons. Recombinations of a few single ring hydrocarbons have been studied previously C_4H_5^+ , 53 amu; C_6H_6^+ (benzene), 78 amu; $\text{C}_6\text{H}_5\text{CH}_3^+$ (toluene), 92 amu; and the seven membered rings benzylium $^+$, 91amu; tropylium $^+$, 91amu; and cycloheptatriene $^+$, 92amu)[10, 11] and there have been some studies with multi-ring systems (e.g., $\text{C}_{14}\text{H}_{10}^+$, anthracene ions).[12] No theoretical calculations of recombination have been made for

ions of this complexity. In the course of our recombination studies[8], and following previous work with CN containing ions,[13, 14] it has been found that association between the protonated reactant vapor [RV] can be competitive with recombination.



This has complicated the studies since the recombination rate constants, α_e , can now vary with the RV concentration and, thus, the composition of the associating gas. Thus, it is essential to determine this variation and identify the reactant vapor concentrations where α_e is independent of the concentration and where single species such as RVH^+ or $(\text{RV})_2\text{H}^+$, dominate the chemistry. This has enabled the recombination of proton bound dimers to be studied in addition to the protonated species. Note that plasma situations cannot always be created where only a single recombining species exists. In such cases the individual α_e were determined through chemical modeling, see figure 3b.

3-3 EXPERIMENTAL

These studies were carried out in a temperature variable flowing afterglow, which has been discussed in detail previously,[15] and, thus, only a brief description will be given here. Helium carrier gas (Airgas UHP grade He) (with throughput 220 Torr l s⁻¹ and pressure 1.5 Torr) is ionized in a microwave cavity and flowed along a flow tube (8 cm dia.; 1 m in length) to a downstream mass spectrometer/electron multiplier under the action of a Roots blower pump. The electron density, [e], in the flowing plasma is determined by an electrostatic Langmuir probe operated in the orbital limited regime.[16] Gases (Ar and H₂) are added upstream sequentially into the flow to create Ar⁺/e and H₃⁺/e plasmas. Downstream of these additions, the reactant vapor (RV) is introduced into the flow to produce the protonated ion of interest by proton transfer from H₃⁺ (reaction 3)

and the proton bound dimer by the association reaction (2) thus, generating the recombining plasmas of interest.



Note that where there is a large difference between the proton affinities of the two neutral species the proton transfer reaction will be very exothermic and can result in fragmentation of the product ion. Where this occurs, an additional step is made in the chemistry to include an additional proton transfer

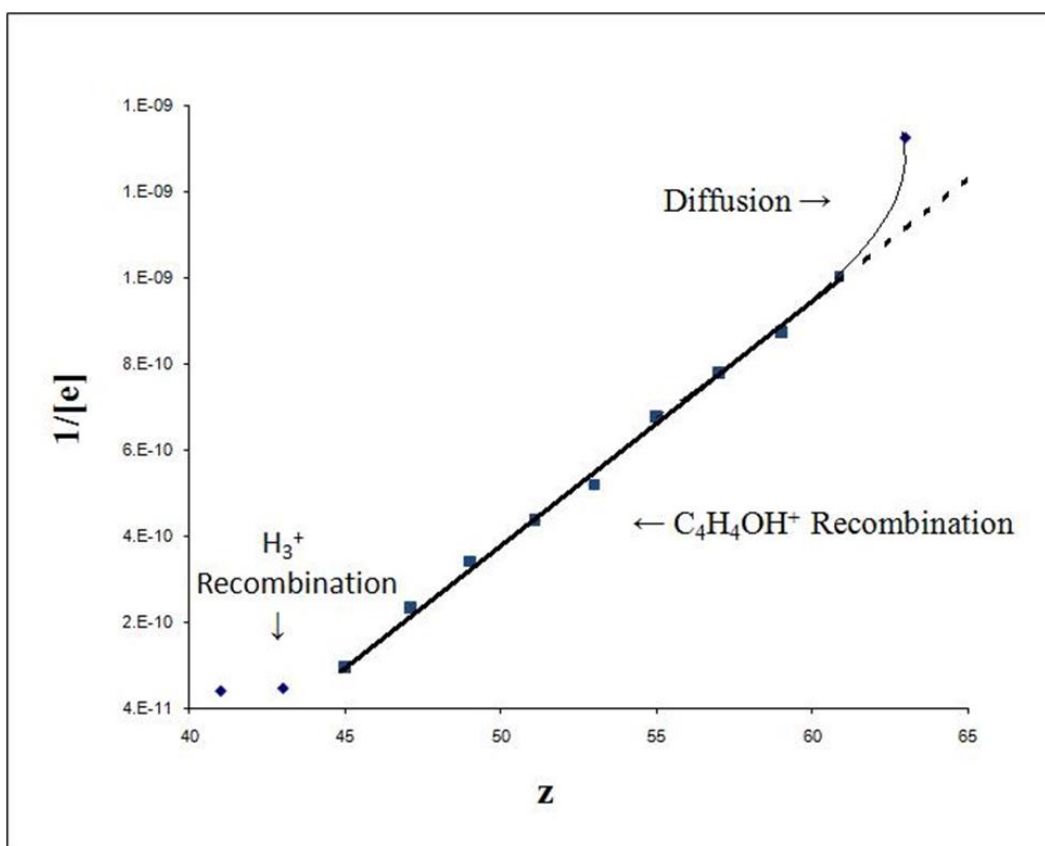


Fig. 3-1. Variation of $1/[e]$ versus distance, z , along the flow for the electron ion recombination of protonated furan at 300K.

from N_2H^+ , HCO^+ or C_6H_7^+ so that the final proton transfer to produce RVH^+ is less exothermic and does not cause fragmentation. This method of proton transfer was utilized for the two ringed compounds cyclohexane and pyrrolidine. The electron density is

observed to reduce along the flow tube as measured by the axially movable Langmuir probe. In this recombination controlled situation, $[e]$ varies with distance, z , as seen in Fig. 3-1 and given by the equation

$$[e]^{-1} - [e]_0^{-1} = \alpha_e z / v_p \quad (4)$$

where α_e is the recombination rate constant, and v_p is the plasma velocity along the flow tube. Recombination rate constants, α_e , for this system are determined as a function of concentration $[RV]$ and yield schematic plots of the form shown in Fig. 3-2 through Fig. 3-4. Fig. 3-2 illustrates plateau regions where

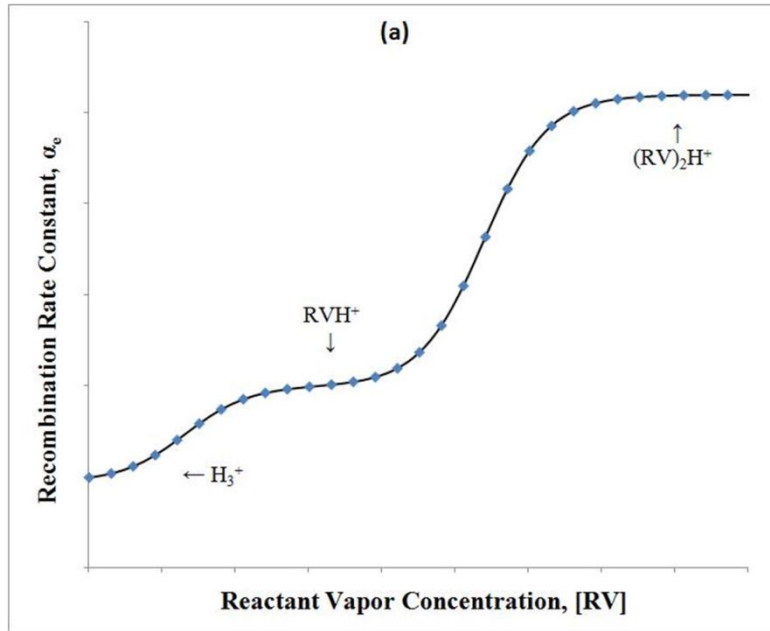


Fig. 3-2. Schematic of the variation of α_e with reactant vapor concentration, $[RV]$, showing the regions where H_3^+ , RVH^+ or $(RV)_2H^+$ dominate the recombination. (a) Plateaus in recombination for RVH^+ and $(RV)_2H^+$ with $\alpha_e(RVH^+) < \alpha_e((RV)_2H^+)$ and asymptotic approach to H_3^+ recombination at low reactant vapor concentrations

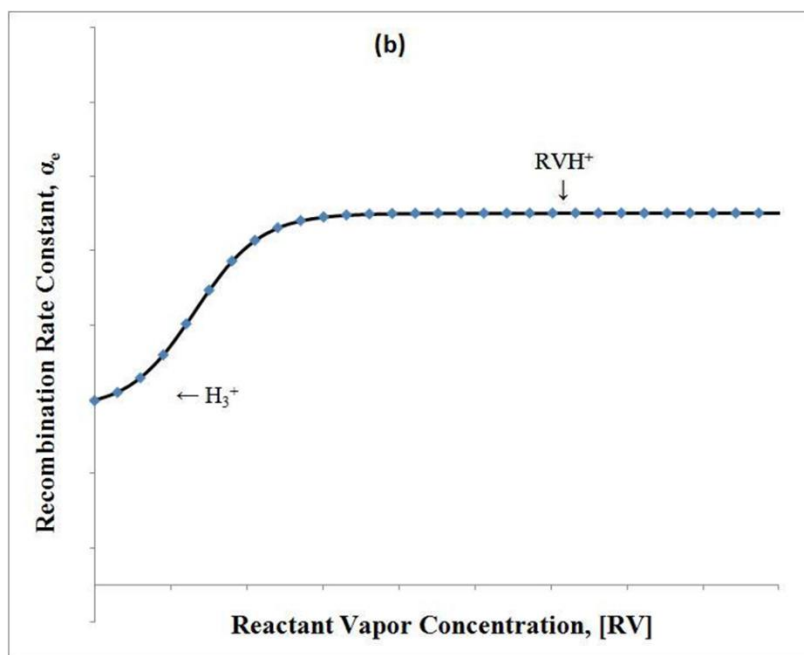


Fig. 3-3. Schematic of the variation of α_e with reactant vapor concentration, $[RV]$, showing the regions where H_3^+ , RVH^+ or $(RV)_2H^+$ dominate the recombination. (b) Plateau in recombination for RVH^+ with no production of $(RV)_2H^+$ and an asymptotic approach to H_3^+ recombination at low reactant vapor concentrations.

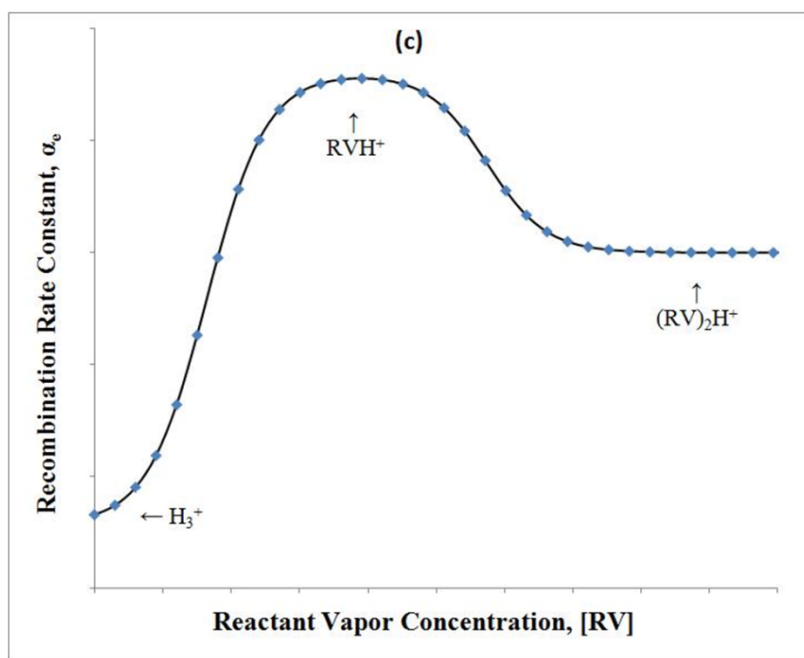


Fig. 3-4. Schematic of the variation of α_e with reactant vapor concentration, $[RV]$, showing the regions where H_3^+ , RVH^+ or $(RV)_2H^+$ dominate the recombination. (c)

Plateaus in recombination for RVH^+ and $(\text{RV})_2\text{H}^+$ with $\alpha_e(\text{RVH}^+) > \alpha_e((\text{RV})_2\text{H}^+)$ and asymptotic approach to H_3^+ recombination at low reactant vapor concentrations

H_3^+ , RVH^+ and $(\text{RV})_2\text{H}^+$ are the recombining ions at the various RV concentrations.

Obviously, it can be seen that without such a plot it is likely that erroneous rate constants would easily be obtained. An example for the 4-picoline system is shown in Fig 3-5

where both the monomer and dimer plateaus can be seen in the data. Note that it is not always possible to cover all three regions as illustrated for RV being pyrrole (see Fig. 3-6). At low [RV], the plasma will be that of H_3^+ since this recombines very slowly[17].

At higher [RV], proton transfer with RV dominates (reaction (3)) and the plasma is then controlled by RVH^+ . This is shown in Fig 2b; note that if recombination of RVH^+



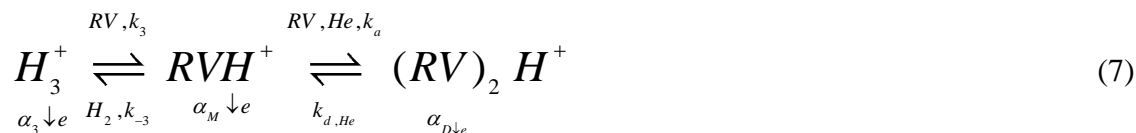
dominates over association then no $(\text{RV})_2\text{H}^+$ is observed. As [RV] is increased further, association (reaction (2)) becomes more rapid and dominates over RVH^+ recombination producing the proton bound dimer $(\text{RV})_2\text{H}^+$, then giving a region dominated by $(\text{RV})_2\text{H}^+$ and the recombination (see Fig. 2a)



If however, this association (reaction (2)) is very slow, RVH^+ will dominate up to large [RV] and this would give the form of α_e versus [RV] as shown in Fig. 2b depending on the association rates. Note that, the steps may not be well defined and curves with only indications of plateaus may be all that can be obtained, such as in Fig. 3b. Fig 3-2

assumes that $\alpha_e((\text{RV})_2\text{H}^+) > \alpha_e(\text{RVH}^+)$. If $\alpha_e((\text{RV})_2\text{H}^+) < \alpha_e(\text{RVH}^+)$ then the form will be as shown in Fig. 3-4; note that this form has not been observed experimentally. An example of actual data for an RV of pyrrole is shown in Fig. 3-5. Here steps are not quite

so well defined, however values of α_e ($(RV)_2H^+$) (with lower accuracy) and $\alpha_e(RVH^+)$ can still be obtained by chemical modeling. The overall model has the form



where α_3 , α_M and α_D are the recombination rate constants of H_3^+ , the monomer RVH^+ and the dimer $(RV)_2H^+$ respectively. Where k_3 and k_{-3} are the forward and reverse rate constants of reaction (3) and k_a and k_d are the forward and reverse rate constants of the association reaction (2). It should be noted that in modeling of the data, fitted values were used for the k rate constants. Changes in these values by a factor of 4 did not significantly influence the fitted recombination rate constants, i.e., by ~15%. To reduce the association, reaction mixes of 0.5-1.5% by volume reactant vapor (RV) in He were made. The reactant vapor was obtained by putting a pure sample of the reactant in to a glass vial and then purifying it through a series of pump-freeze thaw cycles in which all the gaseous impurities suspended within the liquid would be driven off and pumped away. This permits a mix to be made which in low concentrations gives the ability to study a wider dynamic range of concentration [RV] in cases where rapid association is present. This has proven to be the only method by which data could be obtained in the protonated monomer region. Rate constants are accurate to $\pm 15\%$ for protonated monomers and $\pm 20\%$ for the proton bound dimers. Where the proton bound dimer was not clearly observed, only approximate values could be given for the rate constants.

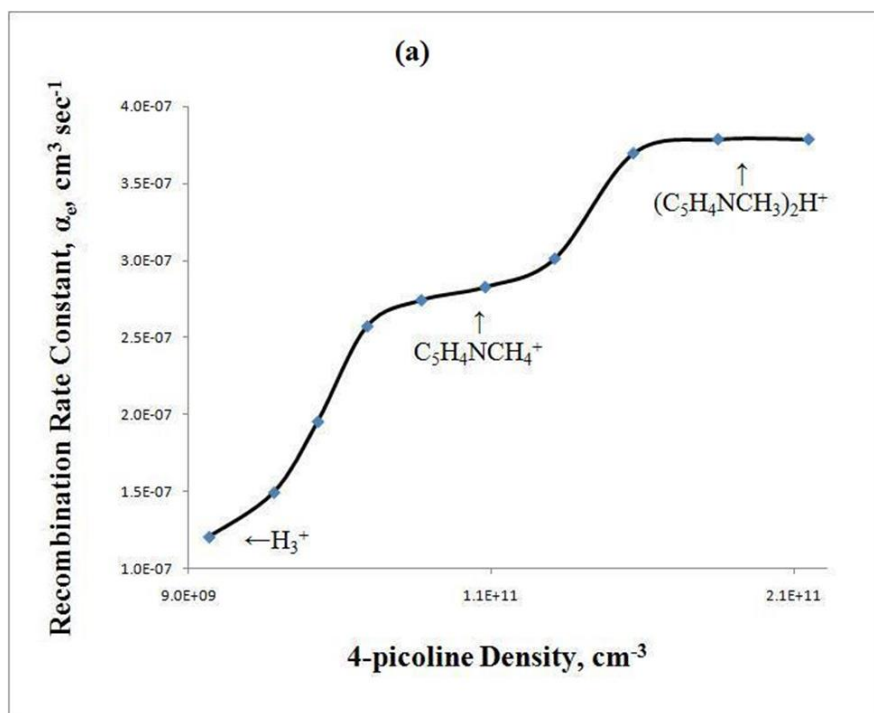


Fig. 3-5. Experimental data for the recombination rate constant, α_e , of protonated 4-picoline as a function of 4-picoline reactant vapor concentration showing both the monomer and the dimer plateaus.

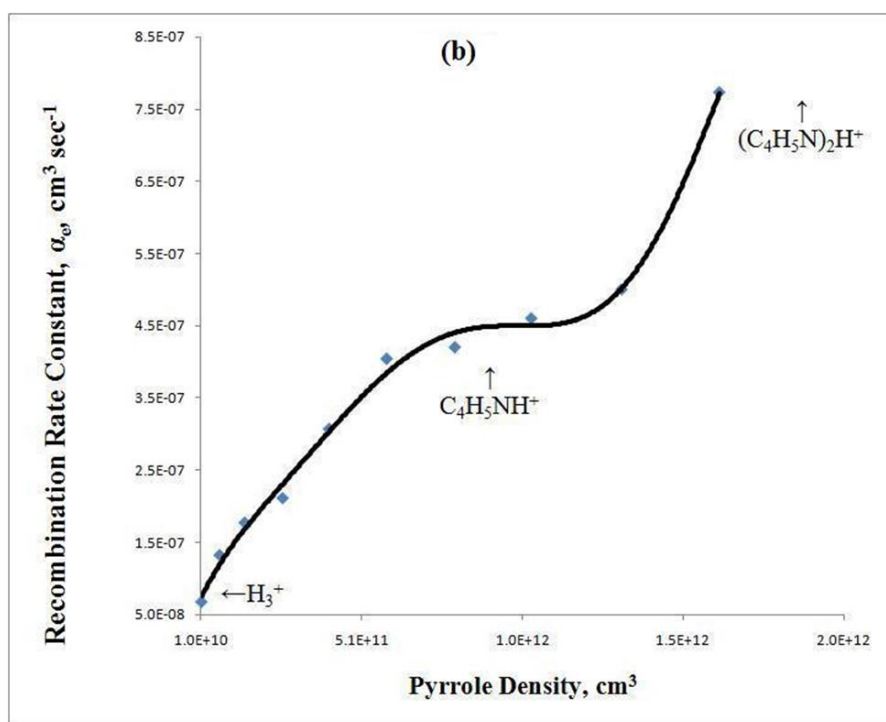


Fig. 3-6. Experimental data for the recombination rate constant, α_e , of protonated pyrrole as a function of pyrrole reactant vapor concentration. This shows that the plateaus for the dimer cannot be seen in all cases.

3-4. RESULTS AND DISCUSSION

The data that have been obtained at room temperature for a series of recombination rate constants for RVH^+ and $(RV)_2H^+$ are given in Table 3-1 for RV being benzene, C_6H_6 (Sigma >99.5%); toluene, $C_6H_5CH_3$ (Sigma 99.8%); pyridine, C_5H_5N (Sigma 99.9%); pyrimidine, $C_4H_4N_2$ (Sigma 99.9%); 4-picoline, C_6H_7N (Sigma 98%); 1,4 dioxane, $C_4H_8O_2$ (Sigma 99.8%); cyclohexane, C_6H_{12} (Sigma \geq 99.7%); six membered rings and the five membered rings, furan, C_4H_4O (Sigma 99+); pyrrole, C_4H_5N (Sigma 98%) and 1-methyl pyrrole, C_5H_7N (sigma 99%); pyrrolidine, C_4H_9N (sigma 99.5%) and thiophene, $C_4H_4SH^+$ (sigma 98%). Note that the data for benzene, pyridine and pyrimidine have been published previously and are included here only for completeness and comparison.[\[8\]](#) To help indicate the relevance that the data may have for Titan, the measured concentration of ions of the same mass to charge as the studied ions has been included in the table. A great deal of information can be gleaned from this table.

Compound, RV	Ion Formulae	Protonated Monomer	Proton Bound Dimer	Monomer Ion Mass (amu)	Ion concentration in the Titan Atmosphere (cm ⁻³)
6-Membered Rings		$\alpha_e(\text{RVH}^+)^a$	$\alpha_e((\text{RV})_2\text{H}^+)^a$		
Benzene	C_6H_7^+	$8.0(-7)^b$	$\sim 5.0(-7)$	79	18.0
Pyridine	$\text{C}_5\text{H}_5\text{NH}^+$	$8.5(-7)^b$	$\sim 6.0(-7)$	80	4.0
Pyrimidine	$\text{C}_4\text{H}_4\text{N}_2\text{H}^+$	$1.35(-6)^b$	$\sim 7.0(-7)$	81	0.7
Toluene	$\text{C}_6\text{H}_5\text{CH}_3\text{H}^+$	$3.8(-7)$	$\sim 1.3(-6)$	93	2.4
4-Picoline	$\text{C}_5\text{H}_4\text{NCH}_3\text{H}^+$	$2.83(-7)$	$3.79(-7)$	94	0.9
1,4 dioxane	$\text{C}_4\text{H}_8\text{O}_2\text{H}^+$	$2.35(-7)$	$\sim 4.3(-6)$	89	4.2
Cyclohexane	$\text{C}_6\text{H}_{13}^+$	$1.3(-6)$	$\sim 3.9(-6)$	85	0.15
5-Membered Rings					
Furan	$\text{C}_4\text{H}_4\text{OH}^+$	$4.1(-7)$	$\sim 7.3(-7)$	69	1.8
Pyrrole	$\text{C}_4\text{H}_5\text{NH}^+$	$4.0(-7)$	$\sim 9.4(-7)$	68	4.0
1-MethylPyrrole	$\text{C}_4\text{H}_4\text{NCH}_3\text{H}^+$	$5.0(-7)$	$\sim 1.0(-6)$	82	0.22
Pyrrolidine	$\text{C}_4\text{H}_9\text{NH}^+$	$2.7(-6)$	$\sim 7.0(-7)$	72	0
Thiophene	$\text{C}_4\text{H}_4\text{SH}^+$	$>7.0(-8)$	N/A ^c	84	0

^a (-7) means $\times 10^{-7}$ ^b values obtained previously [8]. ^c indicates not available

Table 3-1. Room temperature (300K) recombination rate constants, α_e , (cm³ s⁻¹) for the protonated monomer (RVH⁺) and proton bound dimer ((RV)₂H⁺) for the compounds indicated.

The 6-membered rings, for which data are quoted, all have six π electrons excluding 1,4, dioxane and cyclohexane (which have none) and all of the 5-membered rings, except pyrrolidine, also have six π electrons. For the protonated monomers, the rate constants are generally larger for the 6-membered rings relative to the 5-membered rings by about a factor of 2. The only exception is 1,4, dioxane, which has a much smaller rate constant (2.3×10^{-7} cm³ s⁻¹ relative to the average six membered ring rate constant, $\sim 9 \times 10^{-7}$ cm³ s⁻¹) and no π electrons. This indicates that in this case there may be a dependence on the presence and absence of π electrons. Cyclohexane has a large monomer rate constant but no π electrons. However, the rate constants for five and six membered rings would be expected to be similar since the same numbers of π electrons are involved in both cases.

The fact that there is a factor of ~ 2 difference (smaller for five membered rings) may be related to the difference in the mobility of the electrons in the six- and five-membered rings. The situation for the proton bound dimers is very different with the 5-membered rings having rate constants slightly larger than the 6-membered rings. Again 1, 4, dioxane and cyclohexane are the main exceptions, with rate constants larger than the other species. Thus it appears that in this case, the π electrons may be influencing the rate constants. It is also of interest to note that the rate constant given for thiophene is a lower limit for the monomer species due to the adverse effects of thiophene on the metal of which the Langmuir probe was constructed. No information on the thiophene dimer could be obtained. It can also be noted that the addition of a methyl substitution may decrease the rate constant in six membered rings. This can be observed when comparing 6-membered rings with their methyl substituted and non-methyl substituted forms, such as when benzene and pyridine are compared to toluene and 4-picoline. There seems to be the opposite effect with the five membered rings, pyrrole compared to n-methylpyrrole. The protonated ring compounds can also be compared with chain hydrocarbons. Lehfaoui et al.[\[18\]](#) studied the recombination's of a series of such ions varying in complexity from CH_5^+ to $\text{C}_8\text{H}_{17}^+$ (CH_5^+ , 7.0×10^{-7} ; C_2H_5^+ , 6.0×10^{-7} ; C_3H_7^+ , 8.3×10^{-7} ; C_4H_9^+ , 8.3×10^{-7} ; $\text{C}_5\text{H}_{11}^+$, 7.2×10^{-7} ; $\text{C}_6\text{H}_{13}^+$, 7.6×10^{-7} ; $\text{C}_7\text{H}_{15}^+$, 5.5×10^{-7} ; and $\text{C}_8\text{H}_{17}^+$, 8.2×10^{-7} , all $\text{cm}^3 \text{ s}^{-1}$). The α_e for these species are somewhat smaller than those in Table 1 for six membered rings showing that there are factors in play which increase the efficiency of ring recombination. The situation is however not clearly defined as can be seen from comparisons with a series including larger ring compounds varying from C_3H_3^+ , 7×10^{-7} ; C_5H_3^+ , 9×10^{-7} ; C_6H_6^+ , 1×10^{-6} ; C_7H_5^+ , 7×10^{-7} to $\text{C}_{10}\text{H}_8^+$, $3 \times 10^{-7} \text{ cm}^3 \text{ s}^{-1}$.

¹.[\[19\]](#) Here there is no clear pattern of increasing α_e with increasing ion complexity. The overall picture though is followed when O-atoms are added to the ring with its electron withdrawing nature, resulting in a reduction in the rate constant (to $2.35 \times 10^{-7} \text{ cm}^3 \text{ s}^{-1}$) for 1,4 dioxane. This may offer an explanation for the rate constant difference between cyclohexane and the 1,4 dioxane monomer.

Also, previous data on the six membered rings benzylium, $\text{C}_6\text{H}_5\text{CH}_2^+$ and cycloheptatriene, C_7H_8 and the seven membered ring tropylium $\text{c-C}_7\text{H}_7^+$ [\[11\]](#) are in keeping with the present measurements. In our studies for the six membered rings with no side groups, α_e increases as the number of N-heteroatoms in the ring is increased from zero to two. As substituent groups, CH_3 are added, the α_e also increase in some cases.

The situation is dramatically different for the proton bound dimers (see Table1). The α_e for the O-containing six membered ring, dioxane, and for cyclohexane, which have no π electrons are much larger than all of the other six membered rings by about a factor of five. More data are needed to definitely establish these trends and offer possible clues to the origins of these effects.

3-5 CONCLUSIONS

The data on dissociative electron-ion recombination obtained in this study have contributed significantly to chemical modeling of the Titan ionosphere and influencing the ionization balance. It has been shown that protonated six member rings recombine somewhat more rapidly than their proton bound dimers and protonated five member rings. Thus, multi rings made up of six membered rings are likely to grow more rapidly in the Titan atmosphere enhancing naphthalene, anthracene, coronene, etc. rather than azulene with its five membered ring. For substituted rings, the rate constants are

generally larger as the degree of heteroatom and, in limited cases, CH₃ group substitution increases. This has provided more data for modeling the growth of multi-rings which has recently been suggested to occur in association of the major ions, CH₃⁺, C₃H₃⁺, etc. followed by recombination. These ring compounds are known to be stable and it is thus likely that the ring will remain intact upon recombination making these species the precursors to further ring growth.

3-6 ACKNOWLEDGEMENTS

This research was supported by the NASA Planetary Atmospheres program under grant number NNX07AF57.

3-7 REFERENCES

1. Cernicharo, J., et al., *Infrared Space Observatory's Discovery of C₄H₂, C₆H₂ and Benzene in CRL 618*. Ap. J., 2001. **546**: p. L123-126.
2. Waite, J.H., Jr., et al., *The Process of Tholin Formation in Titan's Upper Atmosphere*. Science, 2007. **316**(5826): p. 870-875.
3. Vuitton, V., R.V. Yelle, and M.J. McEwan, *Ion Chemistry and N-containing Molecules in Titan's Upper Atmosphere*. Icarus, 2007. **191**: p. 722-742.
4. Vuitton, V., R.V. Yelle, and J. Cui, *Formation and Distribution of Benzene on Titan*. Journal of Geophysical Research, 2008. **113**: p. E05007(1-18).
5. Cravens, T.E., et al., *Composition and Structure of the Ionosphere and Thermosphere*, in *Titan from Cassini-Huygens*, R.H. Brown, J.-P. Lebreton, and J.H. Waite, Editors. 2009, Springer: Dordrecht. p. 259-295.

6. Leger, A. and L. d'Hendecourt, *Are Polycyclic Aromatic Hydrocarbons the Carriers of the Diffuse Interstellar Bands in the Visible?* *Astron. Astrophys.*, 1985. **146**: p. 81-85.
7. Snow, T.P., *The Unidentified Diffuse Interstellar Bands as evidence for Large Organic Molecules in the Interstellar Medium.* *Spectrochim. Acta, Part A*, 2001. **57**: p. 615-626.
8. Adams, N.G., L.D. Mathews, and D.S. Osborne, *Laboratory Chemistry Relevant to Understanding and Modeling the Ionosphere of Titan.* *Farad. Disc.*, 2010. **147**: p. 1-323-335.
9. Horst, S.M., V. Vuitton, and R.V. Yelle, *Origin of Oxygen Species in Titan's Atmosphere.* *J. Geophys. Res.*, 2008. **113**: p. E10006.
10. Rebrion-Rowe, C., et al., *The Dissociative Recombination of Hydrocarbon Ions: Alkene and Alkyne Derived Species.* *J. Chem. Phys.*, 1998. **108**: p. 7185-9.
11. Rebrion-Rowe, C., et al., *The Dissociative Recombination of Hydrocarbon Ions. III Methyl-substituted Benzene Ring Compounds.* *J. Chem. Phys.*, 2000. **113**: p. 3039-3045.
12. Novotny, O., et al., *Measurement of the Recombination of Photoproduct PAH Ions.* *J. Phys. Conf. Ser.*, 2005. **4**: p. 211-215.
13. McLain, J.L., et al., *Flowing Afterglow Studies of the Electron-Ion Recombination of Protonated Cyanides (RCN)H⁺ and their Proton Bound Dimer Ions (RCN)₂H⁺, where R is H, CH₃, and C₂H₅.* *Int J. Mass Spectrom.*, 2009. **282**: p. 85-90.
14. McLain, J. and N.G. Adams, *Flowing Afterglow Studies of Temperature Dependencies for Electron Dissociative Recombination of HCNH⁺, CH₃CNH⁺,*

- C₂H₅CNH⁺ and their Symmetrical Proton Bound Dimers*. Planet. Space Sci., 2009. **57**: p. 1642-1647.
15. Adams, N.G. and D. Smith, *Flowing Afterglow and SIFT*, in *Techniques for the Study of Ion-Molecule Reactions*, J.M. Farrar and J.W.H. Saunders, Editors. 1988, Wiley Interscience: New York. p. 165-220.
 16. Swift, J.D. and M.J.R. Schwar, *Electrical Probes for Plasma Diagnostics*. 1970, London: Iliffe.
 17. Glosik, J., et al., *Multicollision Character of Recombination of H₃⁺ Ions in Afterglow Plasma*. J. Phys: Conf. Ser., 2009. **192**: p. 012005.
 18. Lehfaoui, L., et al., *The Dissociative Recombination of Hydrocarbon Ions .1. Light Alkanes*. J. Chem. Phys., 1997. **106**(13): p. 5406-5412.
 19. Abouelaziz, H., et al., *Measurements of C₃H₃⁺, C₅H₃⁺, C₆H₆⁺, C₇H₅⁺ and C₁₀H₈⁺ Dissociative Recombination Rate Coefficients*. J. Chem. Phys., 1993. **99**: p. 237-243.

CHAPTER 4

THE EFFECT OF N-HETEROATOMS AND CH₃ SUBSTITUENTS ON
DISSOCIATIVE ELECTRON-ION RECOMBINATION OF PROTONATED SINGLE
SIX MEMBERED RING COMPOUNDS AT ROOM TEMPERATURE⁶

⁶ D.S. Osborne Jr., P. A. Lawson, and N.G. Adams. 2011. International Journal of Mass Spectrometry **308**:114-117. Reprinted here with permission of the publisher.

4-1 ABSTRACT

Electron-ion dissociative recombination rate constants have been determined for protonated single six-membered hydrocarbon rings with varying N-atom substitution in the rings and varying degrees of methyl substitutions to the rings. The species studied have been protonated forms of the xylenes (C_8H_{10} ; with configurations o, m, and p), the picolines (C_6H_7N ; with methyl substitutions located at 2, 3, and 4), mesitylene (C_9H_{12}) and 2, 5- lutidine (C_7H_9N). By operating at high reactant vapor pressures, ternary association has been made to dominate over recombination to create proton bound dimers and the rate constants of these species have been determined. The studies were made at room temperature in a flowing afterglow with a Langmuir probe to determine the reduction in electron density as a function distance along the flow tube. All of the data except for mesitylene showed a consistent trend with the numbers of N-atom substitutions and CH_3 attached to the rings. For the protonated species, the rate constants increase with number of nitrogen's and decreased with number of CH_3 substituents attached to the ring. For proton bound dimers, the rate constants increase with both, the number of N-atoms and number of CH_3 substituents. For the xylene and picoline isomer's the measurements showed that the rate constants were independent of isomeric form, and thus, it is not necessary to study all isomeric forms. The relevance of these studies to the ionosphere of Titan is discussed.

4-2 INTRODUCTION

Recently, single six membered ring compounds have been detected in the atmosphere of Titan (a planetary satellite of Saturn) by the highly successful Cassini spacecraft^[1]. Masses in the range 1 to 99 amu have been detected by the on board

positive ion-neutral mass spectrometer (INMS)[2], positive ion masses up to 350 amu by the Cassini Plasma Spectrometer (CAPS), Ion Beam Spectrometer (IBS), and negative ions 50 to 8,000 amu by the CAPS Electron Spectrometer (ELS)[3]. Within these masses are the six membered rings C_6H_6 (benzene), $C_5H_5N^+$ (ionized pyridine), and $C_7H_9^+$ (protonated toluene). Double rings of naphthalene, anthracene and anthracene dimers have been identified with the IBS[3] and polycyclic aromatic hydrocarbons (PAH's) with the ELS. Since the atmosphere of Titan is composed of 98% nitrogen, it is considered that there may be a great deal of N substitution in the rings. The next most abundant species in this atmosphere is methane (CH_4 ; ~2%), and it can be concluded that the rings present within the Titan atmosphere may have many methyl (CH_3) substitutions. All of these ion species are likely to have different recombination rate constant's and, thus, a body of rate constant data needs to be measured to expose any trends within the nitrogen or methyl substituted (CH_3) ring species. These data will be beneficial to the models which have been produced by Vuitton et al[4] and Cravens et al.[1] Both models show a body of hydrocarbon ion chemistry with cyanides present within the Titan atmosphere. With this in mind, the recombination reactions of protonated and proton bound dimers of benzene (C_6H_6), toluene ($C_6H_5CH_3$), pyridine (C_5H_5N) and pyrimidine($C_4H_4N_2$) have been previously studied and their rate constants determined [5]. More recently, the recombination rate constants for protonated 4- picoline (C_6H_7N), cyclohexane (C_6H_{12}), 1,4 dioxane ($C_4H_8O_2$), furan (C_4H_4O), pyrrole (C_4H_5N), 1-methylpyrrole (C_5H_7N), thiophene (C_4H_4S) and pyrrolidine (C_4H_9N) have also been determined.[6] With more than one substituent in or on the ring, isomeric forms are possible and this has been investigated for all of the isomeric forms of protonated xylenes (C_8H_{10} ; with

configurations o, m, and p) and the picolines (C_6H_7N ; with a methyl substitution located at 2, 3, and 4). The proton bound dimers have also been studied, as well as mesitylene (C_9H_{12}) and 2, 5- lutidine (C_7H_9N) recombination rate constants [6]. Since rate constants for the xylenes and picolines, only varied a little with isomeric form, it is not necessary to study all isomeric forms. This was fortunate since the increasing substituents also corresponds to decreasing vapor pressure which makes it more difficult to introduce the reactant vapor into the reaction vessel. In addition, in these previous studies, only species with few N atoms and CH_3 substituents have been investigated, and the purpose of the present study is to extend this to larger numbers of substituents to look for trends in the recombination rate constants.

4-3 EXPERIMENTAL

The recombination rate constants, α_e , were determined in a flowing afterglow using a Langmuir probe operating within the orbital limited region. This apparatus has been described in detail previously and only features relevant to the present studies are described here [7]. By measuring the decrease in electron density, $[e]$, as a function of distance, z , along the flow tube and utilizing equation 1

$$\frac{1}{[e]_z} - \frac{1}{[e]_0} = \frac{z \alpha_e}{V_p} \quad (1)$$

where V_p is the plasma flow velocity, $[e]_z$ is the measured electron density and $[e]_0$ is the upstream electron density, the recombination rate constant can be determined. The flowing afterglow uses a helium (Airgas UHP He) flow which is ionized upstream in a microwave cavity and allowed to flow to a downstream mass spectrometer under the action of a roots blower pump. Sequential additions of Ar, H_2 and reactant vapors, RV,

to the flow convert the plasmas from $\text{He}^+/\text{He}_2^+/\text{e}$, to Ar^+/e , to H_3^+/e , and to RVH^+/e with the final step being the proton transfer from H_3^+ to RV as seen in equation 2.



This protonated monomer then recombines with the electrons.



However, the addition of larger concentrations of RV allows association



to dominate over recombination (3) generating the dimer $(\text{RV})_2\text{H}^+$ which then recombines [8]. Plots of recombination rate constant, α_e , versus RV concentration, $[\text{RV}]$, then reveals regions

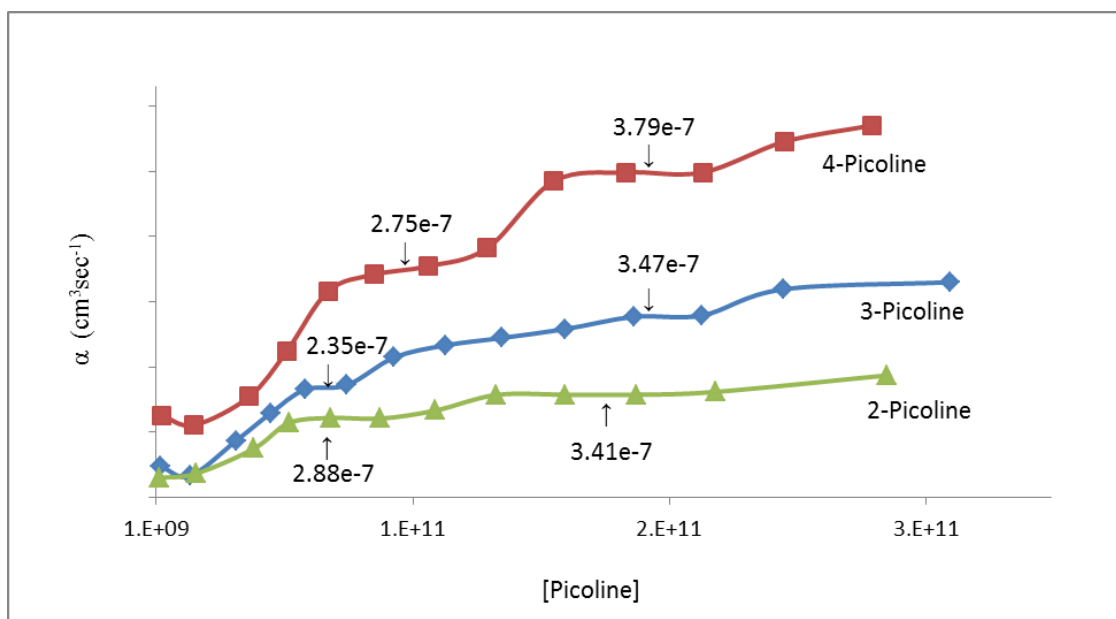
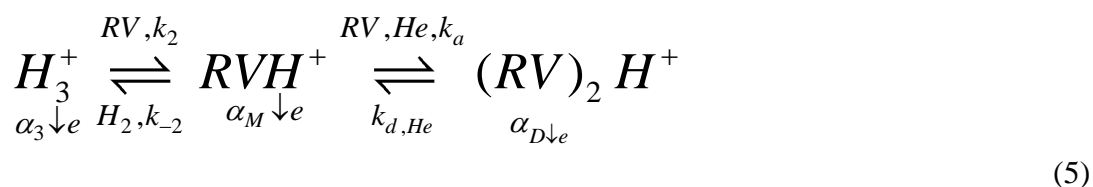


Fig. 4-1. Plot of 2, 3, and 4 picoline rate constant (α_e) versus reactant vapor concentration. The plateaus are well defined for 4-picoline but less so for 2 and 3 picoline. Note: The three plots are vertically offset for viewing ease, but the rates of the protonated form and the proton bound dimer are labeled on each curve.

where $H_3^+ + e^-$, $RVH^+ + e^-$ and $(RV)_2H^+ + e^-$ dominate the flow as seen in the plots shown in Fig. 1 for 2, 3, and 4, picolines. It can be seen that, for 4-picoline, there are well defined plateaus showing the recombination rate constants for RVH^+ and $(RV)_2H^+$. Here the α_e for RVH^+ and $(RV)_2H^+$ can be read directly from the plot, as previously discussed[5]. As the recombination moves to 3-picoline and then to 2-picoline, the plateaus become less distinct and the chemical model in equation (5) has to be used to fit the data to determine the recombination rate constants[6].



Rate constants determined in this way, are accurate to within $\pm 15\%$ for the monomer systems with the dimers less accurate ($\pm 20\%$) because of the fitting procedures. For cross comparison of the isomeric forms, only the relative errors are important, and these have a random error of $\pm 5\%$, this was determined from a series of studies of N_2H^+ recombination under the same experimental conditions.[9] The kinetic data for all of the systems studied are given in Table 1. The purities of the species indicated were 2-picoline (sigma, 98%), 3-picoline (Sigma, $\geq 99.5\%$), 4-picoline (Sigma, 99%), o-xylene (EMD, $> 98\%$), m-xylene (Sigma, 99%), p-xylene (Fisher, 99.9%), mesitylene (Sigma, $\geq 99\%$) and 2,5-lutidine (Sigma, 95%). Since the RV's are liquid at room temperature, they were freeze-pump-thawed several times before use to remove any dissolved gases. The neat vapor was then used to make a 0.5 to 1% mixture in helium (National Welders UPC He). It was always ensured that the vapor was in a concentration substantially less than the saturated vapor pressure to prevent the vapor from condensing on the flow tube

walls. This enabled constant concentrations of these sticky vapors to be introduced into the flow tube. Also included in Table 1 are data previously obtained from the literature [5, 6]. Note that where a plateau for $(RV)_2H^+$ is not obtained (i.e., a sufficiently large $[RV]$ could not be introduced into the flow tube) only approximate values of $\alpha_e((RV)_2H^+)$ could be obtained through modeling.

4-4 RESULTS AND DISCUSSION

A great deal of information can be obtained from a study of Table 1.

CH ₃	Compound	Monomer	Dimer
0	Benzene ^a	8.0(-7)	5.0(-7)
1	Toluene ^a	3.8(-7)	1.25(-6)
2=	o-Xylene	2.8(-7)	1.2(-6)
2=	m-Xylene	2.7(-7)	2.55(-6)
2=	p-Xylene	2.15(-7)	1.7(-6)
3	mesitylene	7.0(-7)	2.5(-6)
N	Compound	Monomer	Dimer
0	Benzene ^a	8.0(-7)	5.0(-7)
1	Pyridine ^a	8.5(-7)	6.0(-7)
2	Pyrimidine ^a	1.35(-6)	7.0(-7)
CH ₃ ;N	Compound	Monomer	Dimer
1, 0	Toluene ^a	3.8(-7)	1.25(-6)
1; 1=	2, Picoline	2.88(-7)	3.4(-7)
1; 1=	3, Picoline	2.42(-7)	3.5(-7)
1; 1=	4, Picoline	2.85(-7)	3.8(-7)
2; 1	Lutidine	5.5(-7)	N/A

^aData from the literature[5, 6].

Table 4-1. Recombination rate constants, α_e , indicated for the protonated species (RVH^+) and their proton bound dimers $((RV)_2H^+)$ together with relevant data from previous studies reported in the literature [5, 6]. These species contain various combinations of CH_3 substituents attached to the rings and N-atoms substituted into the rings.

For the species with CH_3 substituents attached to the single six membered rings, the

RVH^+ rate constants decrease with increasing numbers of CH_3 groups and increase with

increasing numbers of N-atoms. The isomeric forms of xylene all had essentially the same α_e , as did the isomers of picoline indicating that, for species of this complexity, any isomer could be used for determining α_e . Note that mesitylene was not consistent with the trend for other protonated CH_3 containing species. This may be due to its extremely low vapor pressure and the difficulties associated with making a mix in such cases. However, protonated lutidine did conform to the overall trend. These trends can be seen more clearly from the plots in Figs 2 and 3 for the protonated monomers, RVH^+ , and the proton bound dimers, $(\text{RV})_2\text{H}^+$ respectively. It is interesting to note that the CH_3 substituents and N-atoms generally worked in opposite directions. This behavior is surprising since the CH_3 substituents and N-atoms both provide electrons to the ring.

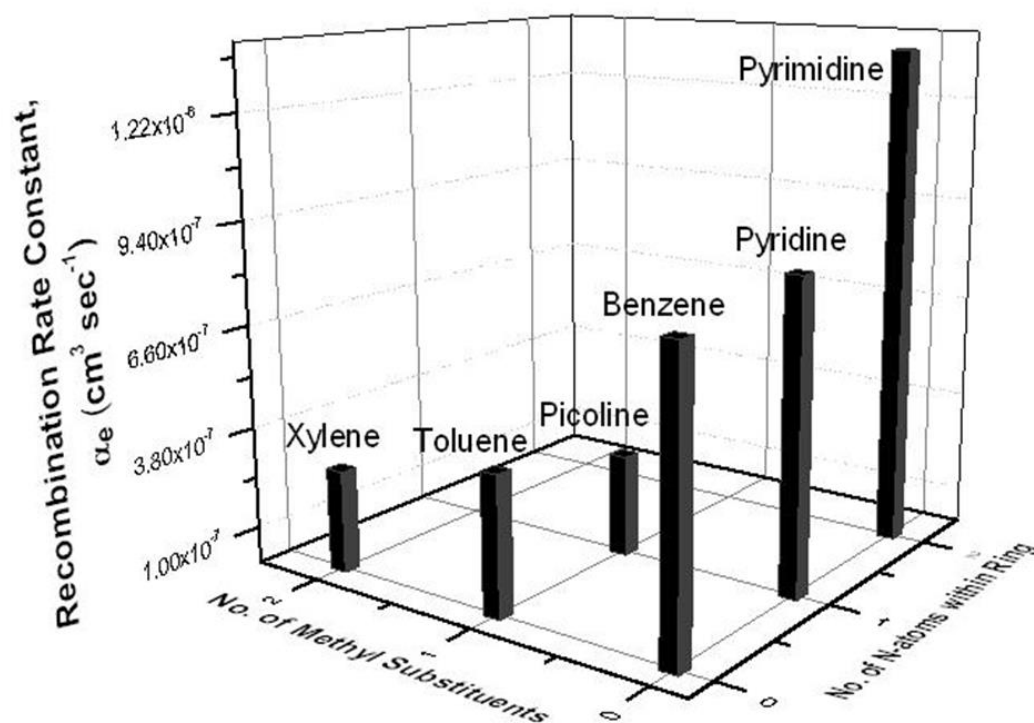


Fig. 4-2. A plot of the rate coefficients, α_e , ($\text{cm}^3 \text{s}^{-1}$) for a series of recombining protonated single six membered ring compounds as a function of the number of CH_3 substituents and N-atoms in the rings. 2,5 lutidine and mesitylene were also studied and

show increasing values and are included in Table 1. However, are omitted for clarity in this figure.

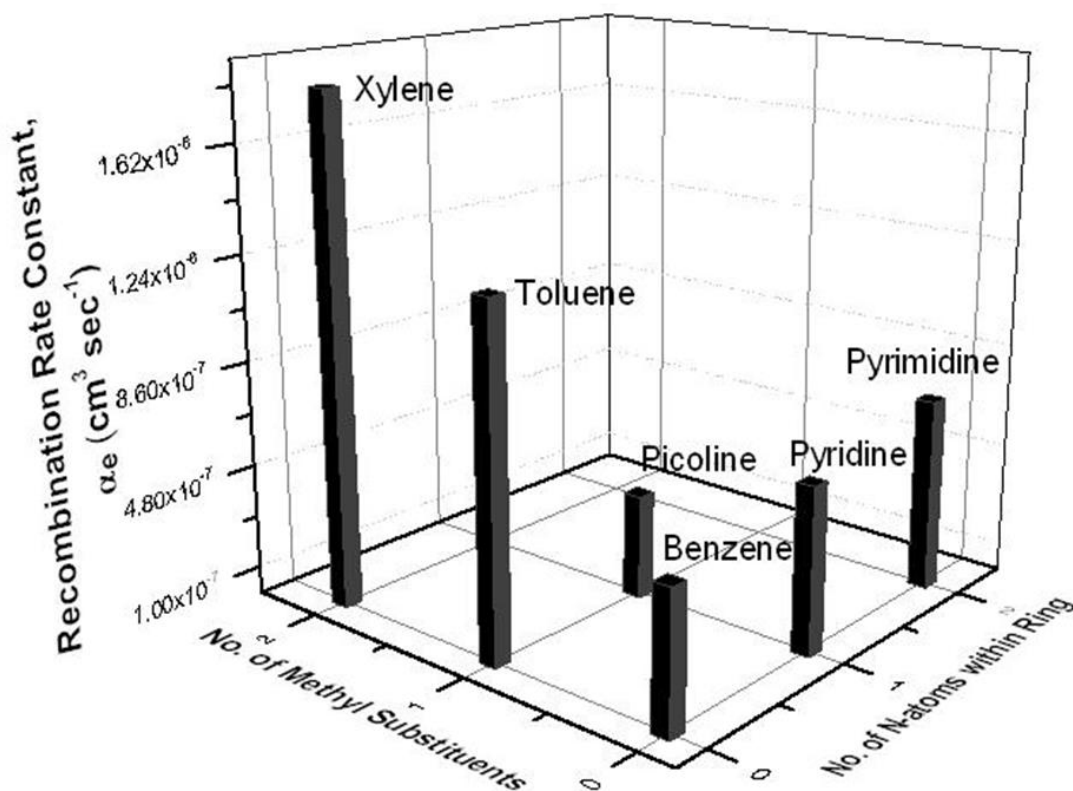


Fig. 4-3. A plot of the recombining proton bound dimer rate constants, α_e , ($\text{cm}^3 \text{ s}^{-1}$) for a series of proton bound dimers of single six membered ring compounds as a function of the number of CH_3 substituents and N-atoms in the rings. Mesitylene shows an increasing value and is included in Table 1. However it is omitted here for clarity.

4-5 CONCLUSIONS

The rate constants for a series of recombination's of single six membered ring compounds with CH_3 substituents and N-atoms substituted in the ring show some degree of consistency. The trends in reactivity are, thus, well established and the data can be included in the chemical models of the Titan atmosphere with confidence. From Fig.2 for the monomers, it is evident that the α_e get larger with increasing numbers of N-atoms in the ring, but smaller with increasing number of methyl substituents. For the dimers,

the situation is very different with α_e being larger and increasing with the number of CH_3 substituents. This trend does not continue for mesitylene, which has three CH_3 groups symmetrically arranged in the molecule. With increasing numbers of N-atoms in the ring, the α_e increases, but the values are smaller than for the monomers. Again the trends are clearer from the plot, as can be seen from Fig. 3. Note that no $\alpha_e((\text{RV})_2\text{H}^+)$ was available for lutidine because an RV high enough could not be introduced into the flow tube to make the dimer dominant. These studies are important due to the Titan atmosphere consisting of 98% N_2 and there are likely to be a significant numbers of N-heteroatoms in the rings and, thus, larger recombination rate constants. Also since the monomer α_e decrease with increasing number of CH_3 substituents, these species have more time to associate to form dimers which then recombine more rapidly with the increasing numbers of CH_3 substituents. These trends should prove useful in chemical models of the Titan atmosphere and allow for the more accurate representation of the ionization balance. Note that within these data, the xylene and the picoline isomers show very little variation. No theoretical calculations have been made for species of this complexity. Such calculations are necessary to fully understand the reaction mechanism which occurs. However, these data may prove critically important to the Titan ionosphere where ring compounds have been detected including one with an N-heteroatom in the ring (pyridine) and one with a CH_3 attached to the ring (toluene). It is likely that, since N_2 and CH_4 are the most abundant species in the Titan atmosphere, the species in this study should be included in the chemical models. Extrapolation of the data to larger numbers of N-atoms and CH_3 groups can now be done with some confidence, and these species could also reasonably be included in the models. Obviously,

recombination rate data need to be obtained for the larger species, including those with more than one ring. Also, association reactions of these species with the abundant ions (CH_3^+ , C_3H_3^+ , C_2H_5^+ , etc) need to be investigated to confirm the suggested reaction paths to larger species [5]. The products of these reactions could be compared with the observations of masses up to 350 amu detected in the CAPS/IBS experiments on the Cassini spacecraft. From the recombination and association data, limited chemical models could be created such as that given below.

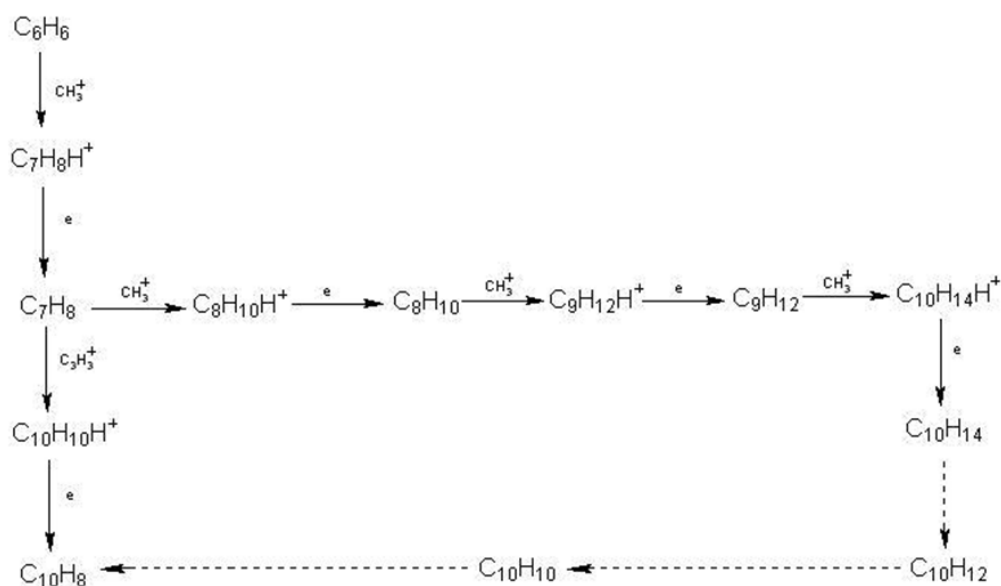


Fig. 4-4. Possible parallel routes to the production of naphthalene through interactions of benzene with ions present within the Titan atmosphere.

This shows parallel routes to naphthalene, due to the associations of species such as CH_3^+ and C_3H_3^+ with single ringed hydrocarbons and followed by recombination. For example, previously discussed CH_3^+ associates with benzene to produce toluene after recombination [5]. This toluene then can associate with C_3H_3^+ which after recombination could produce naphthalene. Alternately, toluene could associate with CH_3^+ followed by

recombination to slowly build up the molecule one CH_2 at a time. Similar sequential association/recombination with CH_3^+ could lead to the buildup to naphthalene. Such mechanisms with other hydrocarbon ions could rapidly generate multi-ring PAH's, and this needs to be investigated.

The study that has been carried out so far has concentrated on the least massive species present. However, the Cassini data has shown that there are also more massive species [1], indicating that there are likely to be both aliphatic and aromatic compounds present with polymer forms and nitrile (CN) and amine (NH_2) group attached. These groups can be attached to carbon atoms in six-membered rings (as in the case of CH_3 groups) or at the end of carbon chains. The studies presented here need to be extended to include these groupings and to determine how the presence of these groupings effects the recombination rate constants and if the dependencies are similar to those for the CH_3 groups. In particular, what is the effect of the electron withdrawing power, how this affect does the association to form proton bound dimers, and the efficiency of ring closing.

As more side groups are added to the six membered rings, the species more closely resemble thymine and cytosine, the nitrogenous base pairs in the nucleotides of nucleic acids. With the recent discovery of non-terrestrial amino acids in the Atmahata Sitta [10] and Murchison [11] meteorites, the role of interstellar production of organic compounds played in the origin of life on the early Earth is becoming increasingly more evident. The data may help in the modeling of the interstellar production of amino acids and complex organic molecules which would have been deposited on the early Earth.

There is a wealth of understanding to be gained from such studies and these situations all need to be investigated.

4-6 ACKNOWLEDGEMENTS

This research was supported by the NASA Planetary Atmospheres program under grant number NNX10AB96G

4-7 REFERENCES

1. Cravens, T.E., et al., *Composition and Structure of the Ionosphere and Thermosphere*, in *Titan from Cassini-Huygens*, R.H. Brown, J.-P. Lebreton, and J.H. Waite, Editors. 2009, Springer: Dordrecht. p. 259-295.
2. Cravens, T.E., et al., *Composition of Titan's Ionosphere*. *Geophys. Res. Lett.*, 2006. **33**: p. L07105.
3. Waite, J.H., Jr., et al., *The Process of Tholin Formation in Titan's Upper Atmosphere*. *Science*, 2007. **316**(5826): p. 870-875.
4. Vuitton, V., R.V. Yelle, and M.J. McEwan, *Ion Chemistry and N-containing Molecules in Titan's Upper Atmosphere*. *Icarus*, 2007. **191**: p. 722-742.
5. Adams, N.G., L.D. Mathews, and D.S. Osborne, *Laboratory Chemistry Relevant to Understanding and Modeling the Ionosphere of Titan*. *Farad. Disc.*, 2010. **147**: p. 1-323-335.
6. Osborne, D.S., P.A. Lawson, and N.G. Adams, *Flowing Afterglow Studies of the Dissociative Electron-Ion Recombination for a Series of Single Ring Compounds at Room Temperature*. *Int. J Mass Spec.*, 2011: p. submitted.

7. Adams, N.G. and D. Smith, *Flowing Afterglow and SIFT*, in *Techniques for the Study of Ion-Molecule Reactions*, J.M. Farrar and J.W.H. Saunders, Editors. 1988, Wiley Interscience: New York. p. 165-220.
8. Plasil, R. and et al., *Formation and recombination of protonated acetonitrile clusters*. Journal of Physics B: Atomic, Molecular and Optical Physics, 1999. **32**(14): p. 3575.
9. Lawson, P.A., D.S. Osborne, and N.G. Adams, *Effect of Isotopic Content on the Rate Constants for the Dissociative Electron-Ion Recombination of N_2H^+* . Int. J. Mass Spectrom., 2011: p. In press.
10. Glavin, D.P., et al., *Extraterrestrial amino acids in the Almahata Sitta meteorite*. Meteoritics & Planetary Science, 2010. **45**(10-11): p. 1695-1709.
11. Martins, Z., et al., *Extraterrestrial nucleobases in the Murchison meteorite*. Earth and Planetary Science Letters, 2008. **270**(1-2): p. 130-136.

CHAPTER 5

TRENDS IN ELECTRON-ION DISSOCIATIVE RECOMBINATION OF BENZENE

ANALOGS WITH FUNCTIONAL GROUP SUBSTITUTIONS: NEGATIVE

HAMMETT σ_{PARA} CONSTANTS⁷

⁷D.S. Osborne, Jr., P.A. Lawson, N.G. Adams, and I. Dotan. Submitted to Icarus, 10/18/2013.

5-1 ABSTRACT

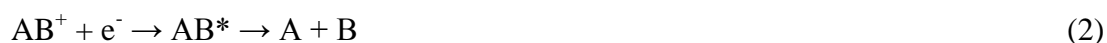
An in-depth study of the effects of functional group substitution on benzene's electron-ion dissociative recombination (e-IDR) rate constant has been conducted. The e-IDR rate constants for benzene, biphenyl, toluene, ethylbenzene, anisole, phenol, and aniline have been measured using a Flowing Afterglow equipped with an electrostatic Langmuir probe (FALP). These measurements have been made over a series of temperatures from 300 to 550K. A relationship between the Hammett σ_{para} values for each compound and rate constant has indicated a trend in both the e-IDR rate constants and their temperature dependence data. Implications of the observed trends to the chemistry of the Titan ionosphere are discussed.

5-2 INTRODUCTION

In 1980, Voyager 1 measured the electron density profile of the Titan ionosphere using remote radio occultation.[1] At about the same time, the haze seen on Titan by Voyagers I and 2 was believed to be due to complex organics.[2] Cassini arrived at Titan in 2004 and has provided a wealth of information about the atmosphere and the surface.[3] It made in-situ measurements of electron density and temperature using the Radio and Plasma Wave (RPWS) detector.[4] Mass spectra were determined by the Ion Neutral Mass Spectrometer (INMS) on Cassini covering the range 1 – 99 amu positive ions with better than 1 amu mass resolution. Additional data for positive ions were obtained with the Ion Beam Spectrometer (IBS) of the Cassini Spectrometer (CAPS) for the mass range 80 to 350 amu and with peaks at ~130, ~170 and 335 amu identified as naphthalene (C_{10}H_8), anthracene ($\text{C}_{14}\text{H}_{10}$) and the anthracene dimer.[5] Negative ions with masses up to 10,000 amu and peaks at 22, 44 and possibly 82 amu were detected by

the Electron Spectrometer (ELS) on CAPS.[6] Conversion of ion masses into molecular compositions requires the modeling of the atmosphere.[5-19] This modeling has shown that the atmosphere is composed of hydrocarbons (including PAH's), nitriles and thiolins with benzene being the most abundant heavy molecule.[13, 20-22]. It is thus possible that benzene compounds with various functional groups are created in the Titan atmosphere. Benzene with a methyl group substitution (protonated toluene) has been identified through modeling of the Cassini data.[6] The presence of benzene compounds with other functional groups, such as amines and nitriles, have been detected in laboratory experiments attempting to replicate the formation of thiolins under Titan like conditions.[23] Thus, kinetic data for these species are required and this has been the objective of the present paper, specifically to determine the effect of electron-ion dissociative recombination (e-IDR) rate constant effects of substituting the functional groups C_6H_5 , CH_2CH_3 , OH , and NH_2 . The functional groups H and CH_3 , corresponding to benzene and toluene, have been studied previously.[24]

The kinetic data obtained for modeling of the Titan ionosphere also gives the opportunity to investigate e-IDR reaction mechanisms. When an electron collides with the protonated species two mechanisms are available for dissociation; the direct mechanism and the indirect mechanism. In the direct mechanism the neutralized ion undergoes a direct transition to a repulsive potential curve, see equation 1.



This has been investigated by Bates[25] and shows a $T_e^{-0.5}$ dependence on electron temperature. In the indirect mechanism, the neutralized ion undergoes a radiationless

transition to high lying Rydberg states. This is followed by a transition to a repulsive potential curve only available to the Rydberg state, see equation 2. Here Bardsley showed that the electron temperature dependence was $T_e^{-1.5}$. [26] For molecules, such as hydrocarbons, where many curve crossings are available, the direct and indirect mechanisms interfere with each other. This interference causes the measured electron temperature dependence to be between $T_e^{-0.5}$ and $T_e^{-1.5}$, showing that both pathways are being accessed. It should be noted that, in a flowing afterglow, the temperatures of the ions and electrons are equal due to thermalization by collisions with the helium buffer gas. To investigate these mechanisms in more detail would require more sophisticated theories, such as Multichannel Quantum Defect Theory (MQDT), but this is beyond the scope of this paper. [27] This paper will probe the effect of electron donating and electron withdrawing functional groups on the e-IDR rate constants and their associated electron temperature dependencies. This can be done in the generalized form of the Hammett σ_{para} values. For σ_{para} negative, the functional group is electron donating to the benzene ring whereas, for σ_{para} positive, the functional group is electron withdrawing from the ring. [28] Values of σ_{para} have been compiled by Hansch et al in a detailed review which served as the source for our σ_{para} values. [29]

5-3 EXPERIMENTAL

Electron-Ion dissociative Recombination (e-IDR) rate constants, α_e , were determined using a Flowing Afterglow equipped with an axial electrostatic Langmuir probe (FALP). This apparatus has been described in detail previously [30-32] and only a basic description is given here. The FALP utilizes a Langmuir probe operating in the orbital limited region to measure the decrease in electron density as a function of distance

along the flow tube, z . When operating in the orbital limited region with only one species undergoing recombination, it is possible to utilize equation (3) to determine α_e .

$$\frac{1}{[e]_z} - \frac{1}{[e]_0} = \frac{z\alpha_e}{V_p} \quad (3)$$

In equation (3) V_p is the plasma velocity, $[e]_0$ is the upstream electron density, and $[e]_z$ is measured electron density as a function of axial position, z . The Flowing Afterglow operates by ionizing a helium (Airgas HP helium) flow upstream in a microwave cavity to create a quasi-neutral plasma. The ionized helium flows downstream under the action of a Roots blower pump. Argon (National Welders UHP Ar) is added to destroy He_2^+ , helium metastables and increases the electron density while creating an Ar^+ plasma. Hydrogen (Airgas UPC Hydrogen) is added to the flow tube following argon to create an H_3^+ plasma. Once an H_3^+ plasma has been created, a reactant vapor (RV) is added and H_3^+ proton transfers to RV creating the desired protonated reactant vapor, RVH^+ . Then the RVH^+ once created undergoes recombination with electrons in the plasma to form neutral products. See reactions (4-10). The ions are identified with a downstream quadrupole mass spectrometer and detected with a discrete dynode electron multiplier.



Temperature dependencies are obtained by varying the temperature of the flow tube using a series of resistive heaters placed along the length of the flow tube. Reactant vapors are introduced into the system with a flow of helium through a bubbler apparatus. The bubbler apparatus causes a flow of helium (Airgas UPC Helium) to be forced through a liquid or a ground up sample of a solid reactant. By this action, the helium carries the reactant vapor of the sample into the system. The helium flow through the bubbler apparatus is varied until the mass spectrum indicating a pure RVH^+ plasma has been obtained. Through the use of the bubbler apparatus, it was possible to get the reactant liquids aniline (Aldrich $\geq 99.5\%$), ethylbenzene (Aldrich 99.8%), and anisole (Fluka $\geq 99\%$); and reactant solids phenol (Aldrich $\geq 99.5\%$) and biphenyl (SAFC $\geq 99\%$) into the flow tube. To minimize fragmentation in the proton transfer reaction (9), the H_3^+ was variously replaced by HCO^+ , N_2H^+ or $\text{C}_6\text{H}_6\text{H}^+$ whose proton transfer reactions are less energetic.

5-4 RESULTS AND DISCUSSION

E-iDR rate constants (α_e) are listed for the species with negative Hammett σ_{Para} values (HV) in Table 5-1; the corresponding power law temperature dependencies are also given. These are plotted in Fig.5-1 and Fig. 5-2 respectively. It can be seen that for the rate constants (Fig. 1) there is a well-defined expression of the form

$$\alpha_e = 4 \times 10^{-7} \text{ HV} + 7 \times 10^{-7} \text{ (cm}^3 \text{ s}^{-1}\text{)}$$

where the α_e decreases with increasingly negative HV. For HV negative, the functional group is donating electron density (electron donating) to the benzene ring.[28] It is possible that this electron density stabilizes the proton located on the benzene ring. It has been proposed by Bates[33], and confirmed experimentally[34], that the mobility of the

electrons within a molecule effects the measured, α_e . In the case of electron donating groups, the extra electron density in the benzene ring appears to limit the mobility of the π -electrons. This limitation increases as the functional group donates more electron density to the benzene ring (i.e. the Hammett σ_{para} value gets more negative). This limitation of the mobility of the π -electron would explain the decrease in the measured α_e as a function of HV negative values. This is further supported by the temperature dependence data. From Fig. 5-2 it can be seen that the electron temperature dependencies, T^x , are decreasing from an average of $T_e^{-1.0}$ to $T_e^{-0.5}$. This suggests that as more electron density is donated to the benzene ring, the number of curve crossings available is decreasing, specifically the curve crossing available to the Rydberg states. A decrease in the number of pathways to dissociation would also lead to a decrease in the measured α_e . For this reason, the electron temperature dependence data further support the trend seen in relation to the Hammett σ_{para} values. It should be noted that only one substituted benzene, i.e. toluene, did not follow this trend. The reason for this has yet to be determined.

Compound	Functional Group	σ_{para}	e-IDR RateConstant (ccsec ⁻¹)	Temperature Dependence
Benzene ^a	H	0	8.0×10^{-7}	$T^{-0.71}$
Biphenyl	C ₆ H ₅	-0.01	7.1×10^{-7}	$T^{-1.2}$
EthylBenzene	CH ₂ CH ₃	-0.15	6.4×10^{-7}	$T^{-0.96}$
Toluene ^a	CH ₃	-0.17	3.8×10^{-7}	$T^{-0.765}$
Anisole	OCH ₃	-0.27	7.0×10^{-7}	-
Phenol	OH	-0.37	5.4×10^{-7}	-
Aniline	NH ₂	-0.66	5.3×10^{-7}	$T^{-0.5}$

Table 5-1: 300K rate constants and electron temperature dependencies (300-550K) for the electron-ion dissociative recombination (e-IDR) of the protonated species indicated. These are all mono substituted with the functional groups indicated and have the negative Hammett (σ_{para}) values shown. The data are plotted graphically in Figs. 1 and 2. a) Data previously published.[35]

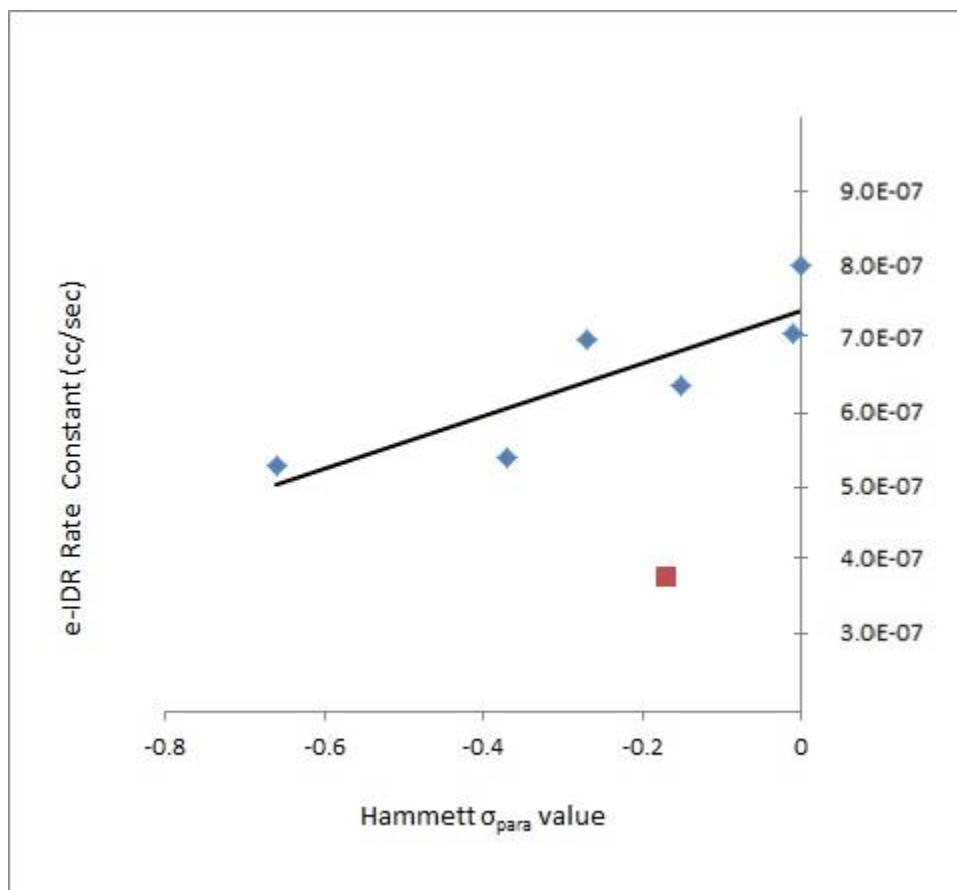


Fig. 5-1: Measured 300K electron-Ion dissociative recombination (e-IDR) rate constants versus their associated negative Hammett σ_{para} values. The red square represents the previously measured e-IDR rate constant for protonated toluene. A trend line, excluding the red square, has been added to show the linearity of the measured data. The toluene data are inconsistent with the trend line for which we have no explanation.

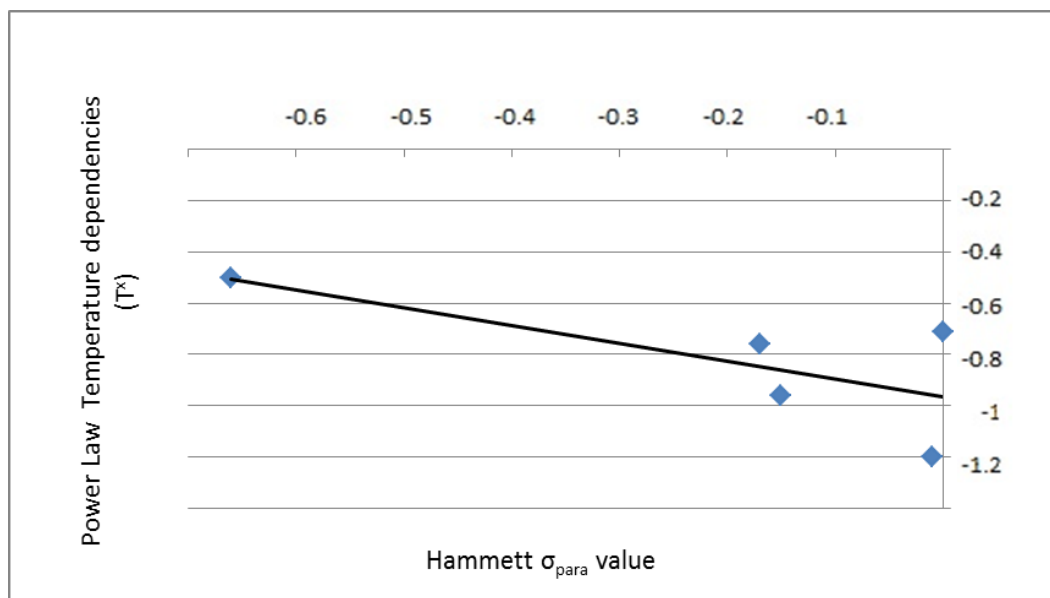


Fig. 5-2: Graph of the power law temperature dependencies for the species in Table 5-1 versus their negative Hammett σ_{para} values.

5-5 CONCLUSION

The data presented here show that the measured α_e , is dependent on many factors, proton location (charge location), electron density around that location, and the mobility of the electrons in a molecule. These trends will help to further explain the complex processes occurring during dissociative recombination. While this represents a large amount of work and gives clues to the complex process of dissociative recombination, very important trends have been established which will allow Titan modelers to predict the temperature dependences and α_e of un-measured substituted benzene compounds. While the current paper has focused on the negative Hammett σ_{para} values, another study needs to be undertaken to investigate the effects which positive Hammett σ_{para} values have on electron-ion dissociative recombination.

5-6 ACKNOWLEDGEMENTS

The authors gratefully acknowledge the support of NASA under grant, NNX10AB96G.

5-7 REFERENCES

1. Bird, M.K., et al., *Detection of Titan's Ionosphere from Voyager 1 Radio Occultation Observations*. Icarus, 1997. **130**: p. 426-436
2. Atreya, S., *Titan's Organic Factory*. Science, 2007. **316**: p. 843-845
3. Wilson, E.H. and S.K. Atreya, *Titan's Carbon Budget and the Case of the Missing Ethane*. J. Phys. Chem. , 2009. **A113**: p. 11221-11226.
4. Wahlund, J.-E., et al., *Cassini Measurements of Cold Plasma in the Ionosphere of Titan*. Science, 2005. **308**: p. 986-988.
5. Waite, J.H., Jr., et al., *The Process of Tholin Formation in Titan's Upper Atmosphere*. Science, 2007. **316**(5826): p. 870-875.
6. Vuitton, V., et al., *Negative Ion Chemistry in Titan's Upper Atmosphere*. Planet. Space Sci., 2009. **57**: p. 1558-1572.
7. Cravens, T.E., et al., *The ionosphere of Titan: an updated theoretical model*. Adv. Space Res., 2004. **33**: p. 212-215.
8. Cravens, T.E., et al., *Composition of Titan's Ionosphere*. Geophys. Res. Lett., 2006. **33**: p. L07105.
9. Cravens, T.E., et al., *Model-Data Comparisons for Titan's Nightside Ionosphere*. Icarus, 2009. **199**: p. 174-188.
10. Vuitton, V. and R.V. Yelle, *The Nitrogen Chemistry of Titan's Upper Atmosphere Revealed*. ApJ 2006. **647**: p. L175-L178.
11. Vuitton, V., et al., *Experimental and Theoretical Study of Hydrocarbon Photochemistry applied to Titan Stratosphere*. Icarus, 2006. **185**: p. 287-300.

12. Vuitton, V., R.V. Yelle, and M.J. McEwan, *Ion Chemistry and N-containing Molecules in Titan's Upper Atmosphere*. Icarus, 2007. **191**: p. 722-742.
13. Vuitton, V., R.V. Yelle, and J. Cui, *Formation and Distribution of Benzene on Titan*. Journal of Geophysical Research, 2008. **113**: p. E05007(1-18).
14. Vuitton, V., et al., *Very High Resolution Mass Spectrometry of HCN Polymers and Tholins*. Farad Disc, 2010. **147**: p. 495-508.
15. Coustenis, A., et al., *Earth-Based Perspective and Pre-Cassini- Huygens Knowledge of Titan*, in *Titan from Cassini-Huygens*, R.H. Brown, J.-P. Lebreton, and J.H. Waite, Editors. 2009, Springer: Dordrecht. p. 9-34.
16. Carrasco, N., et al., *Sensitivity of a Titan Ionospheric Model to the Ion-Molecule Reaction Parameters*. Planet. Space Sci., 2008. **56**: p. 1644-1657.
17. Carrasco, N., et al., *Uncertainty Analysis of Bimolecular Reactions in Titan Ionospheric Chemistry Model*. Planet. Space Sci., 2007. **55**: p. 141-157.
18. Carrasco, N., et al., *Towards a Reduction of the Bimolecular Reaction Model for Titan's Ionosphere*. J. Chem. Kinetic, 2008. **40**: p. 699-709.
19. Waite, J.H., et al., *Ion Neutral Mass Spectrometer Results from the First Flyby of Titan*. Science, 2005. **308**: p. 982-986.
20. Wilson, E.H., S.K. Atreya, and A. Coustenis, *Mechanisms for the Formation of Benzene in the Atmosphere of Titan*. J. Geophys. Res., 2003. **108(E2)**: p. 5014.
21. Vuitton, V., R.V. Yelle, and J. Cui, *Formation and distribution of benzene on Titan*. Journal of Geophysical Research: Planets, 2008. **113(E5)**: p. E05007.

22. Wilson, E.H., S.K. Atreya, and A. Coustenis, *Mechanisms for the formation of benzene in the atmosphere of Titan*. Journal of Geophysical Research: Planets, 2003. **108**(E2): p. 5014.
23. Bernard, J.M., et al., *Reflectance spectra and chemical structure of Titan's tholins: Application to the analysis of Cassini–Huygens observations*. Icarus, 2006. **185**(1): p. 301-307.
24. Adams, N.G., L.D. Mathews, and D.S. Osborne, *Laboratory Chemistry Relevant to Understanding and Modeling the Ionosphere of Titan*. Farad. Disc., 2010. **147**: p. 1-323-335.
25. Bates, D.R., *Dissociative Recombination*. Phys. Rev., 1950. **78**: p. 492-493.
26. Bardsley, J.N., *The Theory of Dissociative Recombination*. J. Phys. B., 1968. **1**: p. 365-380.
27. Florescu-Mitchell, A.I. and J.B.A. Mitchell, *Dissociative Recombination*. Physics Reports-Review Section of Physics Letters, 2006. **430**: p. 277-374.
28. Breslow, R., *Organic Reaction Mechanisms: An Introduction*. 1969, New York: Benjamin/Cummings Publishing Company.
29. Hansch, C., A. Leo, and R.W. Taft, *A Survey of Hammett Substituent Constants and Resonance and Field Parameters*. Chem. Revs., 1991. **91**.
30. Osborne Jr, D.S., P.A. Lawson, and N.G. Adams, *The effect of N-heteroatoms and CH₃ substituents on dissociative electron–ion recombination of protonated single six membered ring compounds at room temperature*. International Journal of Mass Spectrometry, 2011. **308**(1): p. 114-117.

31. Osborne Jr, D., P.A. Lawson, and N.G. Adams, *Flowing afterglow studies of dissociative electron-ion recombination for a series of single ring compounds at room temperature*. International Journal of Mass Spectrometry, 2011. **305**(1): p. 35-39.
32. Adams, N.G. and D. Smith, *Flowing Afterglow and SIFT*, in *Techniques for the Study of Ion-Molecule Reactions*, J.M. Farrar and J.W.H. Saunders, Editors. 1988, Wiley Interscience: New York. p. 165-220.
33. Bates, D.R., *Dissociative recombination of polyatomic ions*. Journal of Physics B: Atomic, Molecular and Optical Physics, 1991. **24**(14): p. 3267.
34. Mitchell, J.B.A. and C. Rebrion-Rowe, *The recombination of electrons with complex molecular ions*. International Reviews in Physical Chemistry, 1997. **16**(2): p. 201-213.

CHAPTER 6

TRENDS IN ELECTRON-ION DISSOCIATIVE RECOMBINATION OF BENZENE
ANALOGS WITH FUNCTIONAL GROUP SUBSTITUTIONS: POSITIVE
HAMMETT σ_{para} CONSTANTS⁸

⁸ D.S. Osborne, Jr., I. Dotan, and N.G. Adams. Submitted to International Journal of Mass Spectrometry, 10/18/2013.

6-1 ABSTRACT

An in-depth study of the effects of functional group substitution on benzene's electron-ion dissociative recombination (e-IDR) rate constants has been conducted. The e-IDR rate constants for nitrobenzene, benzonitrile, acetophenone, benzyl methyl ether, and phenyl isothiocyanate have been measured using a Flowing Afterglow equipped with an electrostatic Langmuir probe (FALP). A trend has been indicated by the comparison between the associated positive Hammett σ_{para} constant for each functional group substitution and the e-IDR rate constants for the protonated form of the benzene analog. Such a plot has indicated that protonated benzene analogs which have functional groups substitutions with a positive Hammett σ_{para} constant value have approximately the same e-IDR rate constant of $4.6 \times 10^{-7} \text{ ccsec}^{-1}$. Implications of the observed trends to the predictions of e-IDR rate constants for unmeasured benzene analogs are discussed.

6-2 INTRODUCTION

Mass spectra of the Titan atmosphere have been obtained by the Cassini spacecraft which arrived at Titan in 2004.[1-4] Since then positive ion mass spectral data were obtained using the Ion Neutral Mass Spectrometer (INMS) on Cassini covering the range 1 – 99 amu positive ions, with a better than 1 amu mass resolution. Less accurate data were obtained for larger mass positive ions using the Ion Beam Spectrometer (IBS) of the Cassini Spectrometer (CAPS); this covered the mass range 80 to 350 amu. From the data accumulated by Cassini, there is the possible identification of naphthalene (C_{10}H_8), anthracene ($\text{C}_{14}\text{H}_{10}$) and the anthracene dimer as present in the Titan atmosphere.[5] The conversion of ion masses, from the spectra taken by Cassini, into molecular compositions requires the modeling of the Titan atmosphere.[5-19] This

modeling has indicated that the atmosphere is composed of hydrocarbons (including PAH's), nitriles and aerosols with benzene being the most abundant heavy molecule.[12, 20-22]. It is thus possible that benzene compounds with various functional groups are being created in the Titan atmosphere. Benzene with a methyl group substitution to the benzene ring, toluene, was identified in the Titan atmosphere.[13] The presence of benzene compounds with other functional groups, such as amines and nitriles, has been suggested based on laboratory experiments. These experiments simulate the Titan atmosphere and attempted to identify the compounds present and the process by which complex compounds are produced therein.[23] Data for these possible species is required to help with atmospheric modeling and providing this, has been the objective of this paper. The data have focused on the effects that substituting the functional groups CH_2OCH_3 , CN , COCH_3 , NCS and NO_2 have on the electron-ion dissociative recombination (e-IDR) rate constant of their protonated forms. The functional groups H and CH_3 , corresponding to protonated benzene and toluene, have been studied previously.[24] Oxygen containing benzene analogs are not suspected to be present in large concentrations in the Titan atmosphere due to the small abundance of oxygen present. Sulfur containing benzene analogs are not suspected to be present since no sulfur has yet been detected by Cassini. While the compounds in this study may only be present in small concentrations in the Titan atmosphere, the trends from the experimental data can help in the prediction of e-IDR rate constants for unmeasured benzene analogs which may be present and in greater concentrations in the Titan atmosphere.

The purpose of this paper is to probe the effect which electron withdrawing functional groups have on e-IDR rate constants for various protonated benzene analogs.

This can be done using the Hammett σ_{para} constants. The Hammett σ constants were first developed by Louis P. Hammett in 1937 as an empirical method to characterize the effects which various functional groups have on organic reactions[25]. From Hammett's work the empirical substituent constant, σ , was developed. This is a unit-less constant which represents the effect due to the functional group [25]. It is defined by equation 1[26].

$$\sigma = \log \left(\frac{K_{\text{Sub}}}{K_{\text{Unsub}}} \right) \quad (1)$$

In equation 1, K_{sub} and K_{unsub} represent the ionization potential of substituted benzene analogs (K_{sub}) and a reference (K_{unsub})[26]. Hammett used benzoic acid as the original reference and determinates the σ constant for various functional groups attached at one of three positions on benzoic acid; ortho, para and meta. The functional group effects, σ , change depending upon which location the functional group occupies. For this reason the value of σ were quoted for different positions. In our study we have used the σ values corresponding to a functional group substituted at the para location, σ_{para} , at the suggestion of Inbal Tuvi-Arad from the Open University of Israel. It is also important to note that the effects of the functional groups can be generalized in terms of electron donating and electron withdrawing to the benzene ring. This generalization can be drawn based upon the sign and magnitude of the functional groups associated Hammett σ_{para} constant value. If σ_{para} is negative, the functional group is electron donating to the benzene ring whereas for σ_{para} positive the functional group is electron withdrawing from the ring.[27] Values of σ_{para} have been compiled by Hansch et al in a detailed review which served as the source for our σ_{para} constant values.[28] This study's focus is to determine if a correlation is present for benzene analogs having positive σ_{para} values.

6-3 EXPERIMENTAL

Electron-Ion dissociative Recombination (e-IDR) rate constants, α_e , were determined using a Flowing Afterglow equipped with an axial electrostatic Langmuir probe (FALP). This apparatus has been described in detail previously [29-31] and thus only a basic description is given here. The FALP utilizes a Langmuir probe operating in the orbital limited region to measure the decrease in electron density as a function of distance along the flow tube. When operating in the orbital limited region with only one species undergoing recombination, it is possible to utilize equation (2) to determine the e-IDR rate constant, α_e .

$$\frac{1}{[e]_z} - \frac{1}{[e]_0} = \frac{z\alpha_e}{V_p} \quad (2)$$

In equation (2), V_p is the plasma velocity, $[e]_0$ is the upstream electron density, and $[e]_z$ is the measured electron density as a function of axial position along the flow tube, z . The Flowing afterglow operates by ionizing a helium (Airgas HP helium) flow upstream in a microwave cavity to create a quasi-neutral plasma. The ionized helium flows downstream under the action of a Roots blower pump. Argon (National Welders UHP Ar) is added to destroy He_2^+ , helium metastables and increases the electron density while creating an Ar^+ plasma. Hydrogen (Airgas UPC Hydrogen) is then added to the flow tube following the argon to create an H_3^+ plasma. Once an H_3^+ plasma has been created, a reactant vapor (RV) is added and H_3^+ proton transfers to RV creating the desired protonated reactant vapor, RVH^+ . The RVH^+ then undergoes recombination with electrons in the plasma to form neutral products, see reactions (3 and 4). The ions are identified with a downstream quadrupole mass spectrometer and detected with a discreet dynode electron multiplier.



Reactant vapors are introduced into the flow tube with a flow of helium through a bubbler apparatus containing a liquid or a ground up sample of a solid reactant. By this, a small flow of helium carries the reactant vapor into the flow tube. This helium flow is varied until the mass spectrum indicates that a RVH^+ dominated plasma is produced. In most cases RVH^+ was 90% or greater of all the ions present within the plasma. In this way, it was possible to get reactant vapors nitrobenzene (Aldrich $\geq 99.5\%$), benzonitrile (Aldrich 99%), acetophenone (Fluka $\geq 99.0\%$), benzyl methyl ether (Aldrich 98%), phenyl isothiocyanate (Aldrich 98%), benzyl cyanide (Aldrich 98%), phenyl isocyanate (Aldrich $\geq 99\%$), benzaldehyde (Aldrich $\geq 99.5\%$), and cinnamaldehyde (Aldrich $\geq 99\%$) into the flow tube. In a similar way, reactant solids benzoic acid (Aldrich $\geq 99.5\%$), and benzamide (Aldrich $\geq 99.5\%$) were introduced into the flow tube. To minimize fragmentation in the proton transfer reaction (3), the H_3^+ was variously replaced by HCO^+ , N_2H^+ or C_6H_6^+ whose proton transfer reactions with RV are less energetic.

6-4 RESULTS AND DISCUSSION

E-IDR rate constants, α_e , are listed for the species with positive Hammett σ_{Para} constant values (HV) in Table 6-1. Previous work for protonated benzene analogs with functional group substitutions which had a negative Hammett σ_{Para} constant value, showed a downward trend in e-IDR rate constants as the HV became increasingly negative[32]. This study showed good agreement for all the compounds, but toluene. The study also showed a trend in the temperature dependence for the e-IDR rate constant. The temperature dependence decreased from T^{-1} at zero HV to $T^{-0.5}$ at -0.66 HV [32]. The

trends in that study showed that the e-IDR rate constant for protonated benzene analogs decreased as the functional group donated more electron density into the benzene ring. The observed data were explained as being possibly due to a stabilization of the proton by the added electron density which resulted in a decrease in the measured e-IDR rate constant [32]. The previous study[32] is at odds with the current study of positive Hammett σ_{para} constant benzene analogs because the withdrawing of electron density from the benzene ring has no effect on the measured e-IDR rate constant. The measured e-IDR rate constant for positive HV remains the same regardless of how much electron density is removed from the benzene ring. This could be due to the location of the proton which is not located on the benzene ring, rather on the functional group. [33-35]. This is different from the previous studied compounds with negative HV's where the proton was located on the benzene ring [36-38]. The data for the e-IDR rate constants are summarized in Table 6-1 and plotted in Fig. 6-1.

Compound	functional Group	σ_{para}	e-IDR RateConstant (ccsec ⁻¹)
Benzyl Methyl Ether	CH ₂ OCH ₃	0.01	4.9x10 ⁻⁷
Phenyl Isothiocyanate	NCS	0.38	≤7.4x10 ⁻⁷
Acetophenone	COCH ₃	0.5	4.2x10 ⁻⁷
Benzonitrile	CN	0.66	4.8x10 ⁻⁷
Nitrobenzene	NO ₂	0.78	4.7x10 ⁻⁷

Table 6-1: 300K rate constants for the electron-ion dissociative recombination (e-IDR) of the protonated species indicated. These are all mono substituted with the functional groups indicated and have the positive Hammett σ_{para} constant values shown. Note that the measured e-IDR rate constants have an associated $\pm 15\%$ error.

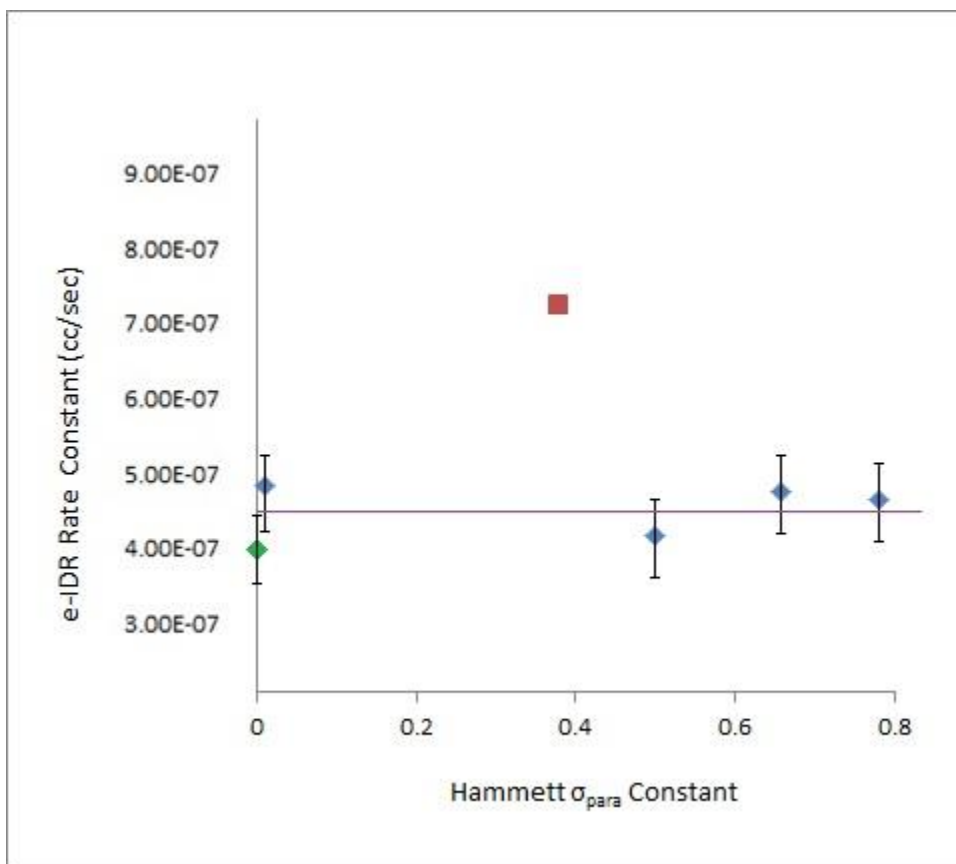


Fig. 6-1: Measured electron-Ion dissociative recombination (e-IDR) rate constants versus their associated Hammett σ_{para} constant values. The red square represents the measured upper limit e-IDR rate constant for protonated phenyl isothiocyanate. The green square represents the e-IDR rate constant for protonated toluene. A purple line, excluding the red square and green square, has been added to show the linearity of the measured data and show the constant value for e-IDR rate constant for benzene analogs whose functional groups have a positive Hammett σ_{para} constant value. The $\pm 15\%$ error associated with each measurement is represented by the error bars attached to each point.

From Fig. 6-1, only one major outlying point is seen; this is phenyl isothiocyanate. The studies of this vapor proved problematic. It was found to attach to the surface of the Langmuir probe causing an insulating layer to build up and produce large errors in the measurement of the e-IDR rate constant. This layer of phenyl isothiocyanate could not be removed and necessitated replacement of the Langmuir probe. This type of problem has been encountered previously with the compound

thiophene.[30] Due to these difficulties, only the upper limit for the α_e could be determined and no further work on this RV was conducted. The upper limit has only been included in Fig. 6-1 for completeness.

It should be noted that the study of a large number of compounds was attempted; however, many of these compounds suffered fragmentation upon proton transfer. A list of these compounds is given in Table 6-2 along with their corresponding Hammett σ_{para} constant values. We surmise that in such cases the protonated species is less stable due to the proton location. In these cases, the amount of energy input into the molecule upon proton transfer is enough to result in fragmentation. In the past, species other than H_3^+ have been used to allow for a “softer” proton transfer and reduce fragmentation. With the compounds in Table 6-2, fragmentation resulted regardless of the species from which proton transfer was attempted, indicating that the fragmentation of the molecule does not require much energy to occur. No data on the various fragments produced upon proton transfer was obtained.

Compound	Functional Group	σ_{para}
Cinnamaldehyde	CHCHCHO	0.13
Benzyl Cyanide	CH ₂ CN	0.18
Phenyl Isocyanate	NCO	0.19
Benzamide	CONH ₂	0.36
Benzaldehyde	CHO	0.42
Benzoic Acid	COOH	0.45

Table 6-2: List of substituted benzene compounds which fragment on proton transfer (see reaction (3)). The associated Hammett σ_{para} constant values and the functional groups are included in the table. Note that all of these species have positive Hammett values, and are less stable.

When comparing the results of this paper with previously published HV data, we see a similarity with protonated toluene. Previous work has shown that the addition of a methyl functional group to benzene reduces the e-IDR rate constant from $8 \times 10^{-7} \text{ ccsec}^{-1}$ for benzene to $\sim 4 \times 10^{-7} \text{ ccsec}^{-1}$ for toluene [29]. If the e-IDR rate constant for protonated toluene, $\sim 4 \times 10^{-7} \text{ ccsec}^{-1}$, is compared to the average e-IDR rate constant of the benzene analogs in the current study, $4.6 \times 10^{-7} \text{ ccsec}^{-1}$, one can see a close agreement in the values. It is important to note that toluene has a negative HV value of -0.17 [39], however this value seems to be inconstant with the current observations. These indicate that toluene should have a HV value which is more positive, than the -0.17 value calculated by Hansch et al [39]. To visually illustrate the similarity with the current study, toluene has been given an HV of zero and included in Fig. 6-1. While protonated toluene can be seen to be just below the line in Fig.6-1, it must be concluded that a similar process is occurring for all the compounds. It is our hope that by understanding what all the protonated compounds in this study have in common with protonated toluene, we will explain the current study's results.

6-5 CONCLUSION

The data presented here show that the measured e-IDR rate constant, is dependent on many factors, proton location (charge location), electron density around that location, and the mobility of the electrons in a molecule. It should be noted that a large number of the compounds with a positive HV, experienced fragmentation upon proton transfer and may not exist in the Titan atmosphere due to this effect. The data in this study will help modelers to predict e-IDR rate constants for compounds which have not been previously measured and are needed in the modeling of the Titan atmosphere. It should also be

noted that the similarity between the results for protonated toluene and the current study should not be overlooked. The similarity between these studies indicates that a similar effect is occurring upon protonation in both cases lowering the measured e-IDR rate constant. Further work is needed to determine what is occurring to the molecule upon protonation.

6-6 ACKNOWLEDGEMENTS

The authors gratefully acknowledge the support of NASA under grant NNX10AB96G. We would also like to thank Inbal Tuvi-Arad from The Open University of Israel for her help and suggestions.

6-7 REFERENCES

1. Bird, M.K., et al., *Detection of Titan's Ionosphere from Voyager 1 Radio Occultation Observations*. Icarus, 1997. **130**: p. 426-436
2. Atreya, S., *Titan's Organic Factory*. Science, 2007. **316**: p. 843-845
3. Wilson, E.H. and S.K. Atreya, *Titan's Carbon Budget and the Case of the Missing Ethane*. J. Phys. Chem. , 2009. **A113**: p. 11221-11226.
4. Wahlund, J.-E., et al., *Cassini Measurements of Cold Plasma in the Ionosphere of Titan*. Science, 2005. **308**: p. 986-988.
5. Waite, J.H., Jr., et al., *The Process of Tholin Formation in Titan's Upper Atmosphere*. Science, 2007. **316**(5826): p. 870-875.
6. Cravens, T.E., et al., *The ionosphere of Titan: an updated theoretical model*. Adv. Space Res., 2004. **33**: p. 212-215.
7. Cravens, T.E., et al., *Composition of Titan's Ionosphere*. Geophys. Res. Lett., 2006. **33**: p. L07105.

8. Cravens, T.E., et al., *Model-Data Comparisons for Titan's Nightside Ionosphere*. Icarus, 2009. **199**: p. 174-188.
9. Vuitton, V. and R.V. Yelle, *The Nitrogen Chemistry of Titan's Upper Atmosphere Revealed*. ApJ 2006. **647**: p. L175-L178.
10. Vuitton, V., et al., *Experimental and Theoretical Study of Hydrocarbon Photochemistry applied to Titan Stratosphere*. Icarus, 2006. **185**: p. 287-300.
11. Vuitton, V., R.V. Yelle, and M.J. McEwan, *Ion Chemistry and N-containing Molecules in Titan's Upper Atmosphere*. Icarus, 2007. **191**: p. 722-742.
12. Vuitton, V., R.V. Yelle, and J. Cui, *Formation and Distribution of Benzene on Titan*. Journal of Geophysical Research, 2008. **113**: p. E05007(1-18).
13. Vuitton, V., et al., *Negative Ion Chemistry in Titan's Upper Atmosphere*. Planet. Space Sci., 2009. **57**: p. 1558-1572.
14. Vuitton, V., et al., *Very High Resolution Mass Spectrometry of HCN Polymers and Tholins*. Farad Disc, 2010. **147**: p. 495-508.
15. Coustenis, A., et al., *Earth-Based Perspective and Pre-Cassini- Huygens Knowledge of Titan*, in *Titan from Cassini-Huygens*, R.H. Brown, J.-P. Lebreton, and J.H. Waite, Editors. 2009, Springer: Dordrecht. p. 9-34.
16. Carrasco, N., et al., *Sensitivity of a Titan Ionospheric Model to the Ion-Molecule Reaction Parameters*. Planet. Space Sci., 2008. **56**: p. 1644-1657.
17. Carrasco, N., et al., *Uncertainty Analysis of Bimolecular Reactions in Titan Ionospheric Chemistry Model*. Planet. Space Sci., 2007. **55**: p. 141-157.
18. Carrasco, N., et al., *Towards a Reduction of the Bimolecular Reaction Model for Titan's Ionosphere*. J. Chem. Kinetic, 2008. **40**: p. 699-709.

19. Waite, J.H., et al., *Ion Neutral Mass Spectrometer Results from the First Flyby of Titan*. Science, 2005. **308**: p. 982-986.
20. Wilson, E.H., S.K. Atreya, and A. Coustenis, *Mechanisms for the Formation of Benzene in the Atmosphere of Titan*. J. Geophys. Res., 2003. **108(E2)**: p. 5014.
21. Vuitton, V., R.V. Yelle, and J. Cui, *Formation and distribution of benzene on Titan*. Journal of Geophysical Research: Planets, 2008. **113(E5)**: p. E05007.
22. Wilson, E.H., S.K. Atreya, and A. Coustenis, *Mechanisms for the formation of benzene in the atmosphere of Titan*. Journal of Geophysical Research: Planets, 2003. **108(E2)**: p. 5014.
23. Bernard, J.M., et al., *Reflectance spectra and chemical structure of Titan's tholins: Application to the analysis of Cassini–Huygens observations*. Icarus, 2006. **185(1)**: p. 301-307.
24. Adams, N.G., L.D. Mathews, and D.S. Osborne, *Laboratory Chemistry Relevant to Understanding and Modeling the Ionosphere of Titan*. Farad. Disc., 2010. **147**: p. 1-323-335.
25. Hammett, L.P., *The Effect of Structure upon the Reactions of Organic Compounds. Benzene Derivatives*. Journal of the American Chemical Society, 1937. **59(1)**: p. 96-103.
26. Muller, P., *Glossary of terms used in physical organic chemistry (IUPAC Recommendations 1994)*. Pure and applied chemistry, 1994. **66(5)**: p. 1077-1184.
27. Breslow, R., *Organic Reaction Mechanisms: An Introduction*. 1969, New York: Benjamin/Cummings Publishing Company.

28. Hansch, C., A. Leo, and R.W. Taft, *A Survey of Hammett Substituent Constants and Resonance and Field Parameters*. Chem. Revs., 1991. **91**.
29. Osborne Jr, D.S., P.A. Lawson, and N.G. Adams, *The effect of N-heteroatoms and CH₃ substituents on dissociative electron-ion recombination of protonated single six membered ring compounds at room temperature*. International Journal of Mass Spectrometry, 2011. **308**(1): p. 114-117.
30. Osborne Jr, D., P.A. Lawson, and N.G. Adams, *Flowing afterglow studies of dissociative electron-ion recombination for a series of single ring compounds at room temperature*. International Journal of Mass Spectrometry, 2011. **305**(1): p. 35-39.
31. Adams, N.G. and D. Smith, *Flowing Afterglow and SIFT*, in *Techniques for the Study of Ion-Molecule Reactions*, J.M. Farrar and J.W.H. Saunders, Editors. 1988, Wiley Interscience: New York. p. 165-220.
32. Osborne Jr, D., et al., *Trends in electron-ion Dissociative Recombination of Benzene Analogs with Functional Group Substitutions: Negative Hammett σ para values*. Icarus, 2013: p. Submitted.
33. Russo, N., et al., *Proton Affinity and Protonation Sites of Aniline. Energetic Behavior and Density Functional Reactivity Indices*. The Journal of Physical Chemistry A, 2000. **104**(17): p. 4017-4021.
34. Eckert-Maksić, M., M. Klessinger, and Z.B. Maksić, *Theoretical calculations of proton affinities in phenol*. Chemical Physics Letters, 1995. **232**(5-6): p. 472-478.
35. Devlin, J.L., et al., *The proton affinities of toluene*. Journal of the American Chemical Society, 1976. **98**(7): p. 1990-1992.

36. Wincel, H., R.H. Fokkens, and N.M.M. Nibbering, *Site of protonation of benzonitrile hydrogen interchange in the protonated species*. Journal of the American Society for Mass Spectrometry, 1990. **1**(3): p. 225-232.
37. Eckert-Maksić, M., et al., *Theoretical model calculations of the absolute proton affinities of benzonitrile, nitroso- and nitrobenzene*. Journal of Molecular Structure: THEOCHEM, 1997. **417**(1-2): p. 131-143.
38. Nourse, B.D. and R. Graham Cooks, *Proton affinity determinations using the kinetic method in an ion trap mass spectrometer*. International Journal of Mass Spectrometry and Ion Processes, 1991. **106**(0): p. 249-272.
39. Hansch, C., A. Leo, and R.W. Taft, *A survey of Hammett substituent constants and resonance and field parameters*. Chemical Reviews, 1991. **91**(2): p. 165-195.

CHAPTER 7

ELECTRON-ION DISSOCIATIVE RECOMBINATION RATE CONSTANTS:
EFFECTS FOR BENZENE ANALOGS WITH VARYING DEGREES OF
METHYLATION⁹

⁹D.S. Osborne, Jr., N.G. Adams, and I. Dotan. 2013. International Journal of Mass Spec. 356:46-48. Reprinted here is permission of the publisher.

7-1 ABSTRACT:

An in-depth study of the effects of varying degrees of methyl substitution on protonated benzene's electron-ion dissociative recombination (e-IDR) rate constants has been conducted. The e-IDR rate constants for protonated benzene, toluene, xylene, trimethylbenzene, tetramethylbenzene, pentamethylbenzene, hexamethylbenzene, and all of their corresponding isomers have been measured at 300K using a Flowing Afterglow equipped with an electrostatic Langmuir probe (FALP). The addition of the first methyl substitution decreases the measured e-IDR rate constant by ~50%. The addition of successive methyl substituents has little effect on the e-IDR rate constant. Isomeric forms also have no effect on the measured e-IDR rate constant. Implications of the observed trends to the chemistry of the Titan ionosphere are discussed.

7-2 INTRODUCTION

In 2004 Cassini arrived at Titan. Since then a wealth of information about the Titan atmosphere and surface has been discovered.[\[1\]](#) In-situ measurements of electron density and temperature have been made using the Radio and Plasma Wave (RPWS) detector[\[2\]](#). Mass spectra were obtained using the Ion Neutral Mass Spectrometer (INMS) on Cassini covering the mass range 1 to 99 amu for positive ions with better than 1 amu mass resolution. Additional data for positive ions were obtained with the Ion Beam Spectrometer (IBS) of the Cassini Spectrometer (CAPS) for the mass range 80 to 350 amu with peaks at ~130, ~170 and 335 amu identified as naphthalene ($C_{10}H_8$), anthracene ($C_{14}H_{10}$) and the anthracene dimer.[\[3\]](#) Negative ions with masses up to 10,000 amu and peaks at 22, 44 and possibly 82 amu were detected by the Electron Spectrometer (ELS) on CAPS.[\[4\]](#) Conversion of ion masses into molecular compositions

requires modeling the complex chemistry which occurs within the Titan atmosphere.[\[3-17\]](#) This modeling has shown that the atmosphere is composed of hydrocarbons (including PAH's), nitriles and thiolins with benzene being the most abundant heavy molecule.[\[11, 18-20\]](#). Benzene with a methyl group substitution (protonated toluene) has been identified through modeling of the Cassini data.[\[4\]](#) This is further confirmed by the identification of benzene, toluene and xylene by the Visual and Infrared Mapping Spectrometer (VIMS) [\[21\]](#). Compounds such as toluene could be formed by ion-neutral association reactions such as in Equation 1.



Such association reactions have been studied using a Selected Ion Flow Tube (SIFT), and this shows that association accounts for ~8% of the products of the reaction between benzene and CH_3^+ .[\[22\]](#) Toluene could be formed as a product following electron-Ion Dissociative Recombination (e-IDR) of protonated toluene. Following the formation of toluene, xylene can be produced by the association reaction of CH_3^+ with toluene. Further methyl substituted benzene compounds could be created through further reactions of Xylene with CH_3^+ . Because of this, there exists a need for a detailed study of the effects of benzene methylation and isomer effects upon e-IDR rate constants; this is the focus of the present paper.

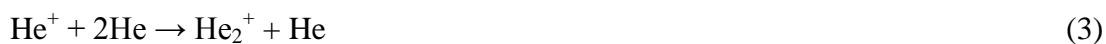
7-3 EXPERIMENTAL

Electron-Ion dissociative Recombination (e-IDR) rate constants, α_e , were determined using a Flowing Afterglow equipped with an axial electrostatic Langmuir probe (FALP). This apparatus has been described in detail previously [\[23-25\]](#) and only a basic description is given here. The FALP utilizes a Langmuir probe operating in the

orbital limited region [26] to determine the decrease in electron density with distance along the flow tube. When only one species is present in the plasma and undergoing recombination, it is possible to utilize equation (2) to determine α_e .

$$\frac{1}{[e]_z} - \frac{1}{[e]_0} = \frac{z\alpha_e}{V_p} \quad (2)$$

In equation (2) V_p , is the plasma velocity, $[e]_0$ is the upstream electron density, and $[e]_z$ is measured electron density as a function of distance along the flow tube, z . A helium (Airgas HP helium) flow is ionized upstream in a microwave cavity to create a quasi-neutral plasma. The ionized helium flows downstream under the action of a Roots blower pump. Argon (National Welders UHP Ar) is added to destroy He_2^+ , helium metastables and increases the electron density creating an Ar^+ plasma. Following argon, hydrogen (Airgas UPC Hydrogen) is added to the flow tube to create an H_3^+ plasma. Once an H_3^+ plasma has been created, a reactant vapor (RV) is added and H_3^+ proton transfers creating the desired protonated reactant vapor, RVH^+ . The RVH^+ once created undergoes recombination with electrons in the plasma forming neutral products. See reactions (3-9). The ions are identified with a downstream quadrupole mass spectrometer and detected with an ETP electron multiplier.



Reactant vapors are introduced into the flow tube with a flow of helium using a bubbler apparatus. The bubbler apparatus causes a flow of helium (Airgas UPC Helium) to be forced through a liquid RV sample. In this way, the helium carries the reactant vapor into the flow tube. The helium flow through the bubbler apparatus is increased until the mass spectrum indicates a pure RVH^+ plasma has been obtained. Through the use of the bubbler apparatus, it was possible to get the reactant liquids mestylene (Aldrich $\geq 99.0\%$), 1,2,4 trimethylbenzene (Aldrich 98%), 1,2,3 trimethylbenzene (Aldrich 90%), and 1,2,3,5 tetramethylbenzene (Aldrich 98%) into the flow tube. Using the same bubbler apparatus, a finely ground solid sample was put in place of the liquid sample. Helium in this way was passed over and through the ground sample. It was possible to get the vapors of reactant solids 1,2,4,5 tetramethylbenzene (Aldrich 98%), pentamethylbenzene (Aldrich 98%), and hexamethylbenzene (Aldrich 99%) into the flow tube using this method. In addition to these data, e-IDR rate constants for protonated benzene, toluene, m-xylene, o-xylene, and p-xylene which have been published previously [[23](#), [27](#)] are included for completeness.

7-4 RESULTS AND DISCUSSION

Electron-ion dissociative recombination rate constants were determined for all possible protonated analogs of benzene with up to six methyl substitutions. These data are plotted in Figure 7-1 and also given in Table 7-1.

Number of methyl Additions	Compound	e-IDR Rate Constant (ccsec ⁻¹)
0	Benzene ^a	8.0x10 ⁻⁷
1	Toluene ^a	3.8x10 ⁻⁷
2	Xylene ^a	2.5x10 ⁻⁷
3	Trimethylbenzene	3.9x10 ⁻⁷
4	Tetramethylbenzene	3.0x10 ⁻⁷
5	Pentamethylbenzene	2.7x10 ⁻⁷
6	Hexamethylbenzene	3.3x10 ⁻⁷

Table 7-1: 300K electron-Ion Dissociative Recombination (e-IDR) rate constants for various methyl substituted benzenes. The data are plotted graphically in Figure 7-1. a) Data previously published.[[23](#), [28](#)]

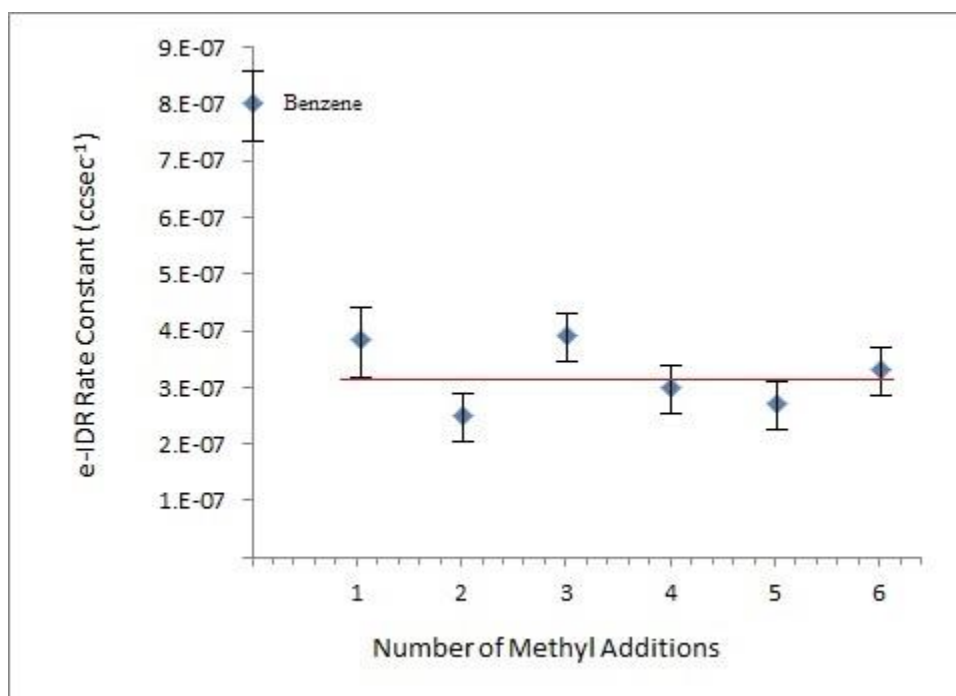


Fig. 7-1: Measured 300K electron-Ion dissociative recombination (e-IDR) rate constants versus the number of benzene methyl additions. The error bars associated with each measurement has been included in the graph, and the benzene value labeled. The red line represents the central value around which all methylated benzene analogs fluctuate.

Figure 7-1, shows that the e-IDR rate constant decreases by ~50% with the addition of a single methyl group; decreasing from $8.0 \times 10^{-7} \text{ ccsec}^{-1}$ for protonated benzene to $3.8 \times 10^{-7} \text{ ccsec}^{-1}$ for protonated toluene at room temperature. The error associated with the e-IDR rate constant measurement is $\pm 15\%$. Given the error associated with the measurement, it could be generalized that, regardless of the number of methyl group substitution above one, the e-IDR rate constant is $\sim 3.2 \times 10^{-7} \text{ ccsec}^{-1}$.

As with the previous studies of isomers of protonated xylene, the protonated isomers of trimethylbenzene and tetramethylbenzene were also studied. The results for the measurements of the individual isomers are given in Table 7-2.

Number of methyl Additions	Isomers	e-IDR Rate Constant (ccsec^{-1})
2	o-Xylene ^a	2.8×10^{-7}
	p-Xylene ^a	2.1×10^{-7}
	m-Xylene ^a	2.7×10^{-7}
3	1,2,3 Trimethylbenzene	4.0×10^{-7}
	1,2,4 Trimethylbenzene	3.9×10^{-7}
	Mestylene	4.0×10^{-7}
4	1,2,4,5 Tetramethylbenzene	2.8×10^{-7}
	1,2,3,5 Tetramethylbenzene	3.2×10^{-7}
5	Pentamethylbenzene	2.7×10^{-7}
6	Hexamethylbenzene	3.3×10^{-7}

Table 7-2: 300K electron-Ion Dissociative Recombination (e-IDR) rate constants for various methyl substituted benzene isomers. a) Data previously published.[[23](#)]

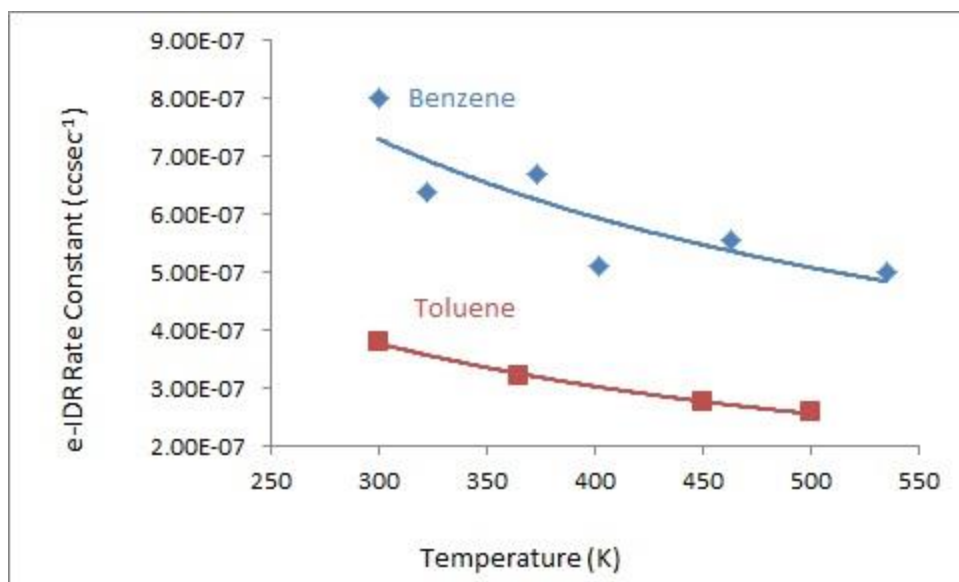


Fig. 7-2: Electron-Ion Dissociative Recombination (e-IDR) rate constants between 300K and 550K for protonated benzene and toluene. Benzene data have been published previously.[27]

For both the protonated trimethylbenzene isomers and the tetramethylbenzene isomers no significant difference in e-IDR rate constant was observed for any of the isomers. These results supported the earlier work on protonated xylene which also showed no e-IDR rate constant dependence upon isomeric form[23]. In Figure 7-2, the temperature dependence data for protonated benzene and toluene are plotted. From the figure, it can be seen that the addition of a single methyl group does not significantly affect the temperature dependence. The measured temperature dependence of protonated benzene is $T^{-0.71}$, while that for protonated toluene is $T^{-0.77}$. It is important to note that the temperature dependencies for protonated benzene and toluene are between that of the direct method[29, 30], $T^{-0.5}$, and the indirect method of recombination[30], $T^{-1.5}$. This indicates that upon neutralization by an electron, the protonated species are accessing both dissociation pathways[31]. Further temperature studies need to be made, to establish if

the temperature dependences of protonated methyl substituted benzene analogs all have the same temperature dependence as protonated benzene and toluene.

7-5 CONCLUSION

The observed trends in the e-IDR rate constants for methyl substituted benzene analogs and isomers will greatly simplify modeling of the Titan ionosphere by reducing the number of reactions that must be input into atmospheric models. For protonated benzene and its methyl substituted analogs, their abundances in the Titan atmosphere will be dependent upon many factors, one of which is their corresponding e-IDR rate constant. Protonated benzene's larger e-IDR rate constant, compared to the protonated methyl substituted benzene analogs, could explain the presence of higher concentrations of benzene in the Titan atmosphere compared to methyl substituted benzene compounds. This knowledge will help with modeling chemical abundances in the Titan atmosphere. Isomeric forms will no longer need to be included in the models. The methyl substituted benzene analogs, and individual compounds will not have to be considered in the atmospheric models. Further, while the reason for the observed sample trend is unknown at this time; the data provided here will give molecular modelers a great deal of evidence through which the process of e-IDR can be better understood. Future work will have to focus on extending the temperature dependent studies to see if there is a difference in the temperature dependences of the other protonated benzene analogs.

7-6 REFERENCES

1. Wilson, E.H. and S.K. Atreya, *Titan's Carbon Budget and the Case of the Missing Ethane*. J. Phys. Chem. , 2009. **A113**: p. 11221-11226.

2. Wahlund, J.-E., et al., *Cassini Measurements of Cold Plasma in the Ionosphere of Titan*. Science, 2005. **308**: p. 986-988.
3. Waite, J.H., Jr., et al., *The Process of Tholin Formation in Titan's Upper Atmosphere*. Science, 2007. **316**(5826): p. 870-875.
4. Vuitton, V., et al., *Negative Ion Chemistry in Titan's Upper Atmosphere*. Planet. Space Sci., 2009. **57**: p. 1558-1572.
5. Cravens, T.E., et al., *The ionosphere of Titan: an updated theoretical model*. Adv. Space Res., 2004. **33**: p. 212-215.
6. Cravens, T.E., et al., *Composition of Titan's Ionosphere*. Geophys. Res. Lett., 2006. **33**: p. L07105.
7. Cravens, T.E., et al., *Model-Data Comparisons for Titan's Nightside Ionosphere*. Icarus, 2009. **199**: p. 174-188.
8. Vuitton, V. and R.V. Yelle, *The Nitrogen Chemistry of Titan's Upper Atmosphere Revealed*. ApJ 2006. **647**: p. L175-L178.
9. Vuitton, V., et al., *Experimental and Theoretical Study of Hydrocarbon Photochemistry applied to Titan Stratosphere*. Icarus, 2006. **185**: p. 287-300.
10. Vuitton, V., R.V. Yelle, and M.J. McEwan, *Ion Chemistry and N-containing Molecules in Titan's Upper Atmosphere*. Icarus, 2007. **191**: p. 722-742.
11. Vuitton, V., R.V. Yelle, and J. Cui, *Formation and Distribution of Benzene on Titan*. Journal of Geophysical Research, 2008. **113**: p. E05007(1-18).
12. Vuitton, V., et al., *Very High Resolution Mass Spectrometry of HCN Polymers and Tholins*. Farad Disc, 2010. **147**: p. 495-508.

13. Coustenis, A., et al., *Earth-Based Perspective and Pre-Cassini- Huygens Knowledge of Titan*, in *Titan from Cassini-Huygens*, R.H. Brown, J.-P. Lebreton, and J.H. Waite, Editors. 2009, Springer: Dordrecht. p. 9-34.
14. Carrasco, N., et al., *Sensitivity of a Titan Ionospheric Model to the Ion-Molecule Reaction Parameters*. Planet. Space Sci., 2008. **56**: p. 1644-1657.
15. Carrasco, N., et al., *Uncertainty Analysis of Bimolecular Reactions in Titan Ionospheric Chemistry Model*. Planet. Space Sci., 2007. **55**: p. 141-157.
16. Carrasco, N., et al., *Towards a Reduction of the Bimolecular Reaction Model for Titan's Ionosphere*. J. Chem. Kinetic, 2008. **40**: p. 699-709.
17. Waite, J.H., et al., *Ion Neutral Mass Spectrometer Results from the First Flyby of Titan*. Science, 2005. **308**: p. 982-986.
18. Wilson, E.H., S.K. Atreya, and A. Coustenis, *Mechanisms for the Formation of Benzene in the Atmosphere of Titan*. J. Geophys. Res., 2003. **108(E2)**: p. 5014.
19. Vuitton, V., R.V. Yelle, and J. Cui, *Formation and distribution of benzene on Titan*. Journal of Geophysical Research: Planets, 2008. **113(E5)**: p. E05007.
20. Wilson, E.H., S.K. Atreya, and A. Coustenis, *Mechanisms for the formation of benzene in the atmosphere of Titan*. Journal of Geophysical Research: Planets, 2003. **108(E2)**: p. 5014.
21. Clark, R.N., et al., *Detection and mapping of hydrocarbon deposits on Titan*. Journal of Geophysical Research: Planets, 2010. **115(E10)**: p. E10005.
22. Fondren, L.D., N.G. Adams, and L. Stavish, *Gas Phase Reactions of CH₃⁺ with a Series of Homo- and Heterocyclic Molecules*. The Journal of Physical Chemistry A, 2008. **113(3)**: p. 592-598.

23. Osborne Jr, D.S., P.A. Lawson, and N.G. Adams, *The effect of N-heteroatoms and CH₃ substituents on dissociative electron-ion recombination of protonated single six membered ring compounds at room temperature*. International Journal of Mass Spectrometry, 2011. **308**(1): p. 114-117.
24. Osborne Jr, D., P.A. Lawson, and N.G. Adams, *Flowing afterglow studies of dissociative electron-ion recombination for a series of single ring compounds at room temperature*. International Journal of Mass Spectrometry, 2011. **305**(1): p. 35-39.
25. Adams, N.G. and D. Smith, *Flowing Afterglow and SIFT*, in *Techniques for the Study of Ion-Molecule Reactions*, J.M. Farrar and J.W.H. Saunders, Editors. 1988, Wiley Interscience: New York. p. 165-220.
26. Swift, J.D.S.M.J.R., *Electrical probes for plasma diagnostics*. 1969, London; New York: Iliffe Books; American Elsevier.
27. Adams, N.G., L.D. Mathews, and D.S. Osborne, *Laboratory Chemistry Relevant to Understanding and Modeling the Ionosphere of Titan*. Farad. Disc., 2010. **147**: p. 1-323-335.
28. Adams, N.G., L.D. Mathews, and D.S. Osborne, *Laboratory Chemistry Relevant to Understanding and Modeling the Ionosphere of Titan*. Farad. Disc., 2010. **147**: p. 323-335.
29. Bates, D.R., *Dissociative recombination of polyatomic ions*. Journal of Physics B: Atomic, Molecular and Optical Physics, 1991. **24**(14): p. 3267.

30. Bardsley, J.N., *The Theory of Electron-Ion Recombination*, in *Linking the Gaseous and Condensed Phases of Matter*, L. Christophorou, E. Illenberger, and W. Schmidt, Editors. 1994, Springer US. p. 495-497.
31. Mitchell, J.B.A. and C. Rebrion-Rowe, *The recombination of electrons with complex molecular ions*. International Reviews in Physical Chemistry, 1997. **16**(2): p. 201-213.

CHAPTER 8

ELECTRON-ION DISSOCIATIVE RECOMBINATION RATE CONSTANTS
RELEVANT TO THE TITAN ATMOSPHERE AND THE INTERSTELLAR
MEDIUM¹⁰

¹⁰ D.S. Osborne, Jr., P.A. Lawson, and N.G. Adams. Submitted to Journal of Chemical Physics, 10/22/2013.

8-1 ABSTRACT

Following the arrival of Cassini at Titan in 2004, the Titan atmosphere has been shown to contain large complex Polycyclic-aromatic hydrocarbons (PAH's). Since Cassini has provided a great deal of data, there exists a need for kinetic rate data to help with modeling this atmosphere. One type of kinetic data needed is electron-ion dissociative recombination (e-IDR) rate constants. These data are not readily available for larger compounds, such as naphthalene, or oxygen containing compounds, such as 1,4 dioxane or furan. Here, the rate constants for naphthalene, 1,4 dioxane and furan have been measured and their temperature dependencies determined when possible, using the University of Georgia's Variable Temperature Flowing Afterglow. The rate constants are compared with those previously published for other compounds; these show trends which illustrate the effects which multi-rings and oxygen heteroatoms substitutions have upon e-IDR rate constants.

8-2 INTRODUCTION

With the arrival of the Cassini space probe at Titan in 2004, a great deal of data has been collected [1]. These data have revealed that the Titan atmosphere is producing large complex molecules which are then deposited upon the planetoid surface. The atmosphere is composed of ~98% nitrogen and ~2% methane with other compounds only found in trace amounts [2]. The nitrogen and methane components of the atmosphere are ionized by solar ultraviolet radiation, high energy electrons and oxygen anions from the Saturn magnetosphere [2-5]. The ionization products then go on to further react with nitrogen or methane leading to the production of larger compounds. These larger

molecules grow further in size as they move towards the planetoid surface with benzene being one of these larger compounds. Benzene has been observed in both the Titan atmosphere and upon the planetoid surface [6-8]. Larger compounds such as naphthalene have also been identified, and it is predicted that these larger compounds could be produced by reactions of ionized benzene with neutral benzene [6]. This would lead to the formation of larger compounds known as polycyclic-aromatic hydrocarbons (PAH's) or perhaps thiolins [7, 9]. Note that naphthalene is the simplest PAH and has already been observed in the Titan atmosphere by Cassini [6].

Naphthalene has also been observed in the Interstellar Medium (ISM).[10] It was identified from observations of unidentified infrared bands (UIR's) and their correlation with laboratory measurements [11-14]. Mid-infrared emission wave lengths have been observed for many years [15] and it has been proposed that these emissions are due to the emission of PAH's which have been excited by ultraviolet radiation [14, 15]. It has been proposed that smaller single ringed compounds also exist in the ISM. While these compounds, such as benzene and furan, have been thought to exist there, it has been proposed that these compounds will have significant heteroatom substitutions [16, 17]. Due to the abundance of nitrogen and oxygen in the ISM, these two atoms could be substituted as heteroatoms in interstellar PAH's [17, 18]. With the growing number of molecules for both Titan and the ISM which must be modeled, there exists a need for much kinetic rate data. Such kinetic rate data are in short supply for larger protonated PAH compounds and single five and six membered rings, especially with heteroatom substitutions. We have focused on measuring electron-ion dissociative recombination (e-IDR) kinetic rate constants in order to help supply some of these needed data. For this,

we have measured the room temperature e-IDR rate constant for protonated naphthalene and completed an extension of our previous e-IDR work on protonated 1,4 dioxane and furan to determine the temperature dependencies of the protonated monomer and proton bound dimer for both species.

8-3 EXPERIMENTAL

Electron-Ion dissociative Recombination (e-IDR) rate constants, α_e , were determined using the University of Georgia's Variable Temperature Flowing Afterglow equipped with an axial electrostatic Langmuir probe (VT-FALP). This apparatus has been described in detail previously [19-21] and only a limited description is given here. The VT-FALP utilizes a Langmuir probe operating in the orbital limited region [22] to determine the decrease in electron density as a function of distance, z , along the flow tube. When only one species is present in the plasma and undergoing recombination, it is possible to utilize equation (1) to determine α_e .

$$\frac{1}{[e]_z} - \frac{1}{[e]_0} = \frac{z\alpha_e}{V_p} \quad (1)$$

Here V_p , is the plasma velocity, $[e]_0$ is the upstream electron density, and $[e]_z$ is measured electron density with distance, z , along the flow tube. Helium (Airgas HP helium) is flowed downstream and ionized in a microwave cavity to create a quasi-neutral plasma. This ionized helium flows under the action of a Roots blower pump. Argon (National Welders UHP Ar) is added to destroy He_2^+ , helium metastables, and increases the electron density creating an Ar^+ plasma. Following the addition of argon, hydrogen (Airgas UPC Hydrogen) is added to the flow to create an H_3^+ plasma. Once an H_3^+

plasma has been created, a reactant vapor (RV) is added and H_3^+ proton transfers to this creating the desired protonated reactant vapor, RVH^+ . The RVH^+ once created undergoes recombination with electrons in the plasma forming neutral products, equations (2-8). In the case where a proton bound dimer is desired, more RV is added to the flow tube. This results in a competition between the recombination of RVH^+ (equation 8) and the collisional association of RVH^+ with RV, equation (9). At large RV flows, association dominates and the proton bound dimer ion is created. Following its creation this dimer ion undergoes recombination with electrons producing neutral products. See reactions (10). The ions are identified with a downstream quadrupole mass spectrometer and detected with an ETP electron multiplier.



Reactant vapors are introduced into the plasma with a flow of helium using a bubbler apparatus or as a dilute reactant vapor mix in helium. Dilute mixes were made by taking a vial of reactant liquid and freezing it while under vacuum. This freezing process drive out any suspended atmospheric gases. Once this freezing process has been completed three times, the neat vapor is flowed into a container and a mix made using helium (Airgas ultra-pure carrier grade Helium). These mixes ranged from 0.5 to 5% in reactant vapor concentration. This range of mixes was needed to allow the complete dynamic range of protonated monomers and proton bound dimers to be created. E-IDR rate constants for the protonated monomer and proton bound dimer are then determined by modeling the experimentally measured e-IDR rate constants. This process is not described here since it has been described in great detail previously [20]. In the case of naphthalene, where significant vapor pressure did not exist to make a mix, the action of bubbler apparatuses was employed. The bubbler apparatus flows helium (Airgas UPC Helium) over and through a finely ground sample of Naphthalene carrying RV into the flow tube. The helium flow through the bubbler apparatus is increased until the mass spectrum indicates that a pure RVH^+ plasma has been obtained. Due to the low vapor pressure and the limits on our helium flow through the bubbler, it was not possible to observe the naphthalene proton bound dimer.

For 1,4 dioxane and furan, the temperature dependence data for the protonated monomer and proton-bound dimer were determined by measuring the e-IDR rate constant at a series of temperatures between 300-550K. Temperatures below room temperature were not possible due to RV condensation upon the flow tube walls.

8-4 RESULTS AND DISCUSSION

Our previous work with 1,4 dioxane was extended to determine the temperature dependence of its recombination rate constant. In the previous study, a comparison of room temperature e-IDR rate constants for six membered rings with and without π electrons was conducted [20]. In that study, it was observed that the presence of π electrons decreased the e-IDR rate constant in six membered rings[20]. This study showed that cyclohexane had a larger 300K e-IDR rate constant than benzene, 1.3×10^{-6} and $8.0 \times 10^{-7} \text{ ccsec}^{-1}$ respectively [20]. This study was extended to see if the π electrons had an effect on the temperature dependence of the six membered ring compounds. To complete the study, we attempted to measured the temperature dependencies for both cyclohexane and 1,4 dioxane. Note that it was not possible to study protonated cyclohexane at temperatures above room temperature due to thermal fragmentation. Lower temperature measurements were also not possible due to the condensation of cyclohexane upon the flow tube walls. For this reason, only a temperature dependence of 1,4 dioxane was possible.

The temperature dependence data for the protonated monomers and proton bound dimers of 1,4 dioxane and benzene are plotted in Figures 8-1 and 8-2.

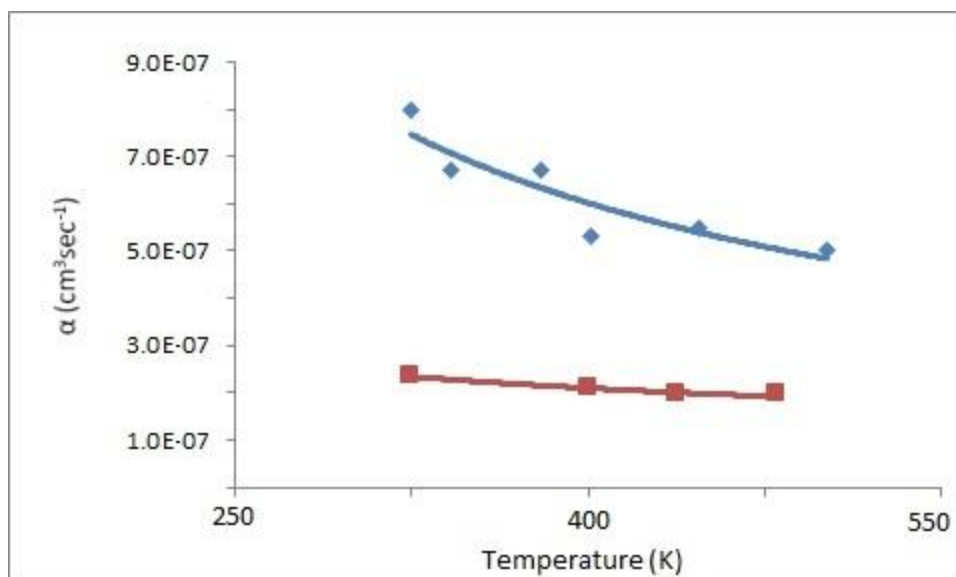


Figure 8-1: A plot of the temperature dependencies of the protonated monomers for 1,4 dioxane (the red squares) and benzene (the blue diamonds). Note that the benzene data have been published previously [23].

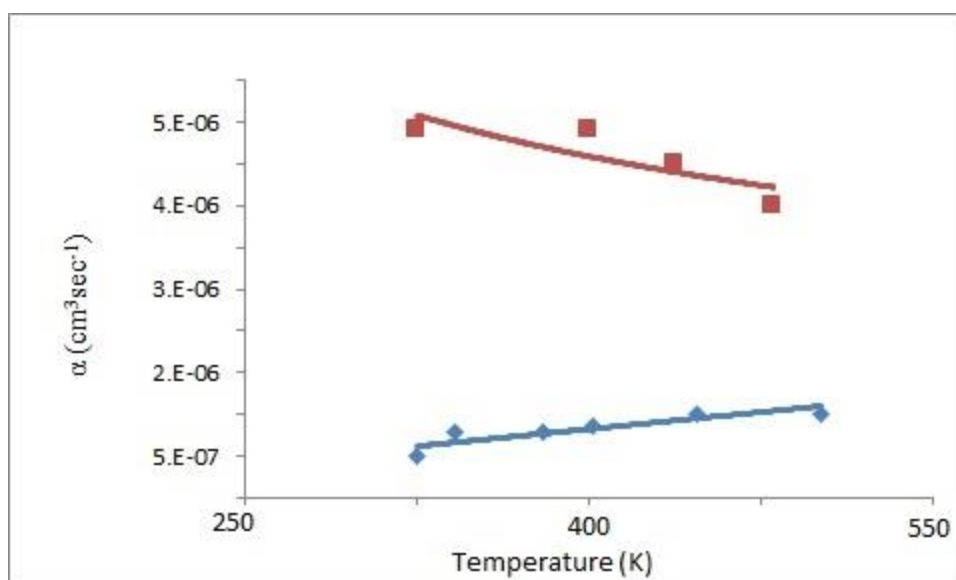


Figure 8-2: A plot of the temperature dependencies of the proton bound dimers for 1,4 dioxane (red squares) and benzene (the blue diamonds). Note that the benzene data have been published previously [23].

The temperature dependence data for benzene, published previously, has been plotted alongside that of 1,4 dioxane for comparison. In Figure 8-1, where the temperature dependence data for both 1,4 dioxane and benzene are presented with benzene's temperature dependence of $T^{-0.7}$ is somewhat different from 1,4 dioxane's temperature dependence of $T^{-0.8}$. In Figure 7-2, where the e-IDR rate constant data for both the proton bound dimers of benzene and 1,4 dioxane are plotted against temperature, it can be seen that there is no similarity. For the proton bound dimer of 1,4 dioxane there is almost no temperature dependence, unlike the proton bound dimer of benzene which has a positive temperature dependence. This difference in temperature dependence may be due to the possible stabilization effects that the π electrons have on the proton bound dimer. Theory will be needed to help explain these results.

Following the work with the six membered rings, the study was extended to five membered rings also with π electrons to see if the size of the ring has an effect upon the temperature dependence. Previously published work has shown that heteroatom substitution and methyl substitution to a five membered ring has little effect on the e-IDR rate constant at 300K [20]. This also showed that the protonated monomer rate constants for five membered rings was approximately half that of benzene at room temperature [20]. In the case of the proton bound dimer, the room temperature rate constants for the various five membered rings varied between 7.25×10^{-7} and 1.0×10^{-6} ccsec⁻¹ [20]. These e-IDR rate constants are slightly larger than the e-IDR rate constants measured for the proton bound dimers of benzene [19, 24]. Protonated six membered ring compounds all showed similar temperature dependences between $T^{-0.55}$ and $T^{-0.96}$. Surprisingly

protonated five membered ringed monomers exhibit a temperature dependence of almost zero.

It is interesting that in the case of the proton bound dimers, six membered ring compounds exhibit a positive temperature dependence as do the five membered ring, furan. See Table 1 for relevant 300K e-IDR rate constants and their corresponding temperature dependencies for the protonated monomers and proton bound dimers.

		Compounds	Protonated Monomer Ions		Proton Bound Dimer Ions	
			α_e (300K) ($\text{cm}^3 \text{s}^{-1}$)	Temperature Dependence	α_e (300K) ($\text{cm}^3 \text{s}^{-1}$)	Temperature Dependence
Compounds with π electrons	Six Membered Rings	Benzene	8.0×10^{-7}	$T^{-0.71}$	5.0×10^{-7}	$T^{0.8}$
	Five Membered Rings	Furan	4.1×10^{-7}	$T^{0.09}$	7.25×10^{-7}	$T^{0.3}$
Compounds without π electrons	Six Membered Rings	1,4 Dioxane	2.3×10^{-7}	$T^{-0.79}$	4.3×10^{-6}	$T^{-0.09}$

Table 8-1: Values for the room temperature electron-ion dissociative recombination rate constants and associated temperature dependencies for benzene, furan, and 1,4 dioxane. Note that the benzene data has been published previously [23]. The 300K data for the protonated monomer and proton bound dimer of both Furan and 1,4 dioxane has been published previously [20].

It is interesting that while the 300K e-IDR rate constant for the proton bound dimer of furan was larger than that for benzene the temperature dependence for furan is approximately half that of benzene's.

Following our work on five and six membered rings we started to study multi-ring systems, such as naphthalene. With the low vapor pressure of the multi-ring compounds a means for introduction of RV into the flow tube had to be developed. By the use of a bubbler apparatus which was previously designed for low vapor pressure liquids; it was possible to introduce naphthalene into the flow tube. By adjusting the flow of helium over and through finely ground naphthalene it was possible to not only get naphthalene into the system but to adjust the amount of naphthalene introduced. The flow of helium through the bubbler apparatus was varied until the mass spectrometer indicated that the plasma was dominated by protonated naphthalene. When this condition was met, the e-IDR rate constant was measured. The results of the protonated naphthalene measurement and a comparison of the 300K e-IDR rate constant for benzene are given in Table 8-2.


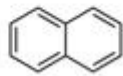
Compound	Number of Benzene Rings	Structure	Rate
Benzene	1		8.0(-7)
Naphthalene	2		9.47(-8)

Table 8-2: Values for the room temperature electron-ion dissociative recombination rate constants of benzene and naphthalene. Note the 300K data for benzene has been published previously [24].

It should also be noted that due to the low vapor pressure and flow limits of the bubbler apparatus it was not possible to introduce enough naphthalene vapor into the flow tube to create any proton bound naphthalene dimer. It can be seen in Table 8-2 that a second

benzene ring has as great effect upon the e-IDR rate constant for the protonated monomer. Here the protonated naphthalene rate constant is an order of magnitude smaller than that for protonated benzene. This large difference in e-IDR rate constants would greatly affect the molecular modeling of large compounds in the ISM and the Titan atmosphere where recombination competes with association.

8-5 FUTURE WORK

Attempts were also made to introduce anthracene (three rings) into the flow tube. Anthracene would allow a detailed study of the effects that multiple rings have on the e-IDR rate constant of protonated compounds. To date, it has not been possible to get sufficient amounts of anthracene into the gas phase. To overcome this limitation, we are currently constructing a new bubbler apparatus which will also allow the sample to be gently heated. It is hoped that by doing this, the vapor pressure will be increased allowing more reactant vapor to be introduced into the flow tube.

8-6 ACKNOWLEDGEMENTS

We would like to thank NASA for their sponsorship under grant NNX10AB96G.

8-7 REFERENCES

1. Coustenis, A., *What Cassini-Huygens has revealed about Titan*. Astronomy & Geophysics, 2007. **48**(2): p. 2.14-2.20.
2. Imanaka, H., et al., *Laboratory experiments of Titan tholin formed in cold plasma at various pressures: implications for nitrogen-containing polycyclic aromatic compounds in Titan haze*. Icarus, 2004. **168**(2): p. 344-366.

3. Vuitton, V., et al., *Negative ion chemistry in Titan's upper atmosphere*. Planetary and Space Science, 2009. **57**(13): p. 1558-1572.
4. Ferris, J., et al., *The role of photochemistry in Titan's atmospheric chemistry*. Advances in Space Research, 2005. **36**(2): p. 251-257.
5. Cravens, T.E., et al., *Composition of Titan's Ionosphere*. Geophys. Res. Lett., 2006. **33**: p. L07105.
6. Clark, R.N., et al., *Detection and mapping of hydrocarbon deposits on Titan*. Journal of Geophysical Research: Planets, 2010. **115**(E10): p. E10005.
7. Delitsky, M.L. and C.P. McKay, *The photochemical products of benzene in Titan's upper atmosphere*. Icarus, 2010. **207**(1): p. 477-484.
8. Bernard, J.M., et al., *Reflectance spectra and chemical structure of Titan's tholins: Application to the analysis of Cassini-Huygens observations*. Icarus, 2006. **185**(1): p. 301-307.
9. Derenne, S., et al., *New insights into the structure and chemistry of Titan's tholins via ^{13}C and ^{15}N solid state nuclear magnetic resonance spectroscopy*. Icarus, 2012. **221**(2): p. 844-853.
10. Iglesias-Groth, S., et al., *Evidence for the naphthalene cation in a region of the interstellar medium with anomalous microwave emission*. The Astrophysical Journal Letters, 2008. **685**(1): p. L55.
11. Ricks, A.M., G.E. Douberly, and M.A. Duncan, *The Infrared Spectrum of Protonated Naphthalene and Its Relevance for the Unidentified Infrared Bands*. The Astrophysical Journal, 2009. **702**(1): p. 301.

12. Hudgins, D.M. and S.A. Sandford, *Infrared Spectroscopy of Matrix Isolated Polycyclic Aromatic Hydrocarbons. 1. PAHs Containing Two to Four Rings*. The Journal of Physical Chemistry A, 1998. **102**(2): p. 329-343.
13. Sloan, G.C., et al., *Direct Spectroscopic Evidence for Ionized Polycyclic Aromatic Hydrocarbons in the Interstellar Medium*. The Astrophysical Journal Letters, 1999. **513**(1): p. L65.
14. Tielens, A.G.G.M., *Interstellar Polycyclic Aromatic Hydrocarbon Molecules**. Annual Review of Astronomy and Astrophysics, 2008. **46**(1): p. 289-337.
15. Allamandola, L.J., D.M. Hudgins, and S.A. Sandford, *Modeling the Unidentified Infrared Emission with Combinations of Polycyclic Aromatic Hydrocarbons*. The Astrophysical Journal Letters, 1999. **511**(2): p. L115.
16. Hudgins, D.M., *Interstellar Polycyclic Aromatic Compounds and Astrophysics*. Polycyclic Aromatic Compounds, 2002. **22**(3-4): p. 469-488.
17. Mattioda, A.L., et al., *Infrared Spectroscopy of Matrix-Isolated Polycyclic Aromatic Compounds and Their Ions. 6. Polycyclic Aromatic Nitrogen Heterocycles*. The Journal of Physical Chemistry A, 2003. **107**(10): p. 1486-1498.
18. Jensen, A.G., F. Markwick-Kemper, and T.P. Snow, *Oxygen in the interstellar medium*. Reviews in Mineralogy and Geochemistry, 2008. **68**(1): p. 55-72.
19. Osborne Jr, D.S., P.A. Lawson, and N.G. Adams, *The effect of N-heteroatoms and CH₃ substituents on dissociative electron-ion recombination of protonated single six membered ring compounds at room temperature*. International Journal of Mass Spectrometry, 2011. **308**(1): p. 114-117.

20. Osborne Jr, D., P.A. Lawson, and N.G. Adams, *Flowing afterglow studies of dissociative electron-ion recombination for a series of single ring compounds at room temperature*. International Journal of Mass Spectrometry, 2011. **305**(1): p. 35-39.
21. Adams, N.G. and D. Smith, *Flowing Afterglow and SIFT*, in *Techniques for the Study of Ion-Molecule Reactions*, J.M. Farrar and J.W.H. Saunders, Editors. 1988, Wiley Interscience: New York. p. 165-220.
22. Swift, J.D.S.M.J.R., *Electrical probes for plasma diagnostics*. 1969, London; New York: Iliffe Books; American Elsevier.
23. Adams, N.G., L.D. Mathews, and D.S. Osborne, *Laboratory Chemistry Relevant to Understanding and Modeling the Ionosphere of Titan*. Farad. Disc., 2010. **147**: p. 1-323-335.
24. Adams, N.G., L.D. Mathews, and J.D. Osborne, *Laboratory chemistry relevant to understanding and modeling the ionosphere of Titan*. Faraday Discussions, 2010. **147**: p. 323-335.

CHAPTER 9

CONCLUSIONS AND FUTURE WORK

Titan has been of great interest for a long time due to the possible similarity between the organic haze formed in the Titan atmosphere and the organic haze that existed in the atmosphere of the early Earth[[1](#), [2](#)]. It is believed that the surface of early Earth was protected from UV radiation and warmed by the presence of an organic haze[[1](#), [3](#), [4](#)]. Titan is the only region in our solar system where organic particles form in the atmosphere to produce a haze[[5](#)]. In the last ~35 years four spacecraft have studied Titan; Pioneer 11, Voyager 1, Voyager 2, and most recently Cassini[[5](#)]. From all this, a great deal has been learned about the process by which large organic particles are produced in the Titan atmosphere.

Decades of study have shown that the Titan atmosphere is composed of ~98% nitrogen, ~2% methane and other gases and compounds in trace amounts[[5](#), [6](#)]. Nitrogen and methane are ionized in the upper atmosphere (above 1200 km) by solar x-rays, ultra-violet radiation, high energy electrons and oxygen anions (O^+) from Saturn's magnetosphere[[7-10](#)]. These ionized compounds undergo a series of reactions where they form larger compounds which diffuse to lower altitudes[[11](#)]. Most important of the organic compounds produced, is benzene. Benzene is produced in great quantities in the Titan atmosphere and has been observed to decrease in concentration with decreasing altitude[[11](#), [12](#)]. It is proposed that benzene reacts with other compounds in the

atmosphere as it diffuses to lower altitudes[[11](#)]. Through this process, large organic compounds (such as Poly-cyclic aromatic hydrocarbons (PAH)) are created. These PAH compounds generate the particles responsible for the characteristic orange haze in the Titan atmosphere[[2](#)]. Between 1000km and 400km these PAH compounds increase in size by two pathways; electron-ion dissociative recombination and ion-ion recombination[[13](#)].

The Cassini spacecraft has obtained a great deal of atmospheric data which require a great deal of kinetic data to turn mass spectra into models of the Titan atmosphere. One type of kinetic data needed is electron-ion dissociative recombination (e-IDR) rate constants. There has not previously been an in-depth study of benzene analogs. Such a study can identify trends which will help the prediction of unmeasured e-IDR rate constants by atmospheric modelers. Such data will greatly increase our understanding of the dissociative recombination process.

The current study of e-IDR rate constants for benzene analogs has shown that there is a correlation between e-IDR rate constants and the electron donating or electron withdrawing nature of the functional group substituted into a benzene ring. With electron donating groups the proton is located on the benzene ring[[14-16](#)]. The additional electron density transferred to the ring by the functional group stabilizes the proton and decreases the mobility of the π -electrons. This decrease in electron mobility causes the e-IDR rate constant to decrease proportionally. For functional groups which are electron withdrawing, the proton is located on the functional group[[17-19](#)]. This has shown that for all electron withdrawing functional groups the e-IDR rate constant is the same, with no dependence on the amount of electron density withdrawn from the benzene ring.

Further investigations of the effects that nitrogen heteroatom substitutions have on e-IDR rate constants for benzene analogs; have shown that the e-IDR rate constant increases with the number of nitrogen heteroatom substitutions to a benzene ring[20, 21]. A study of methyl group substitutions in a benzene ring was also conducted and observed that the e-IDR rate constant decreased by ~50% with the first methyl group addition[21]. Each subsequent methyl addition does not affect the e-IDR rate constant. A study was also conducted which showed that the e-IDR rate constant was smaller for six membered rings than for five membered rings[22]. Another study showed that the e-IDR rate constant decreased by almost an order of magnitude with the addition of a second benzene ring to benzene. While the reasons for these observed trends are not known at this time, these trends still allow Titan modelers to predict e-IDR rate constants for compounds which have yet to be studied.

There is still a great deal of e-IDR rate constant studies to be undertaken. Benzene analogs with multiple functional group substitutions, compounds such as dinitrobenzene and dicyanobenzene, need to be studied. This investigation will determine if a similar effect is present as was observed for methyl substitutions to a benzene ring. These functional group studies need to be conducted for pyridine also. Pyridine is a benzene analog where one carbon heteroatom has been replaced with a nitrogen. With the large amount of nitrogen present within the Titan atmosphere such compounds have been predicted by the Vuitton model[13]. A study of the functional group analogs of pyridine will explain if these compounds have the same e-IDR rate constant trends as benzene analogs. PAH compounds, larger than naphthalene, need to be studied to observe the trends that occur with 3, 4 and 5 benzene ring additions. If the

trend observed for naphthalene continues then the e-IDR rate constant will become so slow that in essence a compound composed of five benzene rings will not recombine with electrons. If this was found to be the case, then for extremely large compounds within the Titan atmosphere, those between 400-800 km, their only loss would be due to ion-ion recombination reactions. There also exists a need for information on the products of e-IDR for benzene analogs. A great deal of kinetic data is still needed for a completely and successful modeling of the Titan atmosphere.

9-1 REFERENCES

1. Wolf, E.T. and O.B. Toon, *Fractal Organic Hazes Provided an Ultraviolet Shield for Early Earth*. Science, 2010. **328**(5983): p. 1266-1268.
2. Trainer, M.G., et al., *Organic haze on Titan and the early Earth*. Proceedings of the National Academy of Sciences, 2006. **103**(48): p. 18035-18042.
3. Kasting, J.F. and M.T. Howard, *Atmospheric composition and climate on the early Earth*. Philosophical Transactions of the Royal Society B: Biological Sciences, 2006. **361**(1474): p. 1733-1742.
4. Feulner, G., *The faint young Sun problem*. Reviews of Geophysics, 2012. **50**(2): p. RG2006.
5. Raulin, F., et al., *Prebiotic-like chemistry on Titan*. Chemical Society Reviews, 2012. **41**(16): p. 5380-5393.
6. Coustenis, A., *What Cassini-Huygens has revealed about Titan*. Astronomy & Geophysics, 2007. **48**(2): p. 2.14-2.20.
7. Ferris, J., et al., *The role of photochemistry in Titan's atmospheric chemistry*. Advances in Space Research, 2005. **36**(2): p. 251-257.

8. Lunine, J. and S. Hörst, *Organic chemistry on the surface of Titan*. Rendiconti Lincei, 2011. **22**(3): p. 183-189.
9. Sittler Jr, E.C., et al., *Heavy ion formation in Titan's ionosphere: Magnetospheric introduction of free oxygen and a source of Titan's aerosols?* Planetary and Space Science, 2009. **57**(13): p. 1547-1557.
10. Wahlund, J.E., et al., *On the amount of heavy molecular ions in Titan's ionosphere*. Planetary and Space Science, 2009. **57**(14–15): p. 1857-1865.
11. Delitsky, M.L. and C.P. McKay, *The photochemical products of benzene in Titan's upper atmosphere*. Icarus, 2010. **207**(1): p. 477-484.
12. Clark, R.N., et al., *Detection and mapping of hydrocarbon deposits on Titan*. Journal of Geophysical Research: Planets, 2010. **115**(E10): p. E10005.
13. Vuitton, V., et al., *Negative ion chemistry in Titan's upper atmosphere*. Planetary and Space Science, 2009. **57**(13): p. 1558-1572.
14. Russo, N., et al., *Proton Affinity and Protonation Sites of Aniline. Energetic Behavior and Density Functional Reactivity Indices*. The Journal of Physical Chemistry A, 2000. **104**(17): p. 4017-4021.
15. Eckert-Maksić, M., M. Klessinger, and Z.B. Maksić, *Theoretical calculations of proton affinities in phenol*. Chemical Physics Letters, 1995. **232**(5–6): p. 472-478.
16. Devlin, J.L., et al., *The proton affinities of toluene*. Journal of the American Chemical Society, 1976. **98**(7): p. 1990-1992.
17. Wincel, H., R.H. Fokkens, and N.M.M. Nibbering, *Site of protonation of benzonitrile hydrogen interchange in the protonated species*. Journal of the American Society for Mass Spectrometry, 1990. **1**(3): p. 225-232.

18. Eckert-Maksić, M., et al., *Theoretical model calculations of the absolute proton affinities of benzonitrile, nitroso- and nitrobenzene*. Journal of Molecular Structure: THEOCHEM, 1997. **417**(1–2): p. 131-143.
19. Nourse, B.D. and R. Graham Cooks, *Proton affinity determinations using the kinetic method in an ion trap mass spectrometer*. International Journal of Mass Spectrometry and Ion Processes, 1991. **106**(0): p. 249-272.
20. Adams, N.G., L.D. Mathews, and J.D. Osborne, *Laboratory chemistry relevant to understanding and modeling the ionosphere of Titan*. Faraday Discussions, 2010. **147**: p. 323-335.
21. Osborne Jr, D.S., P.A. Lawson, and N.G. Adams, *The effect of N-heteroatoms and CH₃ substituents on dissociative electron–ion recombination of protonated single six membered ring compounds at room temperature*. International Journal of Mass Spectrometry, 2011. **308**(1): p. 114-117.
22. Osborne Jr, D., P.A. Lawson, and N.G. Adams, *Flowing afterglow studies of dissociative electron-ion recombination for a series of single ring compounds at room temperature*. International Journal of Mass Spectrometry, 2011. **305**(1): p. 35-39.